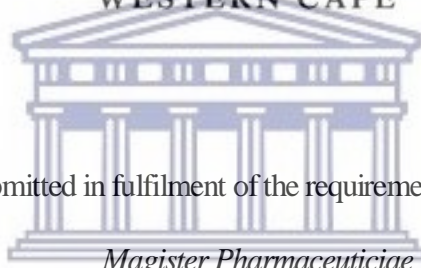# FORMULATION AND EVALUATION OF POLYMERIC MICELLES FOR IMPROVED ORAL DELIVERY OF TENOFOVIR DISOPROXIL FUMARATE AND ZIDOVUDINE USING POLY-LACTIC-CO-GLYCOLIC ACID NANOPARTICLES

By

Lovette Asobo Tenghe

A thesis submitted in fulfilment of the requirements for the degree of

Magister Pharmaceuticiae

Discipline of Pharmaceutics, School of Pharmacy,

Faculty of Natural Sciences,

University of the Western Cape, Bellville, South Africa

Supervisor: Dr Halima Samsodien

Co-supervisor: Dr Oluchi Mbamalu

December 2018

Abstract

ABSTRACT

Background: Tenofovir disoproxil fumarate (TDF) and Zidovudine (AZT) are both nucleotide and nucleoside analogue reverse transcriptase inhibitors (NtRTIs and NRTIs), respectively. They are used for the management and prevention of the Human Immunodeficiency Virus (HIV) infection. These drugs are faced with oral delivery challenges such as low intestinal permeability and extensive first pass liver metabolism for TDF and AZT, respectively. Their use may also be limited by dose-dependent adverse effects, which may result in treatment failure when patients become non-compliant and non-adherent to their prescribed antiretroviral (ARV) regimen. Non-compliance and non-adherence to ARV regimen may lead to drug resistance and a need for change in regimen, which can be very expensive, not only financially but in terms of morbidity and mortality. To solve such issues, a new drug can be formulated, or an existing drug can be modified. The development and formulation of a new drug is time consuming and expensive, especially with no available data and a high probability of failure. Modifying existing drugs is a cheaper, less time-consuming option with lower probability of failure. Such modification can be achieved *via* non-covalent interactions using various methods such as preparation of nano-particulates with polymeric micelles (a non-covalent interaction). Polymeric micelles offer a variety of polymers to choose from for drug modification purposes.

Purpose: The aim of this study was to formulate polymeric nanoparticles of TDF and AZT using different ratios of poly-lactic-co-glycolic acid (PLGA), characterize the formulated nanoparticles (using the following analyses: particle size, zeta potential, encapsulation efficiency, hot stage microscopy, thermogravimetric analysis, differential scanning calorimetry, Fourier transform infrared spectroscopy and scanning electron microscopy), analyze for stability during storage (2-8˚C) and

i

Abstract

determine the release rate of the active pharmaceutical ingredients in the formulated nanoparticles.

Methods: Nanoparticles were prepared using a modified version of the double emulsion (water-in-oil-in-water) solvent evaporation and diffusion method. Two ratios of PLGA (50:50 and 85:15) were used to prepare four formulations (two each of TDF and AZT). Thereafter, the physicochemical and pharmaceutical properties of the formulations were assessed by characterizing the nanoparticles for particle size, zeta potential, polydispersity index, percentage yield, release profile and particle morphology, using the suggested analytical techniques.

Results: For TDF-PLGA 85:15, TDF-PLGA 50:50, AZT-PLGA 85:15 and AZT-PLGA 50:50, nanoparticles of 160.4±1.7 nm,154.3±3.1 nm,127.0±2.32 nm and 153.2±4.3 nm, respectively, were recovered after washing. The polydispersity index (PDI) values were ≤0.418±0.004 after washing, indicating that the formulations were monodispersed. The zeta potential of the particles was -5.72±1 mV, -19.1 mV, -12.2±0.6 mV and -15.3±0.5 mV for TDF-PLGA 85:15, TDF-PLGA 50:50, AZT-PLGA 85:15 and AZT-PLGA 50:50 respectively after washing. The highest percentage yield was calculated to be 79.14% and the highest encapsulation efficiency obtained was 73.82% for AZT-PLGA 50:50, while the particle morphology showed spherical nanoparticles with signs of coalescence and aggregation for all formulated nanoparticles. The release profiles were biphasic; that is, an initial burst which indicated the presence of surface API followed by sustained release. Comparing the release profiles of AZT and TDF at pH 1.2 and 7.4, it was indicative that more AZT was released at pH 1.2 while more TDF was released at pH 7.4. On computing the release data further into various mathematical models, the Weibull model was found to be the best fit. The loaded nanoparticles showed an increase

Abstract

in stability after washing; however, they showed signs of gradual decrease in stability after 10 days of storage at 2-8°C.

Conclusions: Relatively small, spherical and smooth nanoparticles were formulated. The nanoparticle release profile was indicative of sustained release; however, there was no conclusive indication that 48 hours duration was sufficient to release all encapsulated drug. Further studies with an increased API or polymer ratio in the formulation needs to be performed to determine if the encapsulation efficiency can be improved and *in-vivo* studies are required for a better understanding of the API release from formulations as well as its absorption in the body.

UNIVERSITY *of the* WESTERN CAPE

KEYWORDS

Tenofovir disoproxil fumarate

Zidovudine

Nanoparticles

Water-in-oil-in-water double emulsion (W/O/W)

Human Immunodeficiency Virus (HIV)

Poly-lactic-co-glycolic acid (PLGA)

UNIVERSITY *of the*
WESTERN CAPE

DECLARATION

I declare that, *Formulation and evaluation of polymeric micelles for improved oral delivery of tenofovir disoproxil and zidovudine using poly-lactic-co-glycolic nanoparticles,* is my own work. It has not been submitted for examination at this university or any other tertiary institution. All the sources used have been indicated and acknowledged in the references section.

Lovette Tenghe, December 2018

Signed: UWC, Bellville

v

ACKNOWLEDGEMENT

I would like to express my gratitude to both my supervisor Dr. Halima Samsodien and co-supervisor Dr. Oluchi Mbamalu for their relentless efforts in making sure that I do my best at every given opportunity, for their encouragement, patience, motivation and support at every step of the way until the completion of this study.

I would like to acknowledge Dr Marique Aucamp for her guidance in developing the HPLC method used and for always being willing to help.

I would like to acknowledge and thank Mr. Yunus Kippie for his critical input and analysis of the various analytical tools.

I would like to acknowledge Dr. Samsodien's research group: Jean, Yves, Zene, Bjorn, Rami and Dr. Musa for their insight, constructive criticism and support.

DEDICATION

Above all, I would like to give thanks to the Lord Almighty for providing me with good health, wisdom, strength and the perseverance to complete my Master's degree.

❖ A special thanks to my biggest fan in the world, Laura Tengeh (my sister-in-law); without your support, none of this would have come to fruition. Your support and faith in my abilities have no bounds and I cannot thank you enough for the joy and love you and my nieces (Robanura and Ronaldette) and my nephews (Robino and Rovette) have shown me over the years.

❖ I would also like to thank Prof. Robertson K. Tengeh (my brother) for providing me with the means and opportunity to pursue my goals.

❖ To my mom and siblings for constantly putting me in their prayers during my studies.

❖ To my friends Alkassim and Myolisi, for their invaluable advice and support, and for making it a positive competition.

❖ Finally, to the staff and post graduate colleagues at the School of Pharmacy, University of the Western Cape, I say thank you for good working relationships.

Table of content

Table of content

Table of content

Table of content

List of abbreviations

Abbreviation	Full name
API	Active pharmaceutical ingredient
ARV	Antiretroviral (regimen)
AZT	Zidovudine
AZT-PLGA	Zidovudine-poly lactic-co-glycolic acid complex
BA	Bioavailability
BCS	Biopharmaceutical Classification System
˚C	Degrees Celsius
DL	Drug loading
DLS	Dynamic light scattering
DSC	Differential scanning calorimetry
EE%	Encapsulation efficiency
Eq	Equation
FDA	Food and Drug Administration
FTIR	Fourier Transform Infrared spectroscopy
Hrs.	Hours
HSM	Hot stage microscopy
HCl	Hydrochloride
HR-SEM	High resolution scanning electron microscopy
HPLC	High performance liquid chromatography
IR	Infrared spectra
ICH	International Council on Harmonization
Kw	Kilowatts
Mw	Molecular weight
Mg	Milligrams
Ml	Milliliters
mmHg	Millimeters of mercury
Ml	Microliters
Mg	Micrograms

List of abbreviations

Min	Minutes
Nm	Nanometer
NP	Nanoparticle
NtRTI	Nucleotide analogue reverse transcriptase inhibitor
NRTI	Nucleoside analogue reverse transcriptase inhibitor
NPs	Nanoparticles
O/W	Oil-in-water emulsion
PLGA	Poly-lactic-co-glycolic-acid
PBS	Phosphate buffered saline
PDI	Polydispersity index
PCS	Photon correlation spectroscopy
PLA	Poly (lactic acid)
PGA	Poly (glycolic acid)
cm^{-1}	Reciprocal centimeter
RSD	Relative standard deviation
SD	Standard deviation
Sec	Seconds
SEM	Scanning electron microscopy
TDF	Tenofovir disoproxil fumarate
TDF-PLGA	Tenofovir disoproxil fumarate-poly-lactic-co-glycolic acid complex
TGA	Thermogravimetric analysis
TPGS	D-α-tocopheryl polyethylene glycol succinate
UK	United Kingdom
UV	Ultra-violet
USA	United states of America
v/v	Volume per volume
W/O/W	Water-in-oil-in-water emulsion
w/v	Weight per volume
w/w	Weight per weight

Zp	Zeta potential

List of tables

UNIVERSITY *of the*
WESTERN CAPE

List of Appendices

List of Appendices

UNIVERSITY *of the*
WESTERN CAPE

List of figures

List of figures

PEER-REVIEWED CONFERENCE PRESENTATION

The findings reported in this thesis have been presented at the international conference mentioned below:

Poster presentation at international conference:

LOVETTE TENGHE*, OLUCHI MBAMALU, MARIQUE AUCAMP, and HALIMA SAMSODIEN (2018). Formulation and Evaluation of Polymeric Micelles for Improved Oral Delivery of Tenofovir Disoproxil Fumarate and Zidovudine using Poly-Lactic-Co-Glycolic Acid Nanoparticles. Presented at the **First Conference of Biomedical and Natural Sciences and Therapeutics (CoBNeST) 7-10 October 2018, Spier Estate Stellenbosch, Cape Town.**

The asterisk (*) indicates the presenting author.

CHAPTER 1: INTRODUCTION

Chapter 1 introduces the epidemic posed by the Human Immunodeficiency Virus (HIV) in South Africa and around the world, specifically the challenges faced with the drugs used in managing the epidemic, and some of the methods that may be used to attenuate such challenges.

1.1 HIV Background

According to the World Health Organization (WHO), since the dawn of the HIV epidemic, more than 70 million people have been infected with the HIV virus and about 35 million people have died from HIV-related infections. At the end of 2016, 36.7 million [34.0-39.8 million] people globally were living with HIV, with adults between the ages of 15 and 49 years making up about 0.8% [0.7-0.9%] of this population.[1] Sub-Saharan Africa accounts for nearly 70% of the total population of people living with HIV worldwide; about 1 in 25 adults (4.4%) in the region are living with HIV.[1] With South Africa having the highest HIV epidemic profile in the world, an estimated 7 million people in the country were living with HIV at the end of 2016, and an estimated total of 380 000 new infections were reported, with 180 000 deaths from AIDS-related illnesses.[2] Little wonder then that the Antiretroviral Treatment (ART) program in South Africa is the largest globally, with about $1.5 billion invested annually from the country's domestic resources to run the HIV and AIDS programs.[3] The need to prevent the spread of HIV/AIDS cannot be overemphasized. It accounts for severe mortality and morbidity, and has a negative impact on the country's economy, both in the private and public sector. Most people infected fall between the age groups of 20 and 40 years of age. As such, the epidemic affects the most productive years of the infected patient's life and the workforce of the country, leading to a general reduction in the progress of economic development and a decrease in life expectancy.

Consequently, the South African government spends a substantial amount in supporting AIDS-orphaned children, who face several challenges such as migration to relatives, financial stress and food insecurities.[4-5] As aforementioned, the need to contain this scourge cannot be over-emphasized. The current therapy with ARVs has improved the quality and prolonged the lives of many infected individuals. These drugs may however pose delivery challenges, and severe side effect profiles, which may be counterproductive to therapeutic success. Such challenges may be overcome by non-covalent nano-formulation of the drugs with suitable polymers.

Nano-formulations

In the pharmaceutical industry, the various forms of nano-formulations available have become the focal point of many researchers due to their drug delivery capabilities. Nano-formulations have revolutionized cell specific targeting and controlled drug release, and can deliver vaccines, conventional drugs, nucleotides and recombinant proteins.[6,7] Both hydrophobic and hydrophilic drugs can be encapsulated within nanoparticles (NPs), and so a need can be proven for the nano-formulation of almost any agent. Modifying plasma exposure levels *via* sustained release or cell targeting, a technique that can be achieved with nano-formulations, can further reduce toxicities and adverse effects associated with therapeutic agents. An example of an effective therapeutic agent with unacceptable adverse effects and/or toxicities that has been reformulated as NPs to reduce these adverse effects is paclitaxel, an approved drug for chemotherapy. Paclitaxel has been formulated into albumin-based NPs (Abraxane®). Abraxane® has been proven to greatly reduce the adverse effects (such as ocular toxicity, hypersensitivity reactions, myelosuppression, peripheral neuropathy, nausea, vomiting, fatigue, arthralgia, myalgia and alopecia) associated with paclitaxel.[7- 9]

NPs can be optimized by shape and size or functionalized with lipid coatings and protein to facilitate their cellular uptake, drug release, and ability to cross physiologic barriers such as the blood-brain barrier.[10-12] NPs can be further functionalized with ligands such as those with immune system modulating effects, concurrently modifying the cellular immune response and enhancing intracellular drug delivery.[13] Chitosan (CS) has gained attention in the nanomedicine field because it carries a positive charge that can be used for cellular and anatomic targeting of NPs.[14] The electrostatic interactions between positively charged CS NPs and the negatively charged cell surface have been shown to enhance NP uptake[15-20] by using a poly-lactic-co-glycolic acid (PLGA) core in conjunction with a CS shell. This has advanced drug delivery and further specified drug target sites and degradation rates to achieve a specific therapeutic response. Such desirable characteristics can be harnessed for the non-covalent formulation of Tenofovir disoproxil fumarate (TDF) and Zidovudine (AZT) complexes in this study.
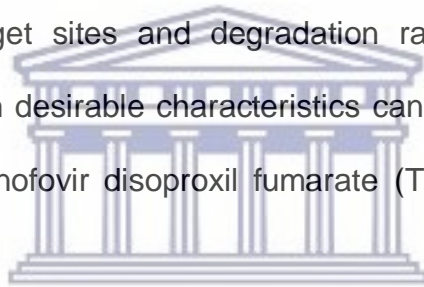
1.2   Tenofovir disoproxil fumarate (TDF) and Zidovudine (AZT)

TDF and AZT are antiretroviral agents. In South Africa, they form part of the first line antiretroviral (ARV) regimen. In patients suffering from renal insufficiency, TDF may be replaced with AZT.[21] The optimal delivery of these drugs is limited by the low bioavailability of TDF (due to its low permeability), and the short plasma half-life and first pass metabolism of AZT (which has resulted in twice daily administration of AZT to achieve and maintain effective plasma concentration levels). The disadvantage of this is a cumulative high drug dose and dose-dependent adverse effects such as neutropenia, hepatotoxicity, myopathy and renal dysfunction.[22] Such adverse effects may result in treatment failure when patients become non-compliant and non-adherent to their prescribed ARV regimen. The result is often drug resistance; the patient may

3

need a change to another regimen which may be more expensive, not only financially but in terms of morbidity and quality of life. Therefore, the field of long-acting, cell-targeted ARVs has become a major area of research.

In this growing field of study, the shortcomings of commonly utilized drugs (e.g. ARVs) are researched. Shortcomings may be resolved by synthesizing a new drug or modifying the existing drugs. Synthesizing a new drug, however is time-consuming and expensive. In addition, with little or no existing data available, there is a very high risk of product failure. On the other hand, modifying existing drugs will likely be less time-consuming and more cost effective, because there is some information about the drug already available and there is a relatively low risk of product failure. Modification of existing drugs can be achieved by:

- ❖ use of polymeric micelles,

- ❖ use of hydrates or solvates,

- ❖ solvent deposition,

- ❖ self-dispersing lipid formulation (SDLF), and

- ❖ lipid based delivery systems.

Polymeric micelle formulation presents a variety of options since there are many polymers to choose from. However, the inability to work with all at the same time to select the best, poses a limitation. One of the most affordable polymers is poly-(D,L)-lactic-co-glycolic acid (PLGA); a co-polymer of poly lactic acid (PLA) and poly glycolic acid (PGA). It is considered one of the best biomaterials for drug delivery based on its design and performance.[20] The toxicities associated with the use of current ARVs such as TDF and AZT may be attenuated using co-polymers such as PLGA. PLGA

4

encapsulates the drug in polymeric micelles which are delivered across lipophilic barriers, thereby increasing drug absorption (bioavailability, BA) across the intestinal mucosa. Formulation with such a co-polymer may result in improved drug absorption/bioavailability by improving permeability, a modification which may very well work to improve TDF bioavailability. The short plasma half-life and first pass metabolism of AZT may also be addressed by co-formulation with appropriate polymers. Such co-formulation may avoid first pass effect through an increase in lymphatic uptake, resulting in the achievement of higher systemic drug concentrations with lower drug doses.[23,24] This may in turn result in reduced incidence of dose-dependent side effects as well as promote sustainable prescribing.[25,26]

Hypothesis

It was hypothesized that, co-formulation of TDF and AZT with PLGA to produce TDF-PLGA and AZT-PLGA nanoparticles, respectively, would improve absorption and reduce the dose of drug required to attain therapeutic concentrations, thereby improving bioavailability and reducing the adverse effects associated with the use of these APIs when administered orally.

1.3   OBJECTIVES

The objectives of this study were:

- ❖ to characterize TDF and PLGA (50:50 and 85:15);

- ❖ to formulate TDF-PLGA and AZT-PLGA nanoparticles;

- ❖ to characterize and compare the physicochemical properties of the formulated complexes using various analytical techniques;

- ❖ to compare the pharmaceutical properties of both formulations (i.e.: *in vitro* release and stability).

Chapter 2 will now follow with a brief literature review on the APIs and poly-lactic-co-glycolic acid.

UNIVERSITY *of the*
WESTERN CAPE

Bibliography

1 World Health Organization (2017). 'HIV/AIDS', [online] available at: *http://www.who int/gho/hiv/en/,* [Accessed 4 Apr 2017].

2 UNAIDS (2014). 'The Gap Report UNAIDS', [online] available at: *http://www.unaids.org/en/resources/documents/2014/20140716_UNAIDS_ gap_report,* [Accessed 10 May 2017].

3 Ndaki, K., (2017). '*SANAC–Global AIDS Response Progress Report (GARPR) 2015* sanac.org.za', [online] available at*: http://sanac.org.za/2016/06/22/global-aids-response-progress-report-garpr-2015/,* [Accessed 15 Jul 2017].

4 Kuo, C., Fitzgerald, J., Operario, D., and Casale, M., (2012). 'Social support disparities for caregivers of aids-orphaned children in south Africa,' *Journal of Community Psychology*, 40(6), pp. 631-644.

5 Dawson, H., (2013). 'HIV/AIDS, the erosion of social capital and the collapse of rural livelihoods in the Nkomazi district of South Africa', *African Journal of AIDS Research*, 12(4), pp. 185-194.

6 Gregory, A., Titball, R., and Williamson, D. (2013). 'Vaccine delivery using nanoparticles', *Frontiers in Cellular and Infection Microbiology*, 3(N/A).

7 Miele, E., Spinelli, G. P., Tomao, F., and Tomao, S., (2009). 'Albumin-bound formulation of paclitaxel (Abraxane ABI-007) in the treatment of breast cancer', *International Journal of Nanomedicine*, 4(N/A), pp. 99–105.

8 Ibrahim, N. K., Samuels, B., Page, R., (2005). 'Multicenter phase II trial of ABI-007, an albumin-bound paclitaxel, in women with metastatic breast cancer,' *Journal of Clinical Oncology*. 23(25), pp. 6019–6026.

9 Tomao, S., (2009). 'Albumin-bound formulation of paclitaxel (Abraxane® ABI-007) in the treatment of breast cancer,' *International Journal of Nanomedicine,* p.99.

10 Mahajan, S. D., Roy, I., and Xu, G., (2010). 'Enhancing the delivery of anti-retroviral drug 'saquinavir' across the blood brain barrier using nanoparticles', *Current HIV Research*, 8(5), pp. 396–404.

11 Alam, M. I., Beg, S., and Samad, A., (2010). 'Strategy for effective brain drug delivery', *European Journal of Pharmaceutical Sciences*, 40(5) pp. 385–403.

12 Nagpal, K., Singh, S. K., and Mishra, D. N., (2013). 'Drug targeting to brain: a systematic approach to study the factors, parameters and approaches for prediction of permeability of drugs across BBB', Expert *Opinion on Drug Delivery*, 10(7), pp. 927–955.

13 Dube, A., Reynolds, J. L., Law, W.C., Maponga, C. C., Prasad, P. N., and Morse, G. D., (2014). 'Multimodal nanoparticles that provide immunomodulation and intracellular drug delivery for Infectious diseases', *Nanomedicine*, 10(4), pp. 831–838.

14 Dai, H., Jiang, X., and Tan, G. C. Y., (2006). 'Chitosan-DNA nanoparticles delivered by intrabiliary infusion enhance liver-targeted gene delivery', *International Journal of Nanomedicine*, 1(4), pp. 507–522.

15 Wang, M., Zhang, Y., and Feng, J., (2013). 'Preparation, characterization, and in vitro and in vivo investigation of chitosan-coated poly (d, l-lactide-co-glycolide) nanoparticles for intestinal delivery of exendin-4', International *Journal of Nanomedicine*, 8(N/A), pp. 1141–1154.

16 Bakhru, S. H., Altiok, E., and Highley, C., (2012). 'Enhanced cellular uptake and long-term retention of chitosan-modified iron oxide nanoparticles for MRI-based cell tracking', *International Journal of Nanomedicine*, 7(N/A), pp. 4613–4623.

17 Chronopoulou, L., Massimi, M., Giardi, M., Cametti, C., Devirgiliis, L., Dentini, M., and Palocci, C., (2013). 'Chitosan-coated PLGA nanoparticles: A sustained drug release strategy for cell cultures', *Colloids and Surfaces B: Biointerfaces*, 103(N/A), pp.310-317.

18 Luo, Y., Teng, Z., Li Y., and Wang, Q., (2015). 'Solid lipid nanoparticles for oral drug delivery: Chitosan coating improves stability, controlled delivery, mucoadhesion and cellular uptake', *Carbohydrate Polymers*, 122(N/A), pp.221-229.

19 Prasad, P., (2012). *Introduction to nanomedicine and nanobioengineering*. Hoboken, NJ: Wiley.

20 The South African Antiretroviral Treatment Guidelines 2013

21 Kutscher, H. L., Makita-Chingombe, F., and DiTursi, S., (2015). 'Macrophage targeted nanoparticles for antiretroviral (ARV) delivery', *Journal of Personalized NanoMedicine*, 1(2), pp. 40–48.

22 Gelmon, K., Montaner, J., Fanning, M., Smith, J., Falutz, J., Tsoukas, C., Gilll, J., Wells, G., O'Shaughnessy, M., Wainberg, M., and Ruedy, J., (1989). 'Nature, time course and dose dependence of zidovudine-related side effects', *AIDS*, 3(9), pp.555-562.

23 Rao, D.A., Forrest, M.L., Alani, A.W.G., Kwon, G.S., and Robinson, J.R., (2010). 'Biodegradable PLGA based nanoparticles for sustained regional

lymphatic drug delivery', *Journal of Pharmaceutical Sciences*, 99(4), pp. 2018–2031

24 Scruggs, E.R., and Dirks, N.A.J., (2008). 'Mechanisms of zidovudine-induced mitochondrial toxicity and myopathy', *Pharmacology*, 82(2), pp. 83–88.

25 Hall, A., Bass, P., and Unwin, R., (2013). 'Drug-induced renal Fanconi syndrome', *QJM: An International Journal of Medicine*, 107(4), pp. 261-269.

26 Daughton, C.G., (2014). 'Eco-directed sustainable prescribing: feasibility for reducing water contamination by drugs', *The Science of the Total Environment*, 493(N/A), pp. 392-404.

CHAPTER 2: LITERATURE REVIEW

Introduction

This chapter reviews the literature on Tenofovir disoproxil fumarate (TDF), Zidovudine (AZT) and poly-lactic-co-glycolic acid (PLGA).

2.1 TENOFOVIR DISOPROXIL FUMARATE
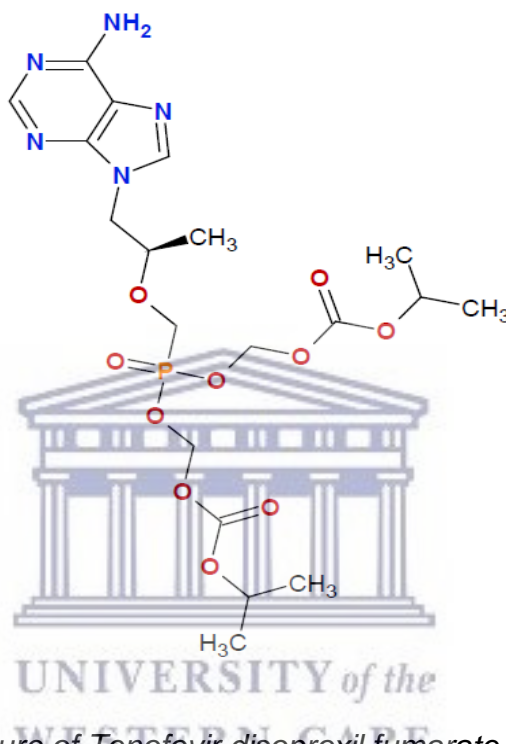
Figure 2.1: *Chemical structure of Tenofovir disoproxil fumarate* (TDF)

Tenofovir disoproxil fumarate (TDF, Figure 2.1) is classified as a nucleotide analogue reverse transcriptase inhibitor (NtRTI). It is a highly effective antiretroviral (ARV) drug used predominantly in combination with other ARVs for the management and prevention of infections by the Human Immunodeficiency Virus (HIV).[1] It is well established as a component of ARV combination therapy regimens in the management of adults with HIV infection. TDF does not inhibit cytochrome P450 enzymes, so few drug interactions are expected with drugs metabolized *via* this route.[2]

11

In addition to its use in ARV therapy, TDF is also used for the treatment of hepatitis B virus (HBV) infection.[3] A substantial amount of HIV-infected individuals are co-infected with HBV[4] and are at a risk of developing HBV-associated diseases such as hepatocellular carcinoma and cirrhosis.[1] TDF is very effective against HBV, hence its continued use as part of the first-line treatment of HIV infected patients, where it serves dual purposes.[1,3]

In terms of physical properties, TDF is a hydrophilic drug, classified as a class III agent according to the Biopharmaceutical Classification System (BCS).[5] This implies that it has high solubility and low intestinal permeability. The latter may account partially for its low bioavailability (BA) (about 25% without food) which can be increased (to about 40%) with a high fat meal.[5] This improved BA however, may still be considered very low. TDF itself is an ester prodrug of tenofovir designed to increase tenofovir's absorption across the intestine. However, this method of drug design to increase efficiency to overcome intestinal barriers can be decreased by the rapid esterase-mediated hydrolysis and P-glycoprotein (P-gp)-related efflux of the drug.[6,7] These factors contribute to the drug's low BA. To address this limitation, a large dose (300 mg) is usually administered to ensure that the minimum plasma concentration required for antiviral activity is attained. Administration of such a large dose may however predispose the patient to dose-dependent drug toxicity, a well-known adverse effect associated with TDF usage.[8]

Another limitation to the use of TDF is its nephrotoxic potential. Studies have documented TDF as the most common cause of nephrotoxicity in HIV patients being referred to nephrologists, accounting for at least 20% of nephrologists' consultations.[9,10] Polyuropolydipsic syndrome has also been associated with TDF use within six months of such use, and full resolution of renal dysfunction

(polyuropolydipsic syndrome) reported within three weeks of withdrawing TDF.[11] In more severe cases of TDF toxicity, patients can develop acute kidney injury, osteomalacia, and Fanconi syndrome (characterized by phosphaturia, tubular proteinuria, bicarbonate wasting, glycosuria, and amino aciduria, which can lead to further complications such as metabolic acidosis).[9,11] The main site of TDF nephrotoxicity seems to be the proximal tubule and the epithelia cells of the conducting ducts. As TDF is eliminated by renal excretion, dose adjustments are necessary in patients with significant renal impairment.

We hypothesize that co-formulation with a suitable polymer will improve solubility and permeability of TDF. With such improved solubility and permeability, therapeutic efficacy may be attained with lower drug doses, resulting in less incidence of dose-dependent drug toxicity.

Table 2.1: Physicochemical properties of Tenofovir disoproxil fumarate[12]

Biopharmaceutical classification	Class III: high solubility and low permeability
Molecular formula	$C_{23}H_{24}N_5O_{14}P$
Molecular weight	635.514922 g/mol
Melting point	114-118 °C
Solubility (in water)	13.4 mg/ml at 25 °C
Appearance	White, fine, powder-like crystals
Log P	1.25 at pH of 6.5

Table 2.2 presents information on the pharmacokinetic and clinical properties of TDF, and its legal status in South Africa (schedule 4). As a schedule 4 medicine, it can only be obtained with a valid prescription from an authorized prescribing doctor.

13

Table 2.2: *Pharmacokinetic and clinical properties of Tenofovir disoproxil fumarate*

Trade Name	Viread® (Gilead Sciences Inc.)
South African legal status	Schedule 4
Bioavailability	25% in fasted state
Half-life	17 hours
Route of administration	Oral
Renal excretion	70-80%
Protein binding	<7%

2.1.1 Mechanism of action

TDF is a prodrug which is hydrolyzed *in vivo* to tenofovir, which then undergoes phosphorylation to tenofovir diphosphate for its antiretroviral effect. Tenofovir diphosphate inhibits the enzyme, HIV reverse transcriptase, by competing with the substrate, deoxyadenosine 5'-triphosphate. It therefore acts as a DNA chain terminator by preventing DNA chain elongation because it lacks the 3-hydroxyl group required for the formation of an ester linkage with the phosphate group of the next nucleotide (Figure 2.2).[13]

14
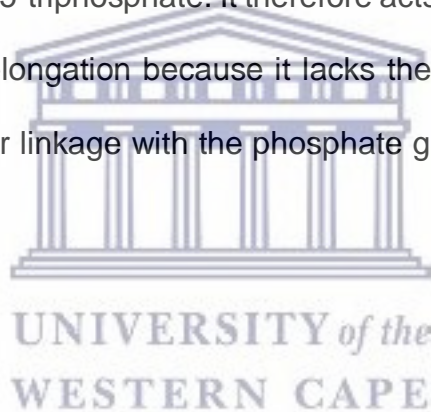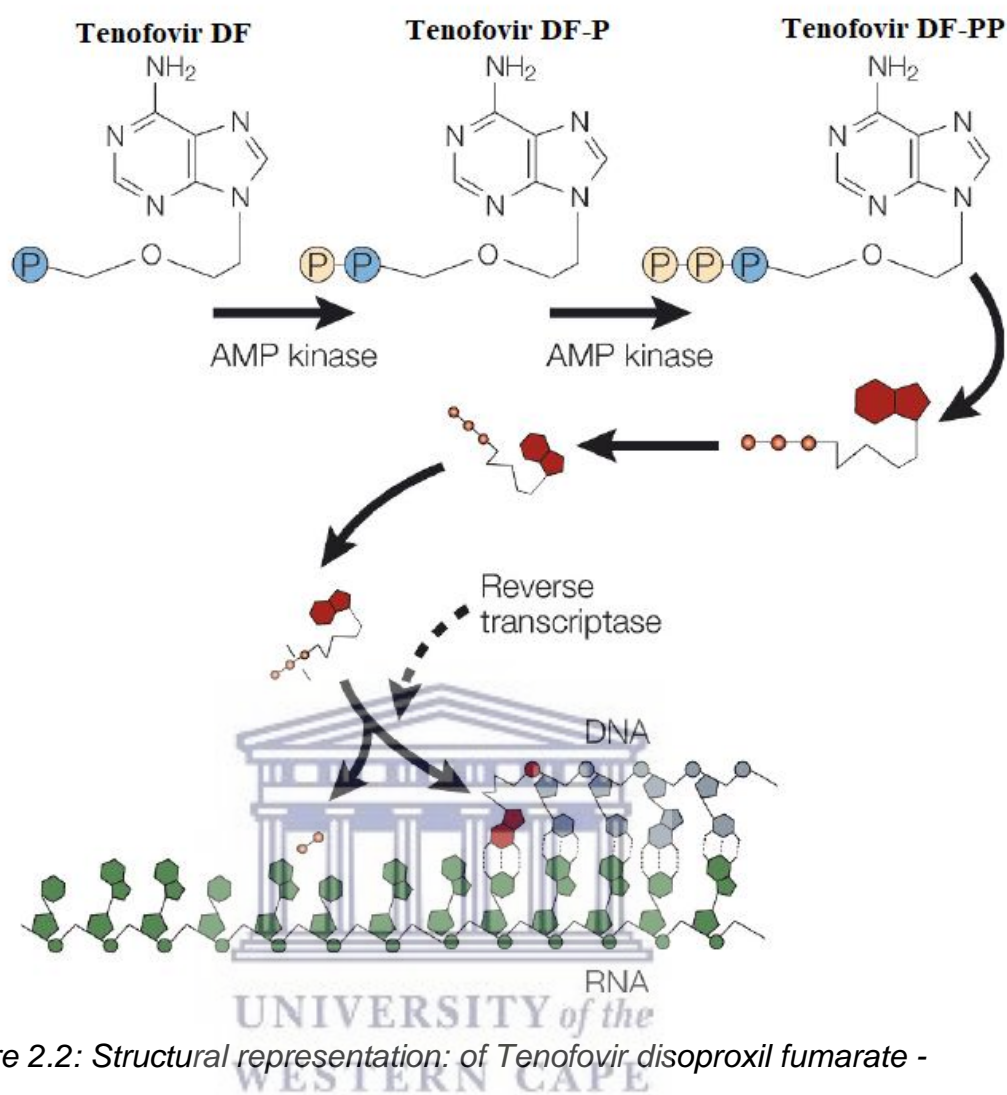
Figure 2.2: Structural representation: of Tenofovir disoproxil fumarate -

mechanism of action

2.1.2 Mechanism of TDF associated toxicities

The kidneys serve as a major route of drug excretion from the body, with several interactions, leading eventually to excretion, taking place in the proximal tubules. As such, there exists the potential for interactions that could lead to toxicity between TDF and other agents in this segment of the nephron.[11] TDF enters the epithelial cells at its basolateral pole using the organic transporter.[14,15] It gets into the tubular lumen *via* multidrug resistant proteins (MRP2, MRP3, MRP4).[16-18] The apical transporter multidrug resistance-associated protein 4 (MRP4) aids its (i.e., TDF's) exit from the

15

cells.[19] Evidence suggests that the proximal tubule is enriched with a high density of mitochondria; and these organelles are targets of TDF toxicity.[11]

The intracellular concentrations of TDF can increase as its plasma concentrations increase or the apical secretion of TDF is inhibited.[14] This leads to oxidative respiratory chain dysfunctions,[19] inhibition of mitochondrial DNA (mtDNA) polymerase γ,[20] and depletion of mtDNA.[14,19,21] As such, structural changes to the mitochondria are induced in the proximal tubular epithelial cells.[19,22] This leads to shortage in the production of ATP, resulting in tubular cells reabsorption of small molecules or ions such as uric acid, amino acids, potassium, glucose, β_2-microglobulin and phosphate. These molecules are secreted abnormally in the urine, a condition referred to as the Fanconi syndrome.

Genetic polymorphism and drug interactions with transporters may also explain why TDF might accumulate in the proximal tubular cells of some patients. Another contributing factor is the inhibition of the enzyme, DNA polymerase γ, which is responsible for the replication of mtDNA.[23] Such inhibition leaves the proximal tubule vulnerable because of the mitochondria's limited ability to anaerobically generate ATP.[24] If these mechanisms of TDF toxicity can be attenuated by non-covalent polymeric micelle formulation parameters, it would be another advantage obtained from the non-covalent formulation of the TDF complexes.

2.2   ZIDOVUDINE
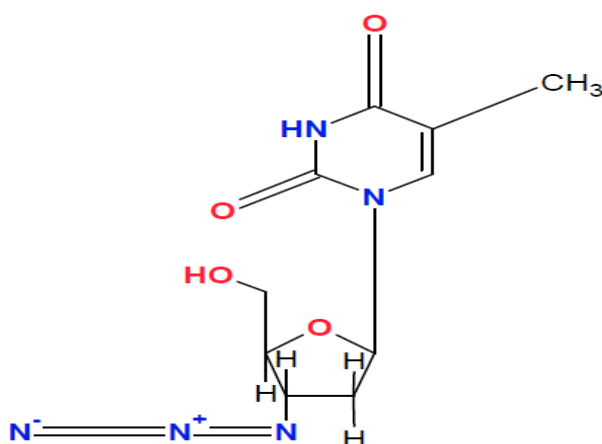
Figure 2.3: *Chemical structure of Zidovudine*

Zidovudine (also known as azido thymidine, or AZT, Figure 2.3) was the first nucleoside analogue reverse transcriptase inhibitor (NRTI) clinically approved by the Food and Drug Administration (FDA) for the management of HIV/AIDS. This was in March 1987, six years after AIDS was first reported.[25] Generally, AZT is administered as an oral dose of 300 mg twice a day, or 1 mg per kilogram over 1 hour every 4 hours for intravenous infusions. In South Africa, AZT is used both as a first- and second-line agent in Highly Active Antiretroviral Therapy (HAART) regimen. [26] It is also used for Post Exposure Prophylaxis (PEP) following exposure of individuals and heath care workers to HIV infection, and especially in the Prevention of Mother to Child Transmission (PMTCT) of HIV. [27,28]

Table 2.3: Chemical and physical properties of Zidovudine [29]

Biopharmaceutical classification	Class III: high solubility and low permeability
Molecular formula	$C_{10}H_{13}N_5O_4$
Molecular weight	267.24132 g/mol
Melting point	120-127 °C
Solubility (in water)	20.1 mg/L (at 25 °C)
Color	White to beige, crystalline solid
LogP	0.05

AZT is a hydrophilic drug, a class III agent according to the BCS classification. Its clinical effectiveness is constrained due to sub-optimal pharmacokinetics *viz.* extensive first pass metabolism, inhibition of mitochondrial machinery, and a short plasma half-life ($t_{1/2}$ = 1 to 2 hours)[24,30-32] (Table 2.4). These lead to a required increase in AZT's dosage and frequency of administration in order to attain and maintain therapeutic plasma levels. High doses may result in unwanted side effects such as anemia, neutropenia, hepatotoxicity, cardiomyopathy, and myopathy.[24,33] HIV patients on AZT have been known to present with hypo-proliferative anemia which resolves on drug withdrawal.[34] Such adverse effect may compromise patient adherence to therapy. Because these adverse effects may be dose-dependent, a reduction in dose may reduce incidents of such adverse effects.[35,36] As proposed for TDF, we hypothesize that co-formulation with a suitable polymer will improve solubility and permeability of AZT, beyond that currently obtainable. With such improved solubility and permeability, therapeutic efficacy may be attained with lower drug (AZT) doses, resulting in less incidence of dose-dependent adverse effects.

As the antiviral effect of AZT is time-dependent,[37] an adequate zero-order delivery system is required to maintain activity as well as to avoid dose-induced toxic responses.[38-41] For instance, the formulation of iron oxide nanoparticles (PLGA) for

18

the delivery of anticancer agents was proven to attenuate the dose-dependent anti-proliferative activity in prostate and cancer cells.[42]

AZT is a substrate of various drug efflux mechanisms that are present in the intestinal epithelium, central nervous system (CNS) and immune system. These efflux systems are mediated by permeability glycoprotein (P-gp), and adenosine triphosphate (ATP) binding cassette of the ABC (transport) protein family.[43] As a result of this efflux, drug resistant strains of the virus might develop.[32] This in effect accounts for cases of inter- and intra-patient non-linearity and variability observed in the bioavailability of AZT.[44,45]

Table 2.4 presents information on the pharmacokinetic and clinical properties of AZT, and its legal status in South Africa (schedule 4). As a schedule 4 medicine, it can only be obtained with a valid prescription from an authorized prescribing doctor.

Table 2.4: *Pharmacokinetic and clinical properties of Zidovudine*

Trade Name	Aspen Zidovudine®
South African legal status	Schedule 4
Bioavailability	65%
Half-life	1-2 hours
Route of administration	Oral
Renal excretion	29%
Protein binding	30-38%

2.2.1 Mechanism of action

AZT (a structural analog of thymidine) is a NRTI that undergoes phosphorylation to its active metabolite, zidovudine triphosphate (AZT-TP). AZT-TP competes with the natural substrate, deoxy guanosine triphosphate (*dGTP*) for incorporation into viral DNA, acting as chain terminator for the synthesis of DNA. It lacks the 3′-OH group in the incorporated nucleoside and it prevents chain elongation by failing to complete the 5′ to 3′ phosphodiester linkage necessary for DNA chain elongation, hence terminating viral DNA growth (Figure 2.4).[13]
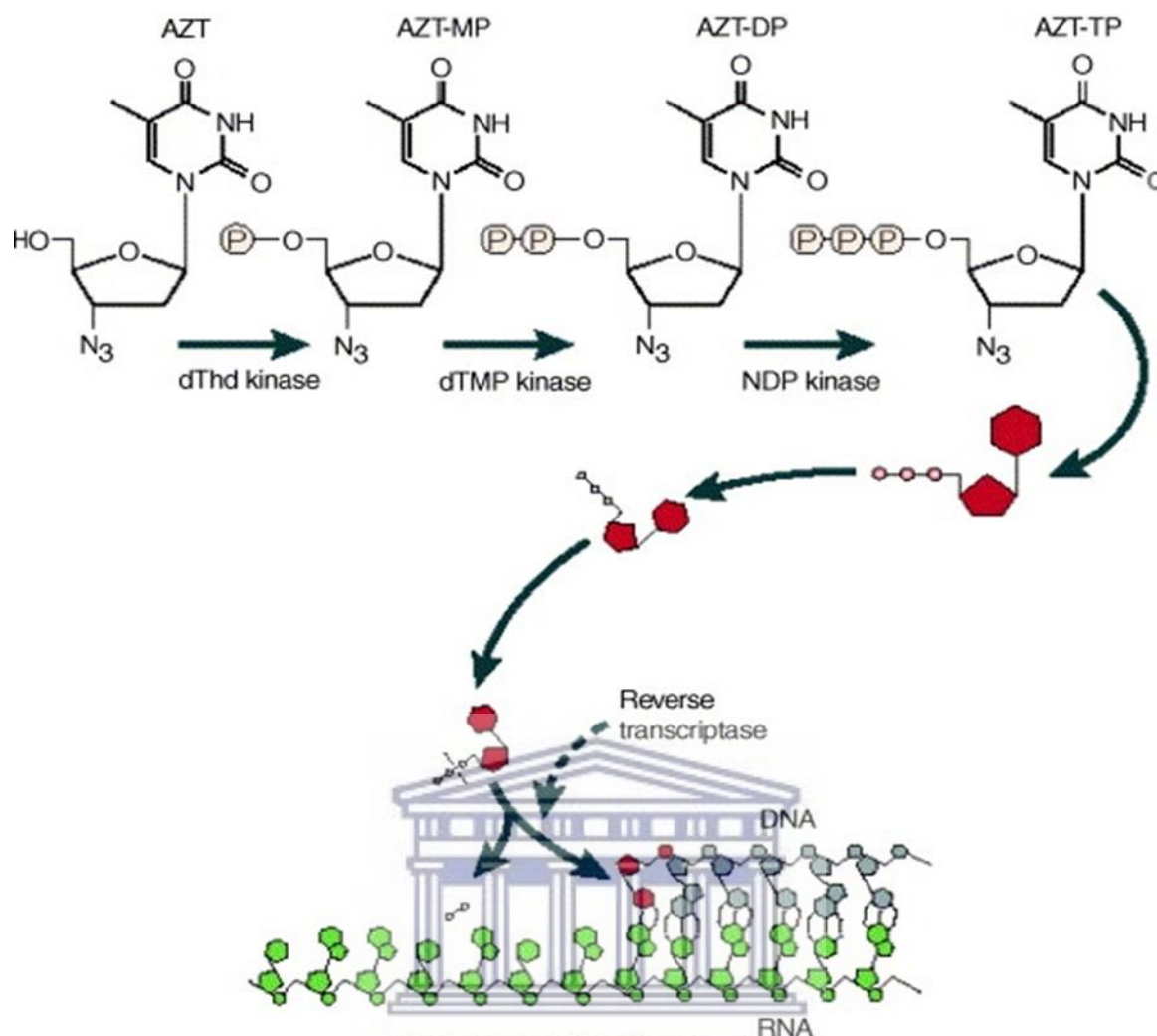
Figure 2.4: Structural representation of Zidovudine - mechanism of action

2.2.2 Mechanism of Zidovudine toxicity

The use of AZT has been associated with adverse effects such as cardiomyopathy, neutropenia, hepatotoxicity, anemia and myopathy.[25] Various mechanisms of AZT-induced toxicity have been postulated to explain how AZT induces toxicity. These mechanisms include mitochondrial DNA (mtDNA) depletion, oxidation stress (mitochondrial dysfunction), and depletion of *l*-carnitine.[25]

mtDNA Depletion

HIV patients who experience AZT-induced myopathy as an adverse effect have been found to present with mtDNA depletion.[46-48] This has led to the deduction that mtDNA depletion leads to dysfunction of the electron transport chain, affecting ATP synthesis

20

and oxidative phosphorylation. Aerobic ATP production fails to produce the minimal energy needed to maintain organ or tissue functions which leads to dysfunction. This however is reversible upon withdrawal of AZT. [46-48]

Studies show that AZT-induced mtDNA depletion is due to mitochondrial thymidine triphosphate pool depletion or inhibition of DNA polymerase, required for DNA synthesis and replication. With reference to the metabolism and mechanism of AZT action, AZT-TP can indeed inhibit DNA-polymerase; however, there is lack of evidence correlating mtDNA depletion and inhibition of DNA polymerase.[49] Literature shows that the ability of mtDNA to replicate is hindered by AZT inhibiting thymidine kinase,[50,51] leading to mtDNA depletion. Lebrecht *et al.*, (2007) reported that administration of dietary supplements rich in uridine to AZT treated mice helped attenuate signs of AZT-induced myopathy, mtDNA depletion and markers of oxidative stress.[50,52] The mechanism by which uridine functions is not fully understood though it is believed to compete with AZT at certain steps such as phosphorylation or intracellular transport, or by correcting a pyrimidine deficit.[50,52]

Oxidative stress

It has been hypothesized that AZT may impair the electron transport chain. This may lead to increased production of reactive oxygen species and oxidative stress, eventually causing loss of mtDNA integrity.[53] AZT was reported to cause a decrease in ATP concentration. It is also responsible for the depletion of glutathione[53] which occurs in conditions of oxidative stress. Glutathione is a cysteine tripeptide whose main objective is the elimination of reactive oxygen species.[53] The concentration of glutathione was seen to dwindle just six days after administration of AZT; by day 15, the values ranged between 32 and 50% of normal levels.[53] Reactive oxygen species can cause cellular and mitochondrial dysfunction through damage to DNA, lipids and

proteins. There is however no direct evidence to suggest that reactive proteins are involved in myopathy and mitochondrial toxicity.[53] The compound, 8-oxo-7,8-dihydro-2'-deoxy guanosine (8-oxo-dG), a marker of oxidative damage to DNA and high levels of oxidized glutathione, was found in AZT-treated mice compared to the control mice;[54] hence showing that oxidative stress plays a role in AZT-induced myopathy.

Reduced Mitochondrial Content of *L*-Carnitine

L-carnitine is a quaternary ammonium compound involved in the metabolism of long chain fatty acids to generate energy. It can be obtained exogenously from the ingestion of dairy products and meat and can also be synthesized endogenously from such amino acids as methionine and lysine. Evidence suggests that AZT is responsible for a reduction in cellular *L*-carnitine levels which may lead to mitochondrial dysfunction,[55-57] promoting accumulation of lipids in the cytoplasm of muscle cells. The mechanism by which AZT causes cellular reduction of *L*-carnitine was shown to be by reduction of *L*-carnitine transport across the plasma membrane.[55] AZT also acts as a non-competitive inhibitor of the sodium-dependent transport of *L*-carnitine.

If one of these mechanisms of AZT toxicity can be attenuated by non-covalent polymeric micelle formulation parameters, it would be another advantage obtained from the non-covalent formulation of the AZT complexes.

2.3 Dosing of TDF and AZT in South Africa

Tenofovir disoproxil is available in South Africa as tablets of 300 mg administered once daily in adults. This dose is modified accordingly in patients with renal impairment. Zidovudine is available in South Africa as capsules of 100 mg and tablets of 300 mg, generally administered at a dose of 300 mg twice a day. It is also available as an oral solution of 10 mg per ml.

2.4 Poly-lactic-co-glycolic acid (PLGA)

Poly (lactic-co-glycolic) acid (PLGA) is a co-polymer of lactic acid and glycolic acid. It is considered one of the best biomaterials for drug delivery based on its design, performance, excellent biocompatibility, biodegradability, and mechanical strength.[58] Among other polymers such as polycaprolactone (PCL), poly-lactic acid (PLA), and poly-glycolic acid (PGA), PLGA is one of many polymers registered by the Food and Drug Administration (FDA) and the World Health Organization (WHO) as material for use in the manufacture or delivery of medicine. PLGA co-polymers are widely used in the pharmaceutical industry for controlled delivery of immunomodulatory drugs, antiviral agents, anticancer agents, antihypertensive agents, hormones and vitamins. Macromolecules such as antibodies, proteins and peptides have also been delivered systemically using PLGA.

In terms of solubility, PLGA is soluble in a wide variety of solvents such as acetone, acetyl acetate, and chlorinated solvents. It can be processed into virtually any size or shape; and can encapsulate molecules of almost any size.

2.4.1 Synthesis of PLGA

PLGA can be synthesized through a polycondensation reaction or ring-opening polymerization of cyclic diesters, which is the random co-polymerization of the two monomers of cyclic dimers (1,4-dioxane-2, and 5-diones) of glycolic and lactic acid (Figure 2.5). The polymers are linked together by ester bonds, and catalysts such as tin (II) 2-ethylhexanoate, tin (II) alkoxides or aluminum isopropoxide are used to produce amorphous aliphatic polyester products. [59] Ring-opening polymerization can be used to synthesize PLGA co-polymer of molecular weight less than 10 kDa (low molecular weight polymer).
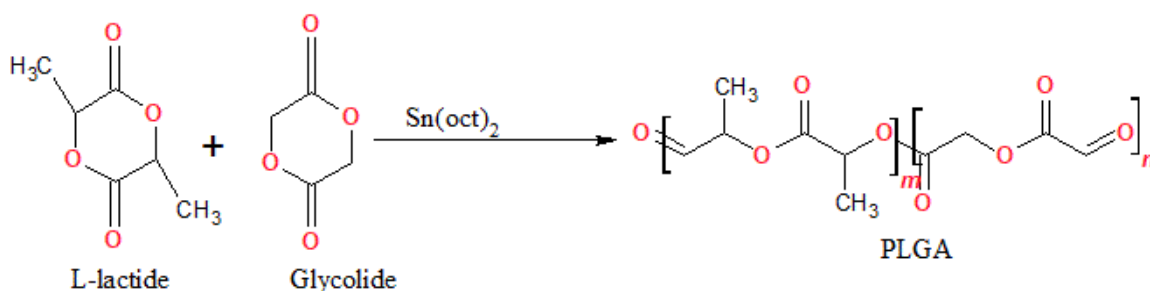
Figure 2.5: *Schematic representation; synthesis of PLGA (**n** represents the number of lactic acid units while **m** represents the number of glycolic acid units).*

2.4.2 Chemistry

The physiochemical properties of PLGA provide it with the ability to entrap hydrophilic drugs and deliver them at the required site. Formulations with PLGA may therefore control drug release rate and increase drug absorption; a feature which may be employed to minimize drug-related adverse effects.[60] The two monomers, poly lactic acid (PLA) and poly glycolic acid (PGA) differ in composition: PLA has an asymmetric α-carbon which is described as the *D* or *L* form while PGA lacks any asymmetric α-carbon. The different forms of PLA are poly *D*-lactic acid (PDLA) and poly *L*-lactic acid (PLLA). PLA has a methyl group in its structure which makes it hydrophobic in nature. This polymer can be manufactured from the two isomers, PDLA and PLLA. The inactive racemic mixture, *D*-lactic acid, is transparent and amorphous in nature due to the irregular distribution of the *D* and *L* units whereas the optically active *L*-lactic acid is semi-crystalline in nature.[61,62] The disordered nature of PLA's polymer chains also permits it to form crystalline (PLLA) or amorphous (PDLA) structures, while its similitude, PGA, lacks any methyl side groups, hence its ability to form highly crystalline structures.[58] This crystallinity is however lost in PLGA copolymers. Amorphous PLGA copolymers are best suited for applications in drug delivery as discussed by Gilding and Reed (1979), reason being that amorphous PLGA provides

a homogenous dispersion of the active pharmaceutical ingredient (API) in the polymer matrix. In the preparation of PLGA using *L*-lactic acid with glycolic acid of 25-70%, the copolymer produced is amorphous. For an amorphous *D*-lactic acid, the ratio of glycolic acid extends from 0-70%; hence the preference for using *D*-lactic acid in the composition of PLGA as compared to the *L*-isomer lactic acid.[61]

As earlier mentioned, PLA is more hydrophobic and is always in a greater percentage in PLGA formulations than glycolic acid. Therefore, a lactide-rich PLGA composition implies that the co-polymer will be hydrophobic. A hydrophobic polymer will absorb less water and will subsequently degrade slowly due to hydrolysis. Studies have shown that PLGA formulations with a ratio of PLA (50):PGA (50) are an exception to this rule, being found to have the fastest degradation rate and shortest half-life.[58,60] This ratio is the most frequently used in preparations. Other ratios of PLGA such as 85:15 and 75:25 have also been used to deliver various drugs such as paclitaxel and rifampicin, while the 50:50 ratio has been used for folic acid delivery. The proportion or molar ratio of each polymer in a PLGA co-polymer therefore influences the rate at which the encapsulated drug is released.[58,63,64]

2.4.3 The effect of particle size and size distribution

The spherical shape and narrow distribution of the polymer play a very important role in the controlled release of an encapsulated drug from the polymer matrix in the body.[65] Interaction and adhesion of the nanoparticles with the cells are largely influenced by the shape and sizes of the nanoparticles. Morphology and porosity also influence the concentration and rate of drug release from the polymer.[66] The morphology of the particles is influenced by properties such as composition, molecular weight, synthesis conditions and chemical structure of the polymer.[65,67] The direct correlation between these parameters and particle morphology have however not

been sufficiently studied, leading to many research areas. Some postulated mechanisms of how particles pass through the gastrointestinal and physiological barriers include:

1. Endocytosis: The uptake of particles is mainly through absorption by the intestinal enterocytes *via* endocytosis. This process mainly absorbs particles < 500 nm.

2. Paracellular passage: The extremely small size of the nanoparticles enables them to knead between intestinal epithelial cells, mainly particles with a size < 50 nm.

3. Lymphatic passage: Particles < 5 µm are mainly absorbed by microfold cells in Peyer's patches of the intestinal tract. Peyer's patches are small masses of lymphatic tissue normally found in the small intestine, which function to prevent growth of pathogenic bacteria and also monitors bacteria population in the intestine.[68] Lymphatic passage in Peyer's patches has been demonstrated by Jani *et al* where particles with mean diameters between 50 and 100 nm were proven to have a higher uptake rate in a rat's intestine compared to larger particles.[69] It was observed that after the administration of equal doses, 26% of the 100 nm and 34% of the 50 nm were detected in gut-associated lymphoid tissues and the intestinal mucosa. With nanoparticle sizes less than 500 nm, only 10% of the particles were detected in intestinal tissues, and particle sizes greater than 1 µm exhibited low uptake and were exclusively found in Peyer's patches. Particle sizes greater than 3 µm were occasionally found in the follicle-associated epithelia.[69,70] The smallest capillaries in the body range between 5 and 6 µm in diameter; therefore, particle distribution in the bloodstream should

be targeted below 5 µm. Care should also be taken to ensure that such particles

do not aggregate.

Several advantages are inherent in the production of nanoparticles with small

sizes. One advantage of making such small nanoparticles (less than 220 nm) is

that they can be easily sterilized by filtration because bacteria and viruses are

larger.[67] Figure 2.6 presents the different nanoparticle size ranges with examples

of various materials that can easily attain such sizes, along with examples of bio-

nanoparticles.
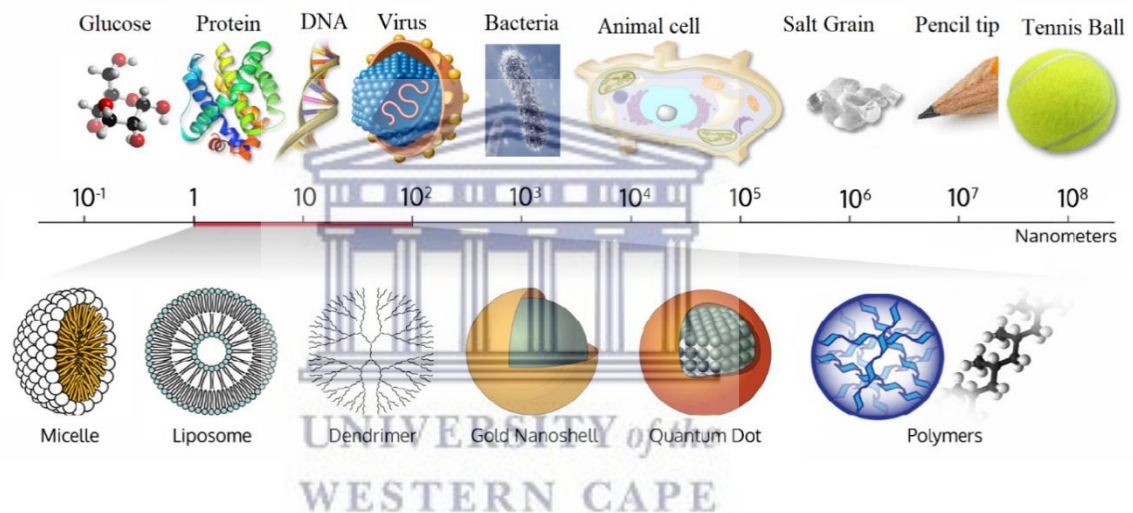
Figure 2.6: *Schematic representation of bio-nanoparticles and nanoparticle sizes (nanometer scale) (Wich Research Lab, 2018)*

2.4.4 Degradation

The degradation of PLGA is not confined to its surface. In an aqueous environment,

PLGA undergoes heterogeneous or bulk erosion. Four distinctive steps – *viz*

hydration, initial degradation and progressive degradation, and solubilization, can be

experienced during PLGA degradation. [64]

2.4.4.1 Hydration

The amorphous region of the polymer is penetrated by water. This disrupts forces such

as hydrogen bonds and weak van der Waals forces, resulting in a decrease in the

polymer's glass transition temperature (Tg).[64]

27

2.4.4.2 Initial degradation

The molecular weight of the polymer decreases, and cleavage of the covalent bonds occurs.

2.4.4.3 Progressive degradation

The degradation process is auto-catalyzed by the carboxyl end groups. This is because of the hydrolytic reactions taking place, hence cleavage of the backbone covalent bonds leading to loss of mass and integrity.

2.4.4.4 Solubilization

The cleaved fragments of the polymer are further cleaved to smaller molecules that are soluble in an aqueous environment. The end products after degradation are lactic acid and glycolic acid (Figure 2.7). These monomers are metabolized and eliminated *via* the Krebs cycle as water and carbon dioxide, [71,72] hence produce minimal, if any, systemic toxicity in the body. Figure 2.7 hydrolysis of PLGA shows how the copolymer is broken down into glycolic acid and lactic acid.
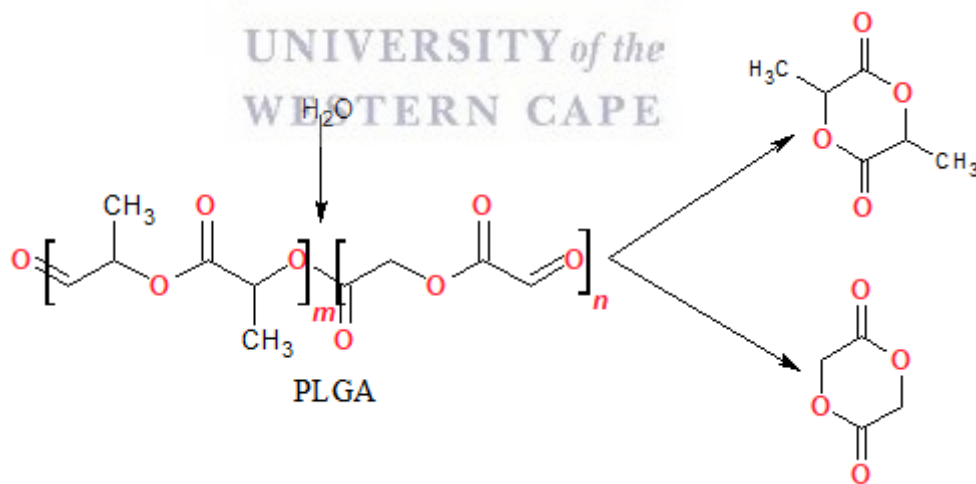
Figure 2.7: *Hydrolysis of PLGA*

The proportion of each monomer in the co-polymer (PLGA) affects its overall physicochemical properties and its ability to undergo degradation. Factors such as mechanical strength, molecular weight, swelling behavior, characteristics of the

surrounding medium, stereochemistry, end-group functional groups chemical derivation and co-polymer composition, also affect the polymer's capacity to undergo hydrolysis to its original monomers, lactic acid and glycolic acid. [60]

2.4.5 Polymer composition

The ratio of lactic acid to glycolic acid in PLGA is very important for control of the degradation process. Lactic acid is more hydrophobic than glycolic acid; this entails that a lactide-rich PLGA will absorb water more slowly and degrade more slowly compared to a glycolic-rich PLGA.

2.4.5.1 Stereochemistry

The degradation process of PLGA is greatly affected to a certain degree by the *D*- and *L*- forms of PLA. This is because water penetration of the *L*- form is slower compared to the *D*- form, hence a faster degradation of the *D*-form.[73]

2.4.5.2 Functional group

The terminal functional group affects the physicochemical properties of PLGA to an extent. *In vivo* studies have shown that an ester-terminated PLGA's degradation time can be delayed for about four to six weeks compared to an acid-terminated PLGA of the same composition and molecular weight. [73]

2.4.5.3 Chain length

Chain length is a very important consideration in the choice of a polymer. The polymer's degradation speed and its physical strength are influenced by the molecular weight of the polymer. It has been shown that increasing the molecular weight of the polymer from 10 to 100 kDa increases the degradation rate of the polymer from weeks to months. [74,75]

2.4.5.4 Chemical derivation

The hydrophobicity of PLGA can be decreased by attaching a hydrophilic moiety (hydroxyl group). A mixture of PLGA and the hydroxyl moiety exhibits a stronger affinity for water than PLGA without a hydroxyl moiety.[76,77]

2.4.5.5 Characterization of the surrounding medium

The medium surrounding the polymer also influences the degradation process. As an example, autocatalysis can be initiated or experienced in an acidic environment; thus, the degradation process is accelerated in acidic conditions compared to non-acidic environments.[78]

2.4.6 Mechanism of drug release

A series of rate limiting steps are involved in the release of a drug from a polymer until exhaustion. There are a few different mechanisms by which an encapsulated drug can be released from the polymer (Figure 2.8). These mechanisms include erosion, degradation of the polymer matrix, diffusion, solvent penetration and polymer swelling. A combination of all these mechanisms may sometimes be involved in the release of drug from the polymer; with different mechanisms occurring at different time intervals.[79]
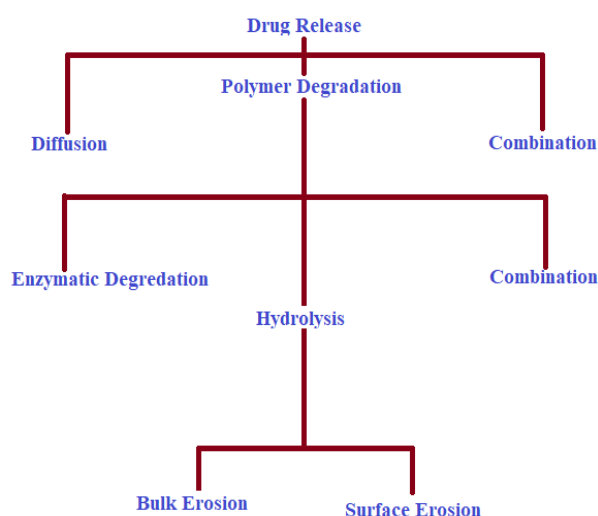
Figure 2.8: Possible mechanisms of drug release from PLGA (Lanao et al., 2013)[79]

With advances made in nanotechnology, several studies have been employed using non-polymeric or polymeric nano-carriers (e.g., micelles or encapsulation into nano conjugates)[80-83] as a means of resolving some of the earlier-mentioned disadvantages associated with the use of these APIs (TDF and AZT). Nanoparticles are advantageous as delivery vehicles; they provide a large surface area to volume ratio and are biomimetic.[84-86] They have been used to enhance oral bioavailability of several drug classes that have low solubility, chemical instability and poor permeation.

Looking at literature, several attempts have been employed by various authors demonstrating the preparations of AZT and TDF into nanoparticles, these authors had one goal which was to optimize the delivery and use of these APIs using PLGA while employing various methods for such formulations. Some of such studies include but are not limited to the following (Table 2.5)

31

Table 2.5: Studies performed by various authors on TDF and AZT involving the use of PLGA nanoparticles

Author and Year of publication	Study	Method	PLGA ratio	Objectives	Particle size
Shailender et al., 2017	Tenofovir disoproxil fumarate loaded PLGA nanoparticles for enhanced oral absorption: Effect of experimental variables and in vitro, ex vivo	Nanoprecipitation	50:50	To develop PLGA based TDF nanoparticles with the goal of minimum particle size and maximum entrapment efficiency for oral absorption	218 nm
Destache et al., 2016	Topical Tenofovir Disoproxil Fumarate Nanoparticles Prevent HIV-1 Vaginal Transmission in a Humanized Mouse Model	Oil-in-water (O/W) emulsion-solvent evaporation	75:25	To improve TDF efficacy in vaginal gel	148.6 nm
Tyo et al., 2017	Multipurpose Tenofovir Disoproxil Fumarate Electrospun Fibers for the Prevention of HIV-1 and HSV-2 Infections In Vitro	Electrospun	50:50	Create electrospun fibers to provide sustained release and in-vitro protection against HIV	1.7-2.0 nm
Peter Christoper et al., 2014	Formulation and optimization of coated PLGA–Zidovudine nanoparticles using factorial design and in vitro in vivo evaluations to determine brain targeting efficiency	Oil-in-water (O/W) emulsion-solvent evaporation	50:50	Develop tween 80 coated AZT loaded PLGA nanoparticles to archive good concerntration of drug in the brain	56-93 nm
Dalpiaz et al., 2013	Development and characterization of PLGA nanoparticles as delivery systems of a prodrug of zidovudine obtained by its conjugation with ursodeoxycholic acid	Nanoprecipitation	Not mentioned	Develop solid-lipid microparticles as a carrier system for nasal administration of AZT	6.77-16.66 µm
Sankar et al., 2012	Formulation and In-vitro Evaluation of Zidovudine-Lamivudine Nanoparticles	Emulsion Polymerization method	50:50	Prepare lower doses of lamivudine Nps to improve BA and minimize drug related side effects	58-224 nm
Jadhav et al., 2013	Development and characterization of gelatin based nanoparticles for targeted delivery of zidovudine.	Two step desolvation technique	Not mentioned	Develop and evaluated AZT loassed gelatin Nps by simple desolvation method and further couple it with mannose	394-797.2 nm
Mandal et al., 1996	Preparation of biodegradable microcapsules containing zidovudine (AZT) using solvent evaporation technique	Solvent evaporation	50:50	Improve the encapsulation efficiency of AZT in PLGA by modifying the secondary aqueous phase	8-8µm

The distinct difference in the studies performed by the above-mentioned authors was their formulation method and the polymer ratio used for the preparation of the nano-formulations (Table 2.5). Each author used a unique approach to increase the encapsulation efficiency to get better nanoparticle uptake such as coating the nanoparticles (Peter Christoper *et al.*, 2014) or even using conjugates (Dalpiaz *et al.*, 2013) etc.

This study shares similarities such as the objective of improving the encapsulation of the APIs, use of PLGA 50:50 ratio used by several of the authors in Table 2.5 and optimizing the delivery of AZT and TDF for the management of HIV using PLGA. However, this study focused on developing a method (modified version of the double emulsion water-in-oil-in-water solvent evaporation/diffusion method) different from those mentioned above which aimed to produce small nanoparticles to facilitate an increase in absorption in the intestines and lymphatic system, thereby increasing bioavailability with increased encapsulation efficiency. The study also makes use of another PLGA ratio (85:15) to compare similarities and differences of AZT and TDF nano-complexes using both ratios.

Chapter 3 presents the methodology for the research. It provides details of the various steps taken to prepare the nano-formulation, characterize the formulations and comparatively test the release profiles.

Bibliography

1. De Clercq, E., (2004). 'Antiviral drugs in current clinical use', *Journal of Clinical Virology*, 30(2), pp.115-133.

2. Carten, M., Aquilante, C., Anderson, P., Wolfe, P., King, T., Delahunty, T., Bushman, L., and Fletcher, C., (2007). 'The Effect of Lopinavir/Ritonavir on the Renal Clearance of Tenofovir in HIV-infected Patients', *Clinical Pharmacology & Therapeutics*, 83(2), pp.265-272.

3. Ristig, M., Crippin, J., Aberg, J., Powderly, W., Lisker-Melman, M., Kessels, L., and Tebas, P., (2002). 'Tenofovir Disoproxil Fumarate Therapy for Chronic Hepatitis B in Human Immunodeficiency Virus/Hepatitis B Virus–Coinfected Individuals for Whom Interferon-α and Lamivudine Therapy Have Failed', *The Journal of Infectious Diseases*, 186(12), pp.1844-1847.

4. Karageorgopoulos, D., (2015). 'Hepatitis C in human immunodeficiency virus co-infected individuals: Is this still a "special population"?', *World Journal of Hepatology*, 7(15), p.1936-1952.

5. Kearney, B. P., Flaherty, J. F., and Shah, J., (2004). 'Tenofovir Disoproxil Fumarate', *Clinical Pharmacokinetics*, 43(9) pp. 595–612.

6. Tong, L., Phan, T. K., Robinson, K. L., Babusis, D., Strab, R., Bhoopathy, S., Hidalgo, I. J., Rhodes, G. R., and Ray, A. S., (2007). 'Effects of human immunodeficiency virus protease inhibitors on the intestinal absorption of Tenofovir Disoproxil Fumarate in vitro', *Antimicrobial Agents and Chemotherapy*, 51(10), pp. 3498–3504.

7. Yoshigae, Y., Imai, T., Aso, T., and Otagiri, M., (1998). 'Species differences in the disposition of propranolol prodrugs derived from hydrolase activity in intestinal mucosa', *Life Sciences*, 62(14), pp. 1231–1241.

8. Calcagno, A., Gonzalez de Requena, D., Simiele, M., D'Avolio, A., Tettoni, M., Salassa, B., Orofino, G., Bramato, C., Libanore, V., Motta, I., Bigliano, P., Orsucci, E., Di Perri, G., and Bonora, S., (2013). 'Tenofovir Plasma Concentrations According to Companion Drugs: a Cross-Sectional Study of HIV-Positive Patients with Normal Renal Function', *Antimicrobial Agents and Chemotherapy*, 57(4), pp.1840-1843.

9. Hall, A. M., Hendry, B. M., Nitsch, D., and Connolly, J. O., (2011). 'Tenofovir-Associated kidney toxicity in HIV-infected patients: A review of the evidence', *American Journal of Kidney Diseases*, 57(5), pp. 773–780.

10. Hall, A. M., Bass, P., and Unwin, R. J., (2013). 'Drug-induced renal Fanconi syndrome', *QJM: An International Journal of Medicine,* 107(4), pp. 261–269.

11. Woodward, C., Hall, A., Williams, I., Madge, S., Copas, A., Nair, D., Edwards, S., Johnson, M., and Connolly, J., (2009). 'Tenofovir-associated renal and bone toxicity', *HIV Medicine*, 10(8), pp. 482–487.

12. Pubchem (2016). 'Tenofovir Disoproxil Fumarate', [online] available at: *https://pubchem.ncbi.nlm.nih.gov/compound/6398764,* [Accessed 24 March 2016)].

13. De Clercq, E., (2005). 'Antiviral drug discovery and development: Where chemistry meets with biomedicine', *Antiviral Research*, 67(2), pp. 56–75.

14. Cihlar, T., Ho, E. S., Lin, D. C., and Mulato, A. S., (2001). 'human renal organic anion transporter 1 (hoat1) and its role in the nephrotoxicity of antiviral nucleotide analogs', *Nucleosides, Nucleotides and Nucleic Acids*, 20(4-7), pp. 641–648.

15. Kohler, J., Hosseini, S., Green, E., Abuin, A., Ludaway, T., Russ, R., Santoianni, R., and Lewis, W., (2011). 'Tenofovir renal proximal tubular

toxicity is regulated By OAT1 and MRP4 transporters', *Laboratory Investigation*, 91(6), pp.852-858.

16. Izzedine, H., Hulot, J., Villard, E., Goyenvalle, C., Dominguez, S., Ghosn, J., Valantin, M., Lechat, P., and Deray, A., (2006). Association betweenABCC2Gene Haplotypes and Tenofovir-Induced Proximal Tubulopathy. *The Journal of Infectious Diseases*, 194(11), pp.1481-1491.

17. Izzedine, H., Launay-Vacher, V., and Deray, G., (2005). 'Antiviral Drug-Induced Nephrotoxicity', *American Journal of Kidney Diseases*, 45(5), pp.804-817.

18. Imaoka, T., Kusuhara, H., Adachi, M., Schuetz, J. D., Takeuchi, K., and Sugiyama, Y., (2006). 'Functional involvement of Multidrug resistance-associated protein 4 (MRP4/ABCC4) in the renal elimination of the antiviral drugs Adefovir and Tenofovir', *Molecular Pharmacology*, 71(2), pp. 619–627.

19. Côté H.C., Magil, A.B., Harris, M., Scarth, B.J., Gadawski, I., Wang, N., Yu, E., Yip B., Zalunardo, N., Werb, R., Hogg, R., Harrigan, PR., Montaner, J.S., (2006). 'Exploring mitochondrial nephrotoxicity as a potential mechanism of kidney dysfunction among HIV-infected patients on highly active antiretroviral therapy', *Antivir Ther*, 11(0), pp.79–86.

20. Lewis, W., Day, B., and Copeland, W., (2003). 'Mitochondrial toxicity of NRTI antiviral drugs: an integrated cellular perspective', *Nature Reviews Drug Discovery*, 2(10), pp.812-822.

21. Tanji, N., Tanji, K., Kambham, N., Markowitz, G., Bell, A., and D'Agati, V., (2001). 'Adefovir nephrotoxicity: Possible role of mitochondrial DNA depletion', *Human Pathology*, 32(7), pp.734-740.

22. Aperis, G., Paliouras, C., Zervos, A., Arvanitis, A., and Alivanis, P., (2011). 'Lactic acidosis after concomitant treatment with metformin and tenofovir in a patient with HIV infection', *Journal of Renal Care*, 37(1), pp.25-29.

23. Lewis, W., and Dalakas, M. C., (1995). 'Mitochondrial toxicity of antiviral drugs', *Nature Medicine*, 1(5), pp. 417–422.

24. Scruggs, E. R., and Dirks Naylor, A. J., (2008). 'Mechanisms of Zidovudine-Induced Mitochondrial toxicity and Myopathy', *Pharmacology*, 82(2), pp. 83–88.

25. FDA (2017). 'HIV/AIDS Historical Time Line 1981-1990', [online] available at: *https://www.fda.gov/ForPatients/Illness/HIVAIDS/History/ucm151074.htm*, [Accessed 7 Mar. 2017].

26. Stephan, C., Dauer, B., Khaykin, P., Stuermer, M., Gute, P., Klauke, S., and Staszewski, S. (2009). 'Quadruple Nucleos(t)ide reverse Transcriptase inhibitors-only regimen of Tenofovir plus Zidovudine/Lamivudine/Abacavir in heavily Pre-Treated HIV-1 infected patients: Salvage therapy or backbone only?', *Current HIV Research*, 7(3), pp. 320–326.

27. Newell, M. L., (2006). 'Current issues in the prevention of mother-to-child transmission of HIV-1 infection', *Transactions of the Royal Society of Tropical Medicine and Hygiene*, 100(1), pp. 1–5.

28. Chitnis, S., Mondal, D., and Agrawal, K. C., (2002). 'Zidovudine (AZT) treatment suppresses granulocyte-monocyte colony stimulating factor receptor type alpha (GM-CSFRα) gene expression in murine bone marrow cells', *Life Sciences*, 71(8), pp. 967–978.

29. PubChem (2016) '*C10H13N5O4*', [online] available at:

    https://pubchem.ncbi.nlm.nih.gov/compound/35370 [Accessed 27 March

    2016].

30. Bozzi, A., D'Andrea, G., and Brisdelli, F., (2008). 'AZT: An old drug with new

    perspectives', *Current Clinical Pharmacology*, 3(1), pp. 20–37.

31. Barbier, O., Turgeon, D., Girard, C., Green, M., D., Tephly, T. R., Hum, D. W.,

    (200). '3'-azido-3'-deoxythimidine (AZT) is glucuronidated by human UDP-

    glucuronosyltransferase 2B7 (UGT2B7) drug metabolism and disposition', *the*

    biological fate of chemicals; 28(5), pp. 497–502.

32. Kumar, P., Lakshmi, Y. S., C., B., Golla, K., and Kondapi, A. K., (2015).

    'Improved safety, Bioavailability and Pharmacokinetics of Zidovudine through

    Lactoferrin Nanoparticles during oral administration in rats', *plos one*, 10(10),

    pp. 140-399.

33. Lewis, W., Gonzalez, B., Chomyn, A., and Papoian, T., (1992) 'Zidovudine

    induces molecular, biochemical, and ultrastructural changes in rat skeletal

    muscle mitochondria', *Journal of Clinical Investigation*, 89(4), pp. 1354–1360.

34. Koduri, P. R., Parekh S., (2003). 'Zidovudine-related anemia with

    reticulocytosis'. *Ann Intern Med* 82(3), pp. 184–185.

35. Kuksal, A., Tiwary, A. K., Jain, N. K., and Jain, S., (2006). 'Formulation and in

    vitro, in vivo evaluation of extended- release matrix tablet of Zidovudine:

    Influence of combination of hydrophilic and hydrophobic matrix formers',

    AAPS PharmSciTech, 7(1), pp. E1–E9.

36. Kieburtz, K. D., Seidllin, M., Lambert, J. S., Dollis, R., Reichman, R., and

    Valentine, T., (1992) 'Extended follow-up of neuropathy in patients with AIDS

and AIDS related complex treated with dideoxyinosine', *J Acquir Immuno Defic Syndrom,* 5 (0), pp.60-64

37. Ganesh, S., Radhakrishnan, M., Ravi, M., Prasannakumar, B., and Kalyani, J., (2008). 'In vitro evaluation of the effect of combination of hydrophilic and hydrophobic polymers on controlled release zidovudine matrix tablets', *Indian Journal of Pharmaceutical Sciences*, 70(4), p. 461

38. Siegel, R. A., Rathbone M. J., (2012) 'Overview of Controlled Release Mechanisms'. In: Siepmann J., Siegel R., Rathbone M. (eds) Fundamentals and Applications of Controlled Release Drug Delivery. Advances in Delivery Science and Technology. Springer, Boston, MA pp.19-43

39. Tiwari, G., Tiwari, R., Bannerjee, S., Bhati, L., Pandey, S., Pandey, P., and Sriwastawa, B., (2012). 'Drug delivery systems: An updated review', *International Journal of Pharmaceutical Investigation,* 2(1), p.2.

40. Celia, C., Ferrati, S., Bansal, S., van de Ven, A., Ruozi, B., Zabre, E., Hosali, S., Paolino, D., Sarpietro, M., Fine, D., Fresta, M., Ferrari, M., and Grattoni, A. (2013). 'Sustained Zero-Order Release of Intact Ultra-Stable Drug-Loaded Liposomes from an Implantable Nanochannel Delivery System', *Advanced Healthcare Materials*, 3(2), pp.230-238.

41. Lee, P., and Good, W., (1987). 'Controlled-release technology', Washington, DC: American Chemical Society, chapter 1, pp.1–13.

42. Jain, T., Morales, M., Sahoo, S., Leslie-Pelecky, D. and Labhasetwar, V., (2005). 'Iron Oxide Nanoparticles for Sustained Delivery of Anticancer Agents', *Molecular Pharmaceutics*, 2(3), pp.194-205.

43. Quevedo, M. A., Nieto, L. E., and Briñón, M. C., (2011) 'P-glycoprotein limits the absorption of the anti-HIV drug zidovudine through rat intestinal

segments', *European Journal of Pharmaceutical Sciences*, 43(3), pp. 151–159.

44. Panhard, X., Legrand, M., Taburet, A., Diquet, B., Goujard, C., and Mentré, F., (2007). 'Population pharmacokinetic analysisof lamivudine, stavudine and zidovudine in controlled HIV-infected patients on HAART', *European Journal of Clinical Pharmacology*, 63(11), pp.1019-1029.

45. Boudinot, F., Schinazi, R., Gallo, J., Mcclure, H., Anderson, D., Doshi, K., Kambhampathi, P. and Chu, C., (1990). '3′-Azido-2′, Polymeric systems for controlled drug release'3′-Dideoxyuridine (AzddU): Comparative Pharmacokinetics with 3′-Azido-3′-Deoxythymidine (AZT) in Monkeys', *AIDS Research and Human Retroviruses*, 6(2), pp. 219-228.

46. Dalakas, M. C., Illa, I., Pezeshkpour, G. H., Laukaitis, J. P., Cohen, B., and Griffin, J. L., (1990). 'Mitochondrial Myopathy caused by long-term Zidovudine therapy', *New England Journal of Medicine'*, 322(16), pp. 1098–1105.

47. Masanés, F., Barrientos, A., Cebrián, M., Pedrol, E., Miró, O., Casademont, J. and Grau, J.M., (1998). 'Clinical, histological and molecular reversibility of zidovudine myopathy', *Journal of the Neurological Sciences*, 159(2), pp. 226–228.

48. Arnaudo, E., Shanske, S., DiMauro, S., Schon, E. A., Moraes, C. T., and Dalakas, M., (1991). 'Depletion of muscle mitochondrial DNA in AIDS patients with zidovudine-induced myopathy', *The Lancet*, 337(8740), pp. 508–510.

49. Martin, J. L., Brown, C. E., Matthews-Davis, N., and Reardon, J. E., (1994). 'Effects of antiviral nucleoside analogs on human DNA polymerases and mitochondrial DNA synthesis', *Antimicrobial Agents and Chemotherapy*, 38(12), pp. 2743–2749.

50. Lynx, M. D., and McKee, E. E., (2006). '3′-Azido-3′-deoxythymidine (AZT) is a competitive inhibitor of thymidine phosphorylation in isolated rat heart and liver mitochondria', *Biochemical Pharmacology*, 72(2), pp. 239–243.

51. Rylova, S. N., Albertioni, F., Flygh, G., and Eriksson, S., (2005). 'Activity profiles of deoxynucleoside kinases and 5′-nucleotidases in cultured adipocytes and myoblastic cells: Insights into mitochondrial toxicity of nucleoside analogs', *Biochemical Pharmacology*, 69(6), pp. 951–960.

52. Lebrecht, D., Deveaud, C., Beauvoit, B., Bonnet, J., Kirschner, J., and Walker, U.A., (2007). 'Uridine supplementation antagonizes zidovudine-induced mitochondrial myopathy and hyperlactatemia in mice', *Arthritis & Rheumatism*, 58(1), pp. 318–326.

53. Yamaguchi, T., Katoh, I., and Kurata, S., (2002). 'Azidothymidine causes functional and structural destruction of mitochondria, glutathione deficiency and HIV-1 promoter sensitization', *European Journal of Biochemistry*, 269(11), pp. 2782–2788.

54. De la Asunción, J. G., del Olmo, M. L., Sastre, J., Millán, A., Pellín, A., Pallardó, F.V. and Viña, J., (1998). 'AZT treatment induces molecular and ultrastructural oxidative damage to muscle mitochondria. Prevention by antioxidant vitamins', *Journal of Clinical Investigation*, 102(1), pp. 4–9.

55. Georges, B., Galland, S., Rigault, C., Borgne, F. L., and Demarquoy, J., (2003). 'Beneficial effects of l-carnitine in myoblastic C2C12 cells', *Biochemical Pharmacology*, 65(9), pp. 1483–1488.

56. Dalakas, M. C., Leon-Monzon, M. E., Bernardini, I., Gahl, W.A., and Jay, C.A., (1994). 'Zidovudine-induced mitochondrial myopathy is associated with

muscle carnitine deficiency and lipid storage', *Annals of Neurology*, 35(4), pp. 482–487.

57. Semino-Mora, M. C., Leon-Monzon, M. E., and Dalakas, M. C., (1994). 'Effect of L-Carnitine on the Zidovudine-Induced Destruction of Human Myotubes. Part I: L-Carnitine Prevents the Myotoxicity of AZT in Vitro', *Lab Invest*, 71(1), pp. 102–112.

58. Makadia, H. K., and Siegel, S. J., (2011). 'Poly Lactic-co-Glycolic acid (PLGA) as biodegradable controlled drug delivery carrier', *Polymers*, 3(4), pp. 1377–1397.

59. Astete, C. E., and Sabliov, C. M., (2006). 'Synthesis and characterization of PLGA nanoparticles', *Journal of Biomaterials Science, Polymer Edition*, 17(3), pp. 247–289.

60. Athanasiou, K., (1996). 'Sterilization, toxicity, biocompatibility and clinical applications of polylactic acid/ polyglycolic acid copolymers', *Biomaterials*, 17(2), pp. 93–102.

61. Gilding, D. K., and Reed, A. M., (1979). 'Biodegradable polymers for use in surgery—polyglycolic/poly(actic acid) homo- and copolymers: 1', *Polymer*, 20(12), pp. 1459–1464.

62. Jain, R. A., (2000). 'The manufacturing techniques of various drug loaded biodegradable poly(lactide-co-glycolide) (PLGA) devices', *Biomaterials*, 21(23), pp. 2475–2490.

63. Wu, X. S., and Wang, N., (2001). 'Synthesis, characterization, biodegradation, and drug delivery application of biodegradable lactic/glycolic acid polymers. Part II: Biodegradation', *Journal of Biomaterials Science, Polymer Edition*, 12(1), pp. 21-34

64. Uhrich, K. E., Cannizzaro, S. M., Langer, R. S., and Shakesheff, K. M., (1999). 'Polymeric systems for controlled drug release', *Chemical Reviews*, 99(11), pp. 3181–3198.

65. Feczkó, T., Tóth, J., and Gyenis, J., (2008). 'Comparison of the preparation of PLGA–BSA nano- and microparticles by PVA, poloxamer and PVP', *Colloids and Surfaces A: Physicochemical and Engineering Aspects*, 319(1-3), pp.188-195.

66. Uskokovic, D., and Stevanovic, M., (2009). 'Poly(lactide-co-glycolide)-based Micro and Nanoparticles for the Controlled Drug Delivery of Vitamins', *Current Nanoscience*, 5(1), pp.1-14.

67. Yin Win, K., and Feng, S., (2005). 'Effects of particle size and surface coating on cellular uptake of polymeric nanoparticles for oral delivery of anticancer drugs', *Biomaterials,* 26(15), pp.2713-2722.

68. Jani, P., Halbert, G., Langridge, J., and Florence, A., (1989). 'The Uptake and Translocation of Latex Nanospheres and Microspheres after Oral Administration to Rats', *Journal of Pharmacy and Pharmacology*, 41(12), pp. 809-812.

69. Jani, P., Halbert, G., Langridge, J., and Florence, A., (1990). 'Nanoparticle Uptake by the Rat Gastrointestinal Mucosa: Quantitation and Particle Size Dependency', *Journal of Pharmacy and Pharmacology,* 42(12), pp.821-826.

70. Gref, R., Minamitake, Y., Peracchia, M., Trubetskoy, V., Torchilin, V., and Langer, R., (1994). 'Biodegradable long-circulating polymeric nanospheres', *Science*, 263(5153), pp.1600-1603.

71. Prabha, S., Zhou, W. Z., Panyam, J., and Labhasetwar, V., (2002). 'Size-dependency of nanoparticle-mediated gene transfection: Studies with

fractionated nanoparticles', *International Journal of Pharmaceutics*, 244(1-2), pp. 105–115.

72. Panyam, J., Dali, M. M., Sahoo, S. K., Ma, W., Chakravarthi, S. S., Amidon, G. L., Levy, R. J. and Labhasetwar, V., (2003). 'Polymer degradation and in vitro release of a model protein from poly(d, l-lactide-co-glycolide) nano- and microparticles', *Journal of Controlled Release*, 92(1-2), pp. 173–187.

73. Tracy, M., (1999). Factors affecting the degradation rate of poly(lactide-co-glycolide) microspheres in vivo and in vitro. *Biomaterials*, 20(11), pp.1057-1062.

74. Yoshioka, T., Kawazoe, N., Tateishi, T., and Chen, G., (2008). 'In vitro evaluation of biodegradation of poly(lactic-co-glycolic acid) sponges', *Biomaterials*, 29(24-25), pp. 3438–3443.

75. Félix Lanao, R. P., Leeuwenburgh, S. C. G., Wolke, J. G. C., and Jansen, J. A., (2011). 'In vitro degradation rate of apatitic calcium phosphate cement with incorporated PLGA microspheres', *Acta Biomaterialia*, 7(9), pp. 3459–3468.

76. Leemhuis, M., van Nostrum, C. F., Kruijtzer, J. A. W., Zhong, Z. Y., ten Breteler, M. R., Dijkstra, P. J., Feijen, J., and Hennink, W. E., (2006). 'Functionalized Poly(α-hydroxy acid)s via ring-opening polymerization: Toward hydrophilic polyesters with pendant Hydroxyl groups', *Macromolecules*, 39(10), pp. 3500–3508.

77. Leemhuis, M., Kruijtzer, J. A. W., van Nostrum, C. F., and Hennink, W. E., (2007). 'In Vitro Hydrolytic degradation of Hydroxyl-Functionalized Poly(α-hydroxy acid)s', *Biomacromolecules*, 8(9), pp. 2943–2949.

78. Pamula, E., and Menaszek, E., (2007). 'In vitro and in vivo degradation of poly (l-lactide-co-glycolide) films and scaffolds', *Journal of Materials Science: Materials in Medicine*, 19(5), pp. 2063–2070.

79. Lanao, R. P. F., Jonker, A. M., Wolke, J. G. C., Jansen, J. A., van Hest, J. C. M., and Leeuwenburgh, S. C. G., (2013). 'Physicochemical properties and applications of Poly(lactic-co-glycolic acid) for use in bone regeneration', *Tissue Engineering Part B: Reviews*, 19(4), pp. 380–390.

80. Calogeropoulou, T., Detsi, A., Lekkas, E., and Koufaki, M., (2003). 'Strategies in the Design of Prodrugs of Anti-HIV Agents', *Current Topics in Medicinal Chemistry*, 3(13), pp.1467-1495.

81. Parang, K., Wiebe, L., and Knaus, E., (2000). 'Novel Approaches for Designing 5-O-Ester Prodrugs of 3-Azido-2, 3-dideoxythymidine (AZT)', *Current Medicinal Chemistry*, 7(10), pp.995-1039.

82. Phillips, N., and Tsoukas, C., (1991). 'Liposomal encapsulation of AZT results in decreased bone marrow toxicity and activity against Murine Acquired Immunodeficiency Syndrome (MAIDS)-induced immunosuppression', *International Journal of Immunopharmacology*, 13(6), pp. 811.

83. Kaur, C., Nahar, M., and Jain, N., (2008). 'Lymphatic targeting of zidovudine using surface-engineered liposomes', *Journal of Drug Targeting*, 16(10), pp.798-805.

84. Goldberg, M., Langer, R., and Jia, X., (2007). 'Nanostructured materials for applications in drug delivery and tissue engineering', *Journal of Biomaterials Science, Polymer Edition*, 18(3), pp.241-268.

85. McNeil, S., (2011). 'Unique benefits of nanotechnology to drug delivery and diagnostics', *Methods in molecular biology*, (697), pp. 3–8.

86. Sanvicens, N., and Marco, M., (2008). 'Multifunctional nanoparticles – properties and prospects for their use in human medicine', *Trends in Biotechnology*, 26(8), pp. 425-433.

87. Wich Research Lab. (2018). 'Size-comparison-Bio-nanoparticles nanometer scale comparison nanoparticle size comparison nanotechnology chart ruler', [online] available at: http://www.wichlab.com/nanometer-scale-comparison-nanoparticle-size-comparison-nanotechnology-chart-ruler-2/, [Accessed 26 Jun. 2018].

88. Dalpiaz, A., Contado, C., Mari, L., Perrone, D., Pavan, B., Paganetto, G., Hanuskovà, M., Vighi, E., and Leo, E., (2013). 'Development and characterization of PLGA nanoparticles as delivery systems of a prodrug of zidovudine obtained by its conjugation with ursodeoxycholic acid', *Drug Delivery*, 21(3), pp.221-232.

89. Destache, C., Mandal, S., Yuan, Z., Kang, G., Date, A., Lu, W., Shibata, A., Pham, R., Bruck, P., Rezich, M., Zhou, Y., Vivekanandan, R., Fletcher, C., and Li, Q. (2016). 'Topical Tenofovir Disoproxil Fumarate Nanoparticles Prevent HIV-1 Vaginal Transmission in a Humanized Mouse Model', *Antimicrobial Agents and Chemotherapy*, 60(6), pp.3633-3639.

90. Jadhav, N., Nadaf, S., Tone, J. and Irny, P. (2013). 'Development and characterization of gelatin based nanoparticles for targeted delivery of zidovudine', *International Journal of Pharmaceutical Investigation*, 3(3), p.126.

91. Peter Christoper, G., Vijaya Raghavan, C., Siddharth, K., Siva Selva Kumar, M., and Hari Prasad, R., (2014). 'Formulation and optimization of coated PLGA – Zidovudine nanoparticles using factorial design and in vitro in vivo

evaluations to determine brain targeting efficiency', *Saudi Pharmaceutical Journal*, 22(2), pp.133-140.

92. Tyo, K., Vuong, H., Malik, D., Sims, L., Alatassi, H., Duan, J., Watson, W., and Steinbach-Rankins, J., (2017). 'Multipurpose tenofovir disoproxil fumarate electrospun fibers for the prevention of HIV-1 and HSV-2 infections in vitro', *International Journal of Pharmaceutics*, 531(1), pp.118-133.

93. Shailender, J., Ravi, P., Saha, P., Dalvi, A., and Myneni, S., (2017). 'Tenofovir disoproxil fumarate loaded PLGA nanoparticles for enhanced oral absorption: Effect of experimental variables and in vitro, ex vivo and in vivo evaluation', *Colloids and Surfaces B: Biointerfaces*, 158, pp.610-619.

UNIVERSITY *of the* WESTERN CAPE

CHAPTER 3: METHODOLOGY

This chapter gives a detailed account of the materials, methods and analytical techniques used in this study. A clear description of the analytical techniques and procedures used is provided in a chronological order.

3.1 MATERIALS

3.1.1 The active pharmaceutical ingredients (APIs)

Tenofovir disoproxil fumarate (TDF) and Zidovudine (AZT) powders, batch numbers BTDFVSP14261113 and ZD3911013, respectively, were donated by Aspen Pharmacare, South Africa.

3.1.2 Chemicals and reagents

Polymer: Resomer® RG 504 ester terminated, lactide: glycolide 50:50, M_w 38,000-54,000 g/mol (*Sigma-Aldrich, Germany*), Poly *D,L*-lactide-*co*-glycolide 85:15 ester terminated, M_w 50,000-75,000 g/mol (*Sigma-Aldrich, Germany*), HPLC grade methanol, HPLC grade orthophosphoric acid, sodium dihydrogen orthophosphate dehydrate (*Sigma-Aldrich, South Africa*), D-α-tocopherol polyethylene glycol succinate (TPGS) (*Sigma-Aldrich, Germany*), gelatin, tween 80, ethyl acetate, acetone (*Sigma-Aldrich, South Africa*), phosphate buffer solution contents (sodium chloride, potassium chloride, disodium hydrogen phosphate, potassium dihydrogen phosphate), sodium hydroxide, and hydrochloric acid (*Sigma-Aldrich, South Africa*).

3.2 INSTRUMENTS

Homogenizer (*IKA® T18 digital Ultra-Turrax®, Germany*), sonicator (*Sonoplus HD GM 2070, Bandelin, Germany*), centrifuge (*Beckman Coulter Allegra® 64R, UK*), analytical balance (Mettler®, model P.E 6000*, USA*), infrared spectrophotometer (*Perkin-Elmer 100 FTIR* instrument fitted with UATR, controlled with Spectrum® software version 6.3.5, *USA*), differential scanning calorimeter (*Perkin-Elmer PC7 series, USA*),

thermogravimetric analyser (*Perkin-Elmer PC thermal system, USA*), scanning electron microscope (*Auriga HR-SEM F50, Zeiss, South Africa*), hot stage microscope *(a Linkam T95 temperature control unit connected to Linkam TH MS600*), ultra violet spectrophotometer (*Cintra 202, GBC Scientific Equipment, Australia),* deep freezer (*Sanyo, USA*), particle size analyzer (*Zeta sizer Nano ZS Malvern Instruments Ltd, UK*), lyophilizer (*Virtis freeze dryer freeze mobile model 125L; Malvern Instruments, Ltd, UK*), pH meter (*Basic 20, Lasec, South Africa*), vortexer (Benchmark Scientific Inc, BV1000 vortex mixer, Taiwan), micropipettes (*Eppendorf, Hamburg, Germany*), water purification system (*Milford, MA, USA*), bath sonicator (*Ultra-sonic Model 702, 100W, Voltage 2030V, LABOTEC, South Africa*), rotary evaporator (*Buchi, LABOTEC, South Africa*), orbital shaker- Incubator ES-80 (*Grant bio, monitoring and control laboratories, South Africa),* HPLC Column (Luna$^{®}$ C_{18} analytical column 250 x 4.6 mm, i.d 5µm), HPLC-system (*Agilent 1200 series)* fitted to a quaternary pump *(G1311A, Germany),* degassing system *(G1322A, Japan),* auto loading sampler *(G1329A, Germany),* Thermostat column compartment *(G13164, Germany),* diode array detector *(G1315B, Germany),* fluorescence detector *(G1521A Germany),* Agilent ChemStation software *(G2173-60101L, Germany),* analyte fraction collector *(G164C, Germany)*

3.3   IDENTIFICATION TECHNIQUES

Identification tests were performed on TDF, AZT, both ratios (50:50 and 85:15) of poly-lactic-co-glycolic acid (PLGA), physical mixtures of TDF with PLGA and physical mixtures of AZT with PLGA. Each API and each different polymer ratio were mixed in a ratio of 1:10 and triturated in a mortar with pestle to obtain uniform mixing. The resulting physical mixture was transferred into a vial for storage. Samples were withdrawn from the vial and analyzed using the following analytical techniques: Differential Scanning Calorimetry (DSC), Thermogravimetric Analysis (TGA), Fourier

Transform Infrared Spectroscopy (FT-IR) Hot Stage Microscopy (HSM) and Scanning electron microscopy (SEM).

3.3.1 Differential Scanning Calorimetry (DSC)

A Perkin Elmer DSC 7 series connected to a Perkin Elmer thermal analysis controller TAC7/DX and a Perkin Elmer gas station were used for this stage of the study. About 1.5 - 3 mg of sample was weighed into an aluminum pan which was then crumpled. An empty aluminum pan of the same dimensions was crumpled and used as a reference. The samples were analyzed at an increasing temperature rate of 10°C/min, with nitrogen as the carrier gas at a flow rate of 20 ml/min. Samples were heated over the temperature range, 30 - 460°C, and Pyris™ software was used to collect and analyze the data.

3.3.2 Thermogravimetric analysis (TGA)

The analysis was performed using a Perkin Elmer thermogravimetric analyzer *TGA 4000*, with the flow rate of nitrogen gas at 20 ml/min. An empty porcelain pan was tarred, the sample placed in the porcelain pan and the weight of the sample recorded. Samples were analyzed over a temperature range from 20 - 600°C at an increasing temperature rate of 10°C per minute. Data was collected and analyzed using Pyris™ software.

3.3.3 Fourier Transform Infrared Spectroscopy (FT-IR)

FT-IR analyses of the nano-formulations were carried out for AZT and TDF nano-formulations made with PLGA (50:50 and 85:15) polymers, using a Perkin Elmer 100 FTIR spectroscope to confirm inclusion of the API's in the nano-formulation. All the spectra were collected using Spectrum® software version 6.3.5. The FT-IR spectra of the complexed formulations were compared to that of the APIs alone. Differences or changes in the characteristic bands of the complexed formulations such as

appearance, disappearance, variations in peak intensity, and shifts in wave number or broadening can be indicative of complex formation. The parameters mentioned above aid in understanding of the physical characteristics of drug/polymer interactions. The infrared absorption spectra were collected at 20°C from 4000 to 650 cm^{-1}.

3.3.4 Hot stage microscopy (HSM)

This is an analytical technique often used in collaboration with DSC to substantiate and elucidate the results obtained from DSC, hence confirming the thermal curves obtained in DSC analysis. A small amount of the nano-formulation was placed on a thin plate of glass and a small drop of silicon oil was used to lubricate the sample. Silicon is an inert element widely used in such procedures because of its lubricating properties and its relatively high thermal stability. Samples were heated at a temperature increase rate of 10°C per minute over a temperature range from 20°C to 200°C. This temperature range included the anticipated melting points of the APIs and polymers. The samples were observed under a microscope and images taken at specific temperature intervals for analyses. The heater was connected to an *Olympus US30* color video camera and the temperature control was a *Linkam TH MS600* connected to a T95 linkpad system controller. Images were recorded using the stream Essential® software.

3.3.5 Scanning Electron Microscopy (SEM)

Scanning electron microscopy is a high-resolution imaging analytical technique used to take images of nanoparticles. It is generally used to the study particle morphology of the sample. The sample is bombarded by a beam of electrons from thermal emission. The interaction between the atoms from the sample and the electrons released presents various signals that in turn provide information on the particle's morphology and composition.

The freeze-dried nano-complexes were smeared on a double-sided carbon adhesive tape attached to an aluminum stub and dried in a fume hood. Thereafter, the nano-complex formulation was coated with gold palladium using an Emitech™ K550X (England) sputter coater. Images were captured using an Auriga™ F50 high resolution scanning electron microscope (HR-SEM), at 6.6 mm and a voltage of 5 kV as the operating parameters.

3.4 Formulation process

3.4.1 Preparation of nanoparticles

The preparation of nanoparticles was achieved using a modified version of the double emulsion (water-in-oil-in-water) solvent evaporation and diffusion method.[1] The steps taken to modify and brief discussion to this eventual method can be seen in Appendix A and B.

Final preparation method of AZT-PLGA and TDF-PLGA nanoparticles

A specified amount (100 mg) of the polymer was weighed on an electrical balance. The weighed polymer was placed in a 50 ml test tube and dissolved in 10 ml mixture of ethyl acetate (EA)/acetone (ACE) at a ratio of 4:1, at which the ensuing mixture had small particle sizes (appendix A). The solution was vortexed to form a polymer solution. An aqueous phase was prepared by dissolving 5 mg of the active pharmaceutical ingredient (API) in 1 ml of distilled water containing 0.2% w/v tween 80. This mixture was vortexed to ensure that the drug was properly dissolved. The aqueous phase was dropped gradually into the polymer solution and homogenized for 2 minutes at a speed of 5000 revolutions per minute (rpm) in an ice bath. The mixture was then probe-sonicated at 87 W energy output (amplitude 87%) for 30 seconds to produce the primary water-in-oil emulsion (w/o). The primary emulsion was poured gradually into 40 ml of water containing 0.12% *D*-α-tocopherol polyethylene glycol succinate (TPGS). This was homogenized for 3 minutes at a speed of 12000 rpm, then

probe sonicated at 87 W energy output (amplitude 87%) for 2 minutes under an ice bath to produce the double water-in-oil-water emulsion (w/o/w). The w/o/w emulsion was solidified by pouring the emulsion into 40 ml of water containing 0.2% tween 80 while stirring at a speed of 800 rpm. The organic phase was evaporated using the rotary evaporator at a speed of 400 rpm and temperature of 34 ± 1°C for 8 hours.

3.4.1.1 Separation of nanoparticles

After evaporation of the organic solvents (EA and ACE), the nanoparticles were collected by pouring the emulsion into 40 ml oak ridge centrifuge tubes. The tubes were then centrifuged at a speed of 16500 rpm at 1°C for 1 hour. The supernatant was discarded while ensuring minimum disruption of the nanoparticles (pellets). The contents of the centrifuge tubes were collected into one test tube and washed three times with distilled water.

3.4.1.2 Lyophilization of nanoparticles

The method of choice to remove water from the nanoparticles was lyophilization, also known as freeze drying. Freeze drying aided in overcoming drug leakage and stability issues such as aggregation. The nanoparticles, after collection and washing, were frozen at a temperature of -70°C and lyophilized to remove the water content. They were then stored between 2 and 8°C and subsequently characterized.

The percentage recovery of the formulated particles was calculated from Equation 3.1 below:

$$Nanoparticle\ recovery\ (\%) = \frac{mass\ of\ nanoparticles\ recovered}{mass\ of\ PLGA\ and\ drug\ used} x100$$

Equation 3.1

3.4.2 Nanoparticle characterization

The following analyses were performed to characterize the nanoparticles: particle size analysis, polydispersity index, zeta potential, percentage yield, drug entrapment efficiency, encapsulation efficiency, FT-IR spectra, DSC, TGA, SEM, and HSM.

3.4.2.1 Particle size analysis

Dynamic light scattering was used to determine the nanoparticle sizes. The instrument used was a Nano-Zeta sizer from Malvern®. This measures the intensity of scattered light which occurs because of the particles being in constant Brownian motion, thus providing information about the particulate system. The particle sizes of nano-formulations are very important because they determine parameters like physicochemical properties, biological half-life and distribution in the body.[2] The measure for width of size distribution is called polydispersity index (PDI). Values of PDI closer to one (1) indicate a heterogeneous distribution of nanoparticles while values closer to zero (0) indicate a homogenous distribution of nanoparticles. Particles sizes were measured immediately after formulation. After collection and after freeze-drying, a small sample of the freeze-dried nano-complex was dispersed in water as a medium, placed in cuvettes (zeta cells) and analyzed. The measurements were all taken in triplicate and the average reported.

3.4.2.2 Zeta potential

Following collection of the pellets and freeze drying, the Malvern® Zetasizer was used to determine the charge of the particles immediately after solvent evaporation. A small sample of the freeze-dried nano-complex was dispersed in distilled water, vortexed and analyzed. The measurements were done in triplicate and the average and standard deviation (SD) values reported.

3.4.2.3 Percentage yield
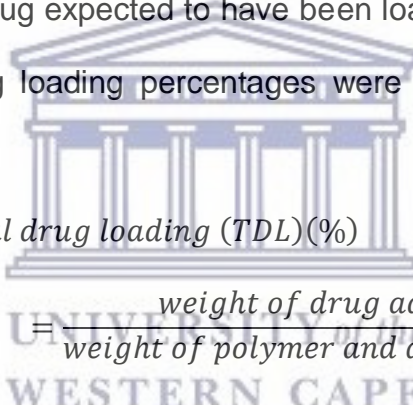
This is the total amount of nanoparticles recovered after formulation expressed as a percentage. The formulated powder was weighed immediately after retrieval from the freeze drier. The percentage yield of TDF-PLGA and AZT-PLGA complexes was determined using the following formula:

$$Percentage\ yield(\%) = \frac{Mass\ of\ nanoparticles\ recovered}{Mass\ of\ PLGA, drug\ and\ excipients\ used\ in\ formulation} x100$$

Equation 3.2

3.4.2.4 Drug entrapment efficiency

Drug entrapment efficiency is defined as the ratio of the drug loaded in the polymer to the theoretical amount of drug expected to have been loaded. To determine this, the theoretical and actual drug loading percentages were first determined, using the following equations:

$$Theoretical\ drug\ loading\ (TDL)(\%)$$
$$= \frac{weight\ of\ drug\ added}{weight\ of\ polymer\ and\ drug\ added} x\ 100$$

Equation 3.3

$$Actual\ drug\ loading\ (\%) = \frac{weight\ of\ drug\ in\ nanoparticles}{weight\ of\ nanoparticles} x100$$

Equation 3.4

$$Drug\ Entrapment\ efficiency(\%) = \frac{actual\ drug\ loading}{theoretical\ drug\ loading} x100$$

Equation 3.5

3.4.2.5 Encapsulation efficiency

The encapsulation efficiency determines the actual amount of drug found in the nano-complex after formulation. The amount of drug encapsulated in the polymer was

determined by dissolving 5 mg of the nano-complex in 0.5 ml of ethyl acetate (in a 5 ml Eppendorf tube) with vortexing. The ethyl acetate was evaporated, and 3 ml of phosphate buffer solution (PBS) was added to the Eppendorf tube. The tube was vortexed, and the contents centrifuged at a speed of 10000 rpm for 15 minutes. Thereafter, the supernatant was collected, and the absorbance measured using the UV-spectrometer and HPLC-DAD system. The concentration of the drug in that sample was determined by extrapolating the absorbance value from a calibration plot of the APIs. The amount of API and the encapsulation efficiency was determined using the equation below:

$$Encapsulation\ efficiency(\%)$$

$$= \frac{total\ amount\ of\ drug\ in\ the\ yield}{amount\ of\ drug\ added\ during\ encapsulation} x100$$

Equation 3.6

3.4.2.6 *In-vitro* drug release

In-vitro release kinetics of TDF and AZT loaded nanoparticles was carried out as described by Cetin, Atila and Kadioglu (2010) with slight modifications (sample and separate method).[3,4] Weighed amounts (20 mg) of each nano-formulation was suspended in an Eppendorf tube with 1 ml of PBS (at either pH 1.2 or pH 7.4) containing 0.1% v/v of tween 80. The sample was incubated at 37°C in a shaker incubator at 120 rpm. Subsequently, 0.5 ml was withdrawn with replacement at predetermined time intervals. The isolated samples were centrifuged at 15000 rpm for 20 minutes and the supernatant analyzed for drug content by the UV-spectrometry and HPLC-DAD methods described below.

3.5 Preparation of phosphate buffer solution (PBS) - pH 7.4 and pH 1.2 for *in-vitro* release

3.5.1 Ingredients

Sodium chloride = 8 g

Potassium chloride = 0.2 g

Disodium hydrogen phosphate = 1.44 g

Potassium dihydrogen phosphate = 0.24 g

The above ingredients were weighed and ground in a mortar with pestle. Thereafter, the ingredients were dissolved in 800 ml of distilled water, while being stirred with a stirring rod to ensure that the solutes dissolved completely. The pH of the solution was measured and adjusted to 1.2 and 7.4 using 0.1 M hydrochloric acid. The final volume was adjusted to 1000 ml with distilled water. The solution was autoclaved to denature any microbiological contamination, allowed to cool and stored for use.

3.6   Method development

Two analytical techniques, that is, ultra violet-visible (UV-VIS) spectrometry and high-performance liquid chromatography with diode array detection (HPLC-DAD), were used to characterize and quantify the amount of drug encapsulated and released from the formulated nanoparticles.

3.6.1   Validation of UV-VIS spectrophotometer analytical procedure for quantification of tenofovir disoproxil fumarate and zidovudine in nanoparticles.

Preparation of standards for calibration

A stock solution was prepared by dissolving 5 mg of API in 100 ml of PBS (at pH 1.2 or pH 7.4) with sonication (for 1 minute) to ensure complete dissolution of the API. Serial dilutions of the stock solution were performed to obtain working solutions of 2 µg/ µl, 4 µg/ µl, 6 µg/ µl, 8 µg/ µl, 10 µg/ µl and 12 µg /µl.

Determination of range and linearity

The absorbance of each API at a specific concentration was measured using the UV-VIS spectrophotometer. A measured amount (3 ml) of PBS solution (at pH 1.2 or pH 7.4) was placed into two quartz cuvettes. The cuvettes were scanned at the lambda

57

maxima (λ_{max}) of 260 nm and 266 nm for TDF and AZT, respectively, and the blank readings were recorded. Thereafter the absorbance of the APIs at different concentrations was measured. Readings were done in triplicate and the mean values were used to plot a graph of absorbance *versus* concentration (µg/ ml).

Determination of accuracy and precision

The accuracy and precision for the method employed in this study was determined thus: three concentrations of the API within the calibration range were used. The precision was determined by inter-day (intermediate precision) and intraday (reproducibility) analyses. Over a period of three consecutive days, the samples were assayed and the average readings, standard deviation and % relative standard deviation (RSD) were calculated and compared to determine the inter-day and intra-day precision. The accuracy of the method was determined by taking the mean of the measurements and calculating the percentage difference. All readings and measurements were done in triplicate.

3.6.2 Validation of HPLC-DAD analytical procedure for quantification of tenofovir disoproxil fumarate and zidovudine in PLGA-nanoparticles

Chromatographic conditions

The mobile phase comprised of HPLC grade methanol and phosphate buffer (sodium dihydrogen orthophosphate, 10 mM, at pH 5.0) mixed in a ratio of 70:30 (v/v), and operated at a flow rate of 0.8 ml/min. A Luna C_{18} column (250 mm x 4.6 mm, 5 µm) was used as the stationary phase. Samples were analyzed over a range of wavelengths from 254 to 266, with the specific wavelengths of interest at 260 nm and 266 nm for TDF and AZT, respectively.

Preparation of standards for calibration

Stock solutions were prepared by dissolving 4 mg of the API (TDF and AZT) in 200 ml of PBS (at pH 1.2 or pH 7.4) with sonication (for 1 minute) to ensure complete

dissolution of the API. Serial dilutions of the stock solution were performed to obtain working solutions of 0.02 µg/ µl, 0.04 µg/ µl, 0.06 µg/ µl, 0.08 µg/ µl, 0.10 µg/ µl and 0.12 µg/ µl.

Optimization of chromatographic conditions

The HPLC method was based on the method developed by Bhavsar et *al* (2012) with some slight modification to the flow rate. The final chromatographic conditions consisted of 70 volumes of methanol to 30 volumes of PBS (pH adjusted to 5.0 using 10% orthophosphoric acid) as the mobile phase. A flow rate of 0.8 ml/min was observed to be suitable for elution for both APIs within 10 minutes, with good symmetrical peaks that were acceptable when compared to those obtained at a flow rate of 1.0 ml/min. The final column temperature was set to 40°C.

Method validation

The method for simultaneous estimation of TDF and AZT separately in PLGA nanoparticles was developed and validated in accordance with the International Conference on Harmonisation (ICH) guidelines [5,6].

Linearity

The linearity of the method was assessed by preparing standard solutions of different concentrations (0.02 µg/ µl to 0.12 µg/ µl) for both TDF and AZT in different PBS solutions (at pH 1.2 or pH 7.4). Each preparation and measurement was done in triplicate as per the chromatographic conditions mentioned above. The obtained peaks were used to plot a graph of absorbance against concentration to obtain a calibration graph for each compound (API).

Sensitivity

The sensitivity of the analytical method was evaluated by determining the limits of detection (LOD) and the limits of quantification (LOQ) in accordance with the ICH guidelines.

Determination of accuracy and precision

The accuracy and precision for this method was determined by taking sample readings in triplicate. Three concentrations of the API within the calibration range were used, and the precision was determined by inter-day (intermediate precision) and intraday (reproducibility) analyses. Over a period of three consecutive days, the samples were assayed and the average values, standard deviation and % relative standard deviation (RSD) were compared to determine the inter-day and intra-day precision. The accuracy of the method was determined by the percentage difference of the mean measurements.

3.7   Assessment of loaded nanoparticle stability

Following preparation, the nano-formulations were stored between 2 and 8°C. The particle size, zeta potential and PDI were assessed over a period of 10, 20, 30, 60 and 90 days after formulation.

Chapter 4 will follow with the results obtained during formulation and characterization of the formulated nanoparticles using TDF, PLGA 50:50 and PLGA 85:15.

Bibliography

1. Liu, J., Qiu, Z., Wang, S., Zhou, L., and Zhang, S., (2010). 'A modified double-emulsion method for the preparation of daunorubicin-loaded polymeric nanoparticle with enhancedin vitroanti-tumor activity', *Biomedical Materials*, 5(6), pp. 065002.

2. Blanco, E., Shen, H., and Ferrari, M., (2015). 'Principles of nanoparticle design for overcoming biological barriers to drug delivery', *Nature Biotechnology*, 33(9), pp.941-951.

3. Cetin, M., Atila, A., and Kadioglu, Y., (2010). 'Formulation and In vitro Characterization of Eudragit® L100 and Eudragit® L100-PLGA Nanoparticles Containing Diclofenac Sodium', *AAPS Pharm SciTech*, 11(3), pp.1250-1256.

4. Agnihotri, S., and Vavia, P., (2009). 'Diclofenac-loaded biopolymeric nanosuspensions for ophthalmic application', *Nanomedicine: Nanotechnology, Biology and Medicine*, 5(1), pp.90-95.

5. Bhavsar, D., Patel, B. and Patel, C. (2012). 'RP-HPLC method for simultaneous estimation of tenofovir disoproxil fumarate, lamivudine, and efavirenz in combined tablet dosage form', *Pharmaceutical Methods*, 3(2), pp.73-78.

6. Bapatla J, Sai N, Hari HD, Theja K, Ramalingam P, Reddy Y., (2011). 'Validated HPTLC Method for the Determination of Tenofovir as Bulk Drug and in Pharmaceutical Dosage Form', *Pelagia Res Library*, (2), pp.163–8.

CHAPTER 4: RESULTS AND DISCUSSION FOR TENOFOVIR DISOPROXIL

FUMARATE LOADED NANOPARTICLES

This chapter presents the results and discussion obtained when Tenofovir disoproxil fumarate (TDF) was investigated. Emphasis is placed on the different ratios of poly-lactic-co-glycolic acid (PLGA 50:50 and 85:15) used in this study.

4.1   Introduction

The objective of this study was two-fold of which the formulation of TDF as a nanoparticle presented the following specific sub-objectives:

- ❖ to characterize TDF and PLGA (50:50 and 85:15)

- ❖ to formulate non-covalent complexes of TDF with PLGA of different ratios (50:50 and 85:15);

- ❖ to characterize and compare physicochemical properties of the formulated complexes using various analytical techniques;

- ❖ to compare the pharmaceutical properties (i.e. particle size, stability and *in-vitro* release) of both formulations (TDF-PLGA 50:50 and TDS-PLGA 85:15) as a means of addressing some of the limitations associated with optimal oral delivery of TDF (i.e. low permeability, low bioavailability).

4.2   Characterization of TDF and PLGA (50:50 and 85:15)

Prior to formulation of the nanoparticle proper, TDF and two PLGA ratios (PLGA 50:50 and PLGA 85:15) were characterized individually, and in combination as a physical mixture (TDF-PLGA 50:50 and TDF-PLGA 85:15). Data from the characterization studies are as follows:

4.2.1   Fourier-transform infra-red (FT-IR) spectroscopy

Infra-red spectroscopy (FTIR) was used to identify the functional groups in TDF, PLGA (50:50 and 85:15), and the TDF-PLGA (50:50 and 85:15) formulations. This was done

to identify the susceptibility of these functional groups to chemical reactions *via* reduction in band intensities or complete disappearance of characteristic bands. The samples were also used as reference samples for assessment of the nano-formulation process. Figure 4.2 presents the spectra of TDF, PLGA 50:50, PLGA 85:15 and a combination of TDF-PLGA 50:50 and TDF-PLGA 85:15 physical mixtures. TDF was ground with each polymer separately to form the physical mixtures. The FTIR spectra of these mixtures were compared to those of the single component compounds (TDF, PLGA 50:50 and PLGA 85:15) to identify characteristic functional groups as a physical mixture, as well as the appearance of or disappearance of such functional groups in the combination (Figure 4.2 and Table C1.3 in appendix C).

TDF (Figure 4.2a) showed a characteristic peak band at 3459.12 cm^{-1}, attributed to the N-H stretching vibration bands of the amine group. The intensity bands at 2981.38 cm^{-1} and 2814.22 cm^{-1} were assigned to the hydroxyl (O-H) stretching, the band at 2081.44 cm^{-1} was attributed to the C=C, and the intensity bands at 1752.31 cm^{-1} and 1671.87 cm^{-1} were assigned to C=O. Figure 4.1a presents the structure of TDF.

The pure PLGA 50:50 (Figure 4.2b) showed characteristic peak bands at 2950.52 cm^{-1} which was attributed to the chelated O-H stretching vibrations. The peak band at 1750.32 cm^{-1} was attributed to the C=O stretching of the carbonyl group. The pure PLGA 85:15 (Figure 4.2c) also showed characteristic peak bands at 2996.25 cm^{-1} which was attributed to chelated O-H bridge stretching and 1746.64 cm^{-1} attributed to strong C=O stretching of the carbonyl group. Figure 4.1b below presents the structure of PLGA.
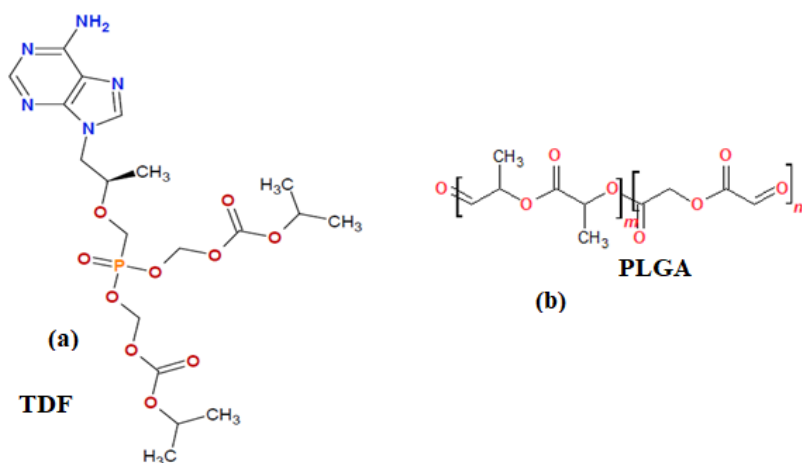
*Figure 4.1: Structure of (a) TDF and (b)PLGA (**n** represents the number of lactic acid units while **m** represents the number of glycolic acid units)*
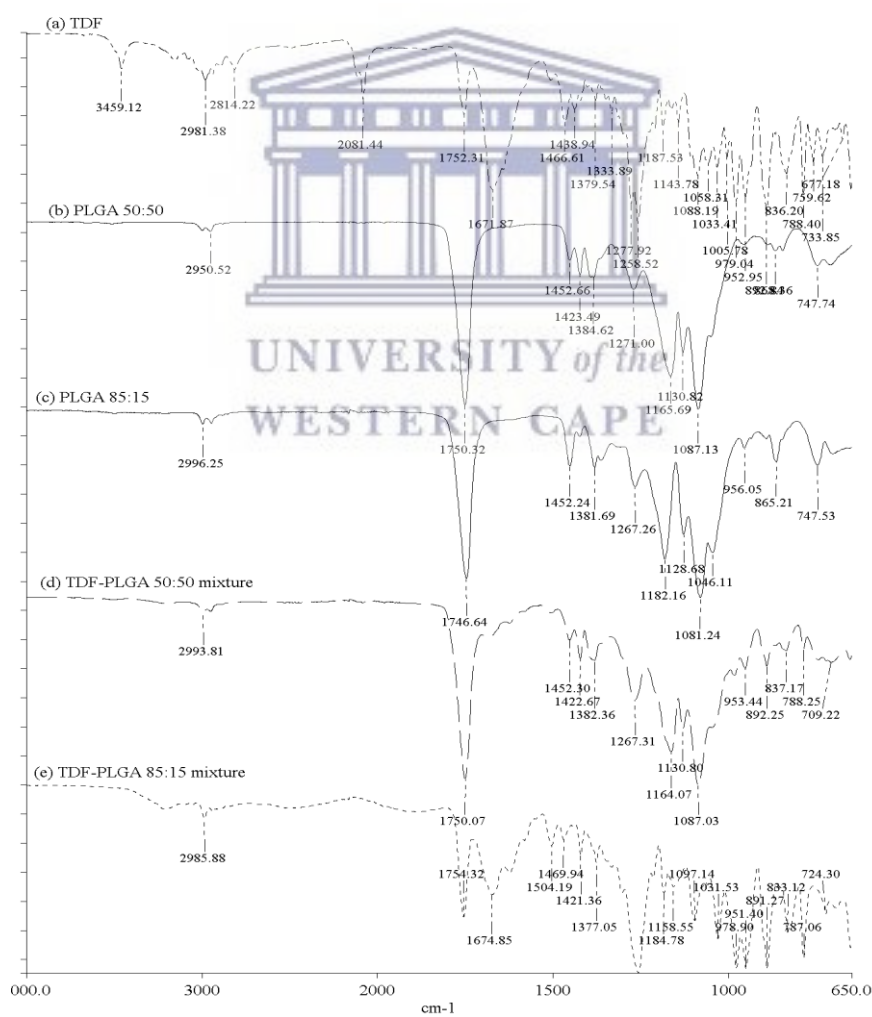
Figure 4.2: *FT-IR spectra of (a) TDF, (b) PLGA 50:50, (c) PLGA 85:15, (d) TDF-PLGA 50:50 physical mixture, (e) TDF-PLGA 85:15 physical mixture*

64

The FT-IR spectra of TDF-PLGA 50:50 and TDF-PLGA 85:15 physical mixtures (Figure 4.2d and Figure 4.2e, respectively) showed shifts in the characteristic peak bands of the components in the resulting physical mixture. TDF-PLGA 50:50 physical mixture (Figure 4.2d) showed characteristic peak bands at 2993.81 cm^{-1}, attributed to chelated O-H bridge stretching and at 1750.07 cm^{-1}, attributed to the C=O stretching vibration. The peaks at 3459.12 cm^{-1} 2814.22 cm^{-1} 2081.44 cm^{-1} and 1671.87 cm^{-1} had disappeared while the intensity of the peak at 1752.31 cm^{-1} had increased when compared to the parent AZT. On the other hand, TDF-PLGA 85:15 physical mixture (Figure 4.2e) also showed similar characteristic peak bands at 2985.88 cm^{-1} attributed to chelated O-H bridge stretching, and at 1754.32 cm^{-1} and 1674.85 cm^{-1}, both attributed to the C=O stretching vibration. The spectra also presented with peaks that had disappeared just like in AZT-PLGA 50:50 with the exception of the peak at 1671.87 cm^{-1} which was available but with decrease intensity and we also experienced a decrease in intensity for the peak at 1754.32 cm^{-1} when compared to the parent compounds.

Overall both physical mixtures showed slight shifts, disappearance, increase and decrease in intensity of characteristic peaks when compared to the parent compounds, thus indicating an interaction between the TDF and PLGA. A summary of the bands is in Table C1.3 in appendix C.

4.2.2 Hot stage microscopy (HSM)

The results presented below were obtained during sample analysis using hot stage microscopy (HSM). The compounds were analyzed individually (TDF, PLGA 50:50, PLGA 85:15) and in combination as a physical mixture of the polymer with TDF (mixed by grinding). The samples where heated up to a maximum temperature of 200°C at a temperature increase rate of 10°C per min.

Figure 4.3(a) shows images of TDF taken during HSM analysis. The melting of TDF commenced in the temperature range, 113°C to 118°C. At 120°C, the sample had completely melted, and at this temperature, bubbles were noticed. The appearance of bubbles could be because of gas (due to sublimation) accumulation between the glass slides (cover slide and sample holder). The results obtained from this analysis were in line with the certificate of analysis which indicated that the melting point of TDF was between 114°C and 118°C. The degradation of TDF started at about 180°C, observed by discoloration of the sample.
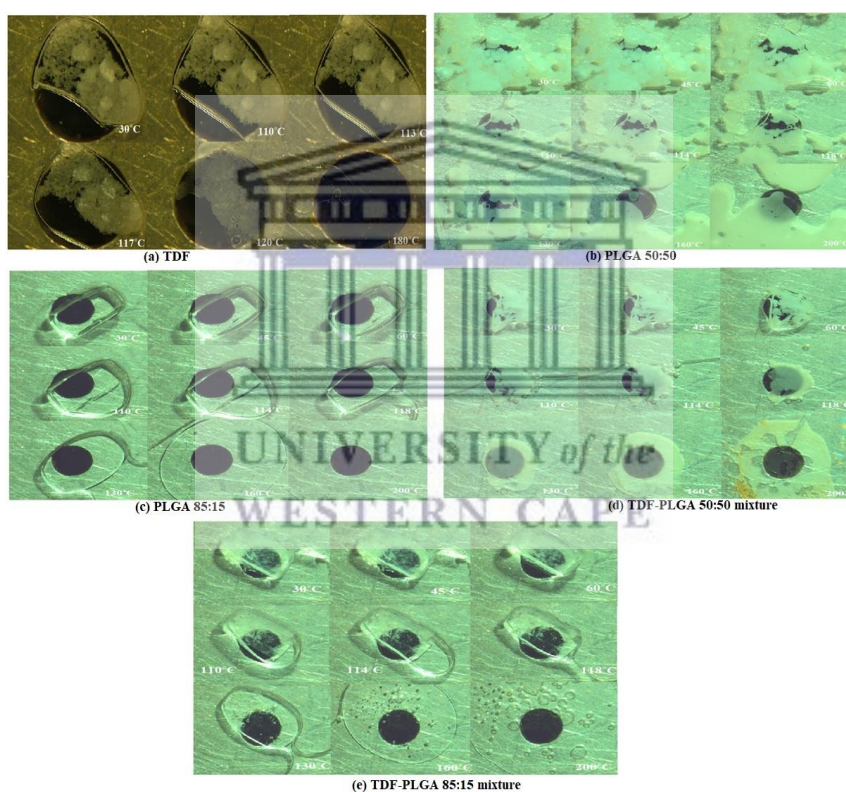
Figure 4.3: *HSM images of (a) TDF, (b) PLGA 50:50, (c) PLGA 85:15, (d) TDF-PLGA 50:50 physical mixture, and (e) TDF-PLGA 85:15 physical mixture*

The melting of PLGA 50:50 when analyzed using HSM is shown in Figure 4.3(b). Melting commenced at about 45°C; the sample gradually melted with no appearance of bubbles, an indication that no moisture was entraped in the samples. At temperatures above 60°C, the sample had passed its indicated glass transition

66

temperature, and appeared to be oily and viscous. There were however no visible signs of degradation (discolouration) even at temperatures up to 200°C.

Figure 4.3(c) presents HSM analysis of PLGA 85:15, with melting commencing at about 55°C. The sample gradually melted with no appearance of bubbles, like what was obtained with PLGA 50:50, also an indication that no moisture was entrapped in the samples. At temperatures above 60°C, the sample had passed its indicated glass transition temperature, and appeared to be oily and viscous. As happened with PLGA 50:50, the samples did not show any visible signs of degradation even at temperatures up to 200°C.

Figure 4.3(d) shows images from the HSM analysis of the polymer mixture (TDF-PLGA 50:50). Signs of melting were observed from temperatures around 56°C, with the appearance of bubbles at temperature changes between 110°C and 114°C. This was around the melting point of the API, confirming the presence of the API in the physical mixture. The appearance of the bubbles was also an indication of moisture entrapment between the slides covering the sample. The bubbles eventually disappeared, and signs of degradation such as browning of the sample appeared at a temperature of 160°C.

Figure 4.3(e) presents images from the HSM analysis of TDF-PLGA 85:15 physical mixture. Signs of sample melting were observed around 56°C, with the appearance of bubbles at temperatures between 110°C and 114°C. This was also around the melting point of TDF, confirming its presence in the physical mixture. The appearance of the bubbles was an indication of moisture being entrapped between the slides covering the sample, or fumes from the API melting. Unlike what was obtained with TDF-PLGA 50:50 physical mixture [Figure 4.3(d)] however, the bubbles did not disappear on

continued heating and instead grew bigger, indicating degradation. Another sign of degradation, browning of the sample, appeared at a temperature of 160°C. Given that the copolymers, PLGA 50:50 and PLGA 85:15, did not show any signs of degradation under HSM analyses [Figure 4.3 (b) and (c)] while TDF did, the presence of TDF in the physical mixture can be inferred from the degradation observed on HSM of TDF-PLGA 85:15.

4.2.3 Thermogravimetric analysis (TGA)

Changes in thermal stability, organic solvent evolution and the degradation of TDF, PLGA 50:50, PLGA 85:15, and a mixture(physical) of both polymers with TDF (mixed by grinding) was evaluated using TGA. Figure 4.4 shows the TGA curves obtained when the samples were analyzed. There was release of volatile substance from the samples and weight loss due to moisture was observed. The temperature at which mass loss began (T_{onset}°C) and ended (T_{endset}°C) as well as the temperature at which maximum mass loss occurred ($T_{deg.max.}$°C) were determined and are presented in Table C1.4 in appendix C.
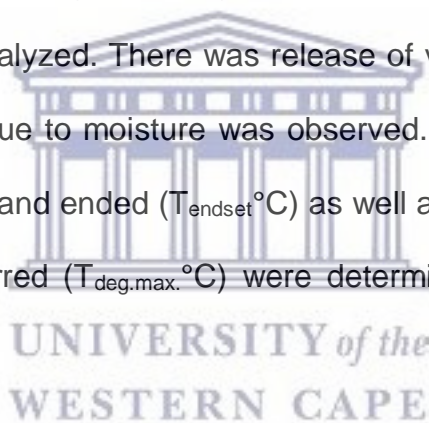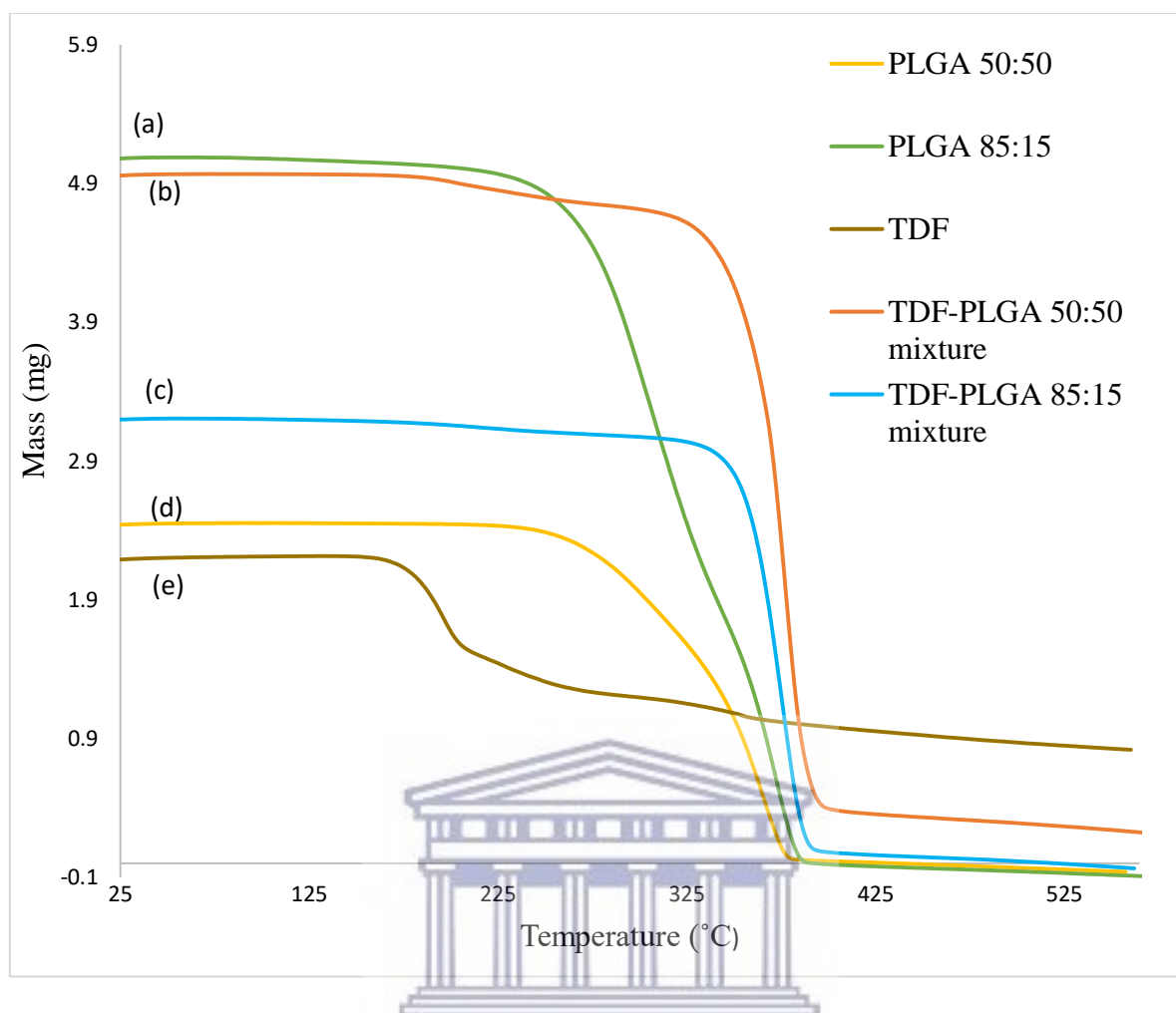
Figure 4.4: *TGA curves of (a) PLGA 85:15, (b) TDF-PLGA 50:50 physical mixture, (c) TDF-PLGA 85:15 physical mixture, (d) PLGA 50:50, and (e) TDF.*

Both polymers (PLGA 50:50 and 85:15) displayed two mass loss events associated with the degradation process of the polymer [Figure 4.4 (a) and (d)]. PLGA 50:50 had a first and second mass loss of about 30% and 68%, respectively, while PLGA 85:15 showed mass loss values of about 65% and 35%, respectively. When compared to each other, PLGA 50:50 did not obtain a 100% mass loss; it proceeded with a 2% inert residue. When the physical mixtures of TDF with PLGA 50:50 and TDF with PLGA 85:15 were analyzed, both samples showed a single mass loss event compared to the individual polymers and TDF [Figure 4.4 (b) and (c)]. The percentage mass loss for TDF-PLGA 50:50 and TDF-PLGA 85:15 were about 93% and 98%, respectively.

The T_{onset} values for TDF-PLGA 50:50 and TDF-PLGA 85:15 were at a lower temperature when compared to that of both polymers and higher than that of TDF alone (Table C1.4) in appendix C. The physical mixture of TDF and PLGA showed an overall increase in thermal stability when compared to the individual polymers and TDF[1]. The differences in the mass loss percentages in the polymers could be attributed to their differences in molecular mass and composition since each polymer has a different ratio of lactic and glycolic acid.

4.2.4 Differential Scanning Calorimetry (DSC)

Prior to formulation of the nanoparticles, the melting points of the samples were determined using DSC. Figure 4.5a shows the thermograms of PLGA 50:50 and PLGA 85:15; both co-polymers showed a single endothermic peak, indicating that the melting points for both polymers were at about 55.41°C and 45.84°C, respectively.

Figure 4.5b shows the DSC thermogram of TDF. Two endothermic peaks were observed, within the range of temperatures, 111°C-118°C; these peaks corresponded to the melting points of two different polymorphic forms of TDF, according to literature there are about three different polymorphic forms (A, B and I).[2,3] The first endothermic peak was because of polymorphic form I_{-1} melting, which was then followed by recrystallisation (an exothermic event) of the melted API into form I which presented with a melting peak of 118°C[2,4], thus both endothermic peaks can be attributed to the different forms of TDF.
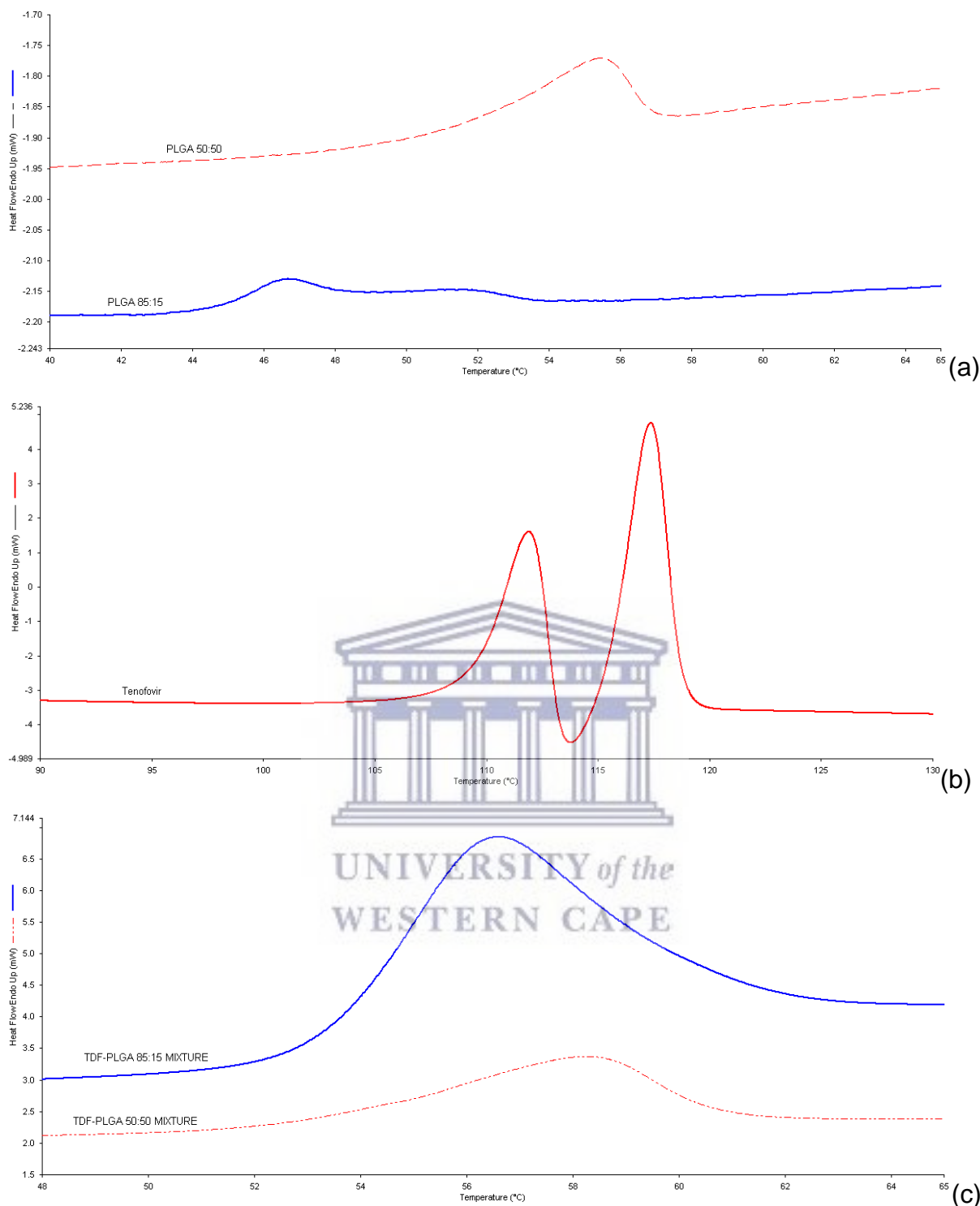
Figure 4.5: DSC thermograms of (a) PLGA (50:50 and 85:15), (b) Tenofovir disoproxil fumarate, (c) TDF-PLGA 50:50 and TDF-PLGA 85:15 physical mixtures.

Figure 4.5c presents thermograms of TDF when it was analyzed as a physical mixture

by grinding separately with PLGA 50:50 and PLGA 85:15. A single endothermic event

was observed for each sample, with highest peaks at 58.27°C and 56.51°C for TDF-

71

PLGA 50:50 and TDF PLGA 85:15 physical mixture, respectively. Comparing these peaks with PLGA alone, a slight shift of about 3-4°C can be observed. This indicates a slight increase in stability of the physical mixture, which might also indicate that there is some form of interaction taking place in the physical mixture.

4.3 Formulation and characterisation of TDF loaded nanoparticles

Figure 4.6 below shows diagrammatically each step in the formulation of TDF-loaded nanoparticles. Formulation was done using the water-in-oil-in-water double emulsion solvent evaporation and diffusion method by Liu *et al*., 2010 with modifications to decrease nanoparticle size and increase encapsulation efficiency.
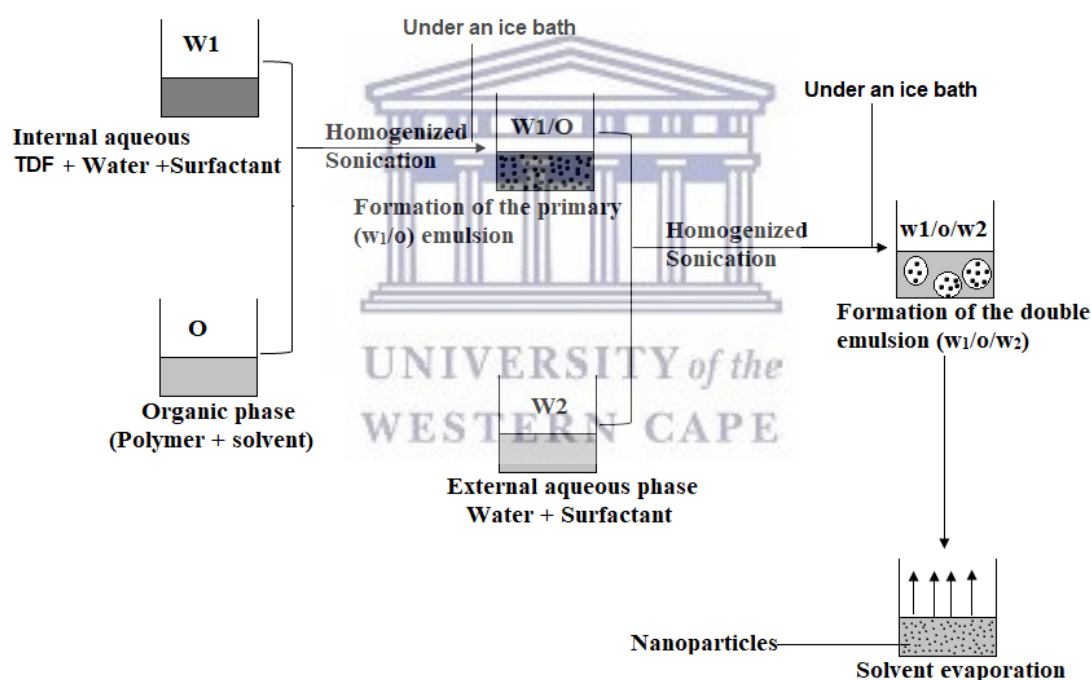
Figure 4.6: Schematic presentation of TDF-loaded nanoparticle formulation process.
After formulation, the loaded nanoparticles were freeze dried and characterized for particle size and distribution, surface morphology, zeta potential, percentage yield, drug entrapment and encapsulation efficiency.

4.3.1 Particle size and distribution (polydispersity index) PDI

The particle size distribution of the TDF-PLGA (50:50 and 85:15) loaded nanoparticles was determined immediately after formulation and evaporation of the organic solvents from the sample, using dynamic light scattering in the Malvern particle-sizing system. The mean particle sizes for TDF-PLGA 50:50 and TDF-PLGA 85:15 were found to be 117.3 ± 0.45 nm and 103.0 ± 1.62 nm, respectively. There was an increase in particle sizes after the TDF-PLGA (50:50 and 85:15) loaded nanoparticles were washed three times with distilled water. The average sizes after washing for TDF-PLGA 50:50 and TDF-PLGA 85:15 were found to be 153.2 ± 4.3 nm and 127 ± 2.32 nm, respectively. The increase in particle size (Table 4.1) could have resulted from particle aggregation after the surfactants and emulsifiers had been removed by the washing process.

Table 4.1: *Particle size distribution of TDF-loaded nanoparticles.*

Formulated nanoparticle	Particle size (nm)	
	Before wash	After wash
TDF-PLGA 50: 50	117.3 ± 0.45	153.2 ± 4.3
TDF-PLGA 85: 15	103.0 ± 1.62	127.0 ± 2.32

The particle size of formulated nanoparticles plays an important role in their therapeutic efficacy. The smaller the particle size, the higher the rate of particle absorption from the intestine into the blood stream.[5,6] Therefore, a high uptake of particles is expected from the formulation prepared, given the particle sizes obtained. The postulated mechanisms to show how particles pass through the gastrointestinal and physiological barriers highlights endocytosis as one of the mechanisms, for particles < 500 nm. It can therefore be seen that the sizes of TDF-PLGA 50:50 and TDF-PLGA 85:15 nanoparticles immediately after formulation (117.2 ± 2.33 nm and 103.0 ± 1.62 nm, respectively) and immediately after washing (153.2 ± 4.3 nm and 127.0 ± 2.32 nm, respectively) favors uptake *via* endocytosis. As such, it may be

inferred that the formulated nanoparticles would easily permeate physiological barriers to promote absorption.

Table 4.2: Polydispersity index of TDF-loaded nanoparticles.

Formulated nanoparticle	Polydispersity index	
	Before wash	After wash
TDF-PLGA 50: 50	0.160 ± 0.01	0.303 ± 0.06
TDF-PLGA 85: 15	0.152 ± 0.04	0.355 ± 0.01

The polydispersity index (PDI) values (Table 4.2) for TDF-PLGA (50:50) and TDF-PLGA (85:15) after formulation were found to be an average of 0.160 ± 0.01 and 0.152 ±0.07, respectively. These PDI values increased to 0.303 ± 0.06 and 0.355 ± 0.01 (Table 4.2) for TDF-PLGA 50:50 and TDF-PLGA 85:15, respectively, after washing of the loaded nanoparticles. These values are indicative of a homogenous distribution of the nanoparticles. PDI values between 0.1 and 0.4 are indicative of monodisperse samples; the nanoparticles are relatively of the same size, width and/or shape while PDI value greater than 0.5 indicate a polydispersed sample.[7] The increase in the PDI after washing of the pellets could be due to such pellets aggregating or coalescing after removal (washing) of the surfactants and emulsifiers, hence making the distribution a bit more heterogeneous post washing.

4.3.2 Evaluation of surface morphology of the nanoparticles

The morphology (shape and properties) of the nanoparticles was determined using high resolution scanning electron microscopy (HR-SEM). Blank nanoparticles were prepared and the morphology (shape and properties) of the nanoparticles were determined. Figure 4.7 [(a) and (b)] shows images of blank PLGA 50:50 and blank PLGA 85:15 nanoparticles; the images showed that the particles were spherical in shape with smooth surfaces.

Figure 4.7c shows images of TDF-PLGA 85:15 loaded nanoparticles. The images showed spherical shaped particles with smooth surfaces. The average particle size was above 200 nm which was greater than the sizes provided by the zeta sizer (127 nm). As mentioned previously, the increase in size might be due to aggregation and coalescence of the nanoparticles. Such aggregation and coalescence may be attributed to the freeze-drying process, which may have caused irreversible fusion of the nanoparticles. The freeze-drying process can also cause mechanical stress on the nanoparticles leading to a change in particle morphology.[8] As shown by (Pirooznia *et al.*, 2012), the addition of cryoprotectants in the final step before lyophilization can decrease the tendency for the nanoparticles to aggregate, thus preventing changes in particle morphology.
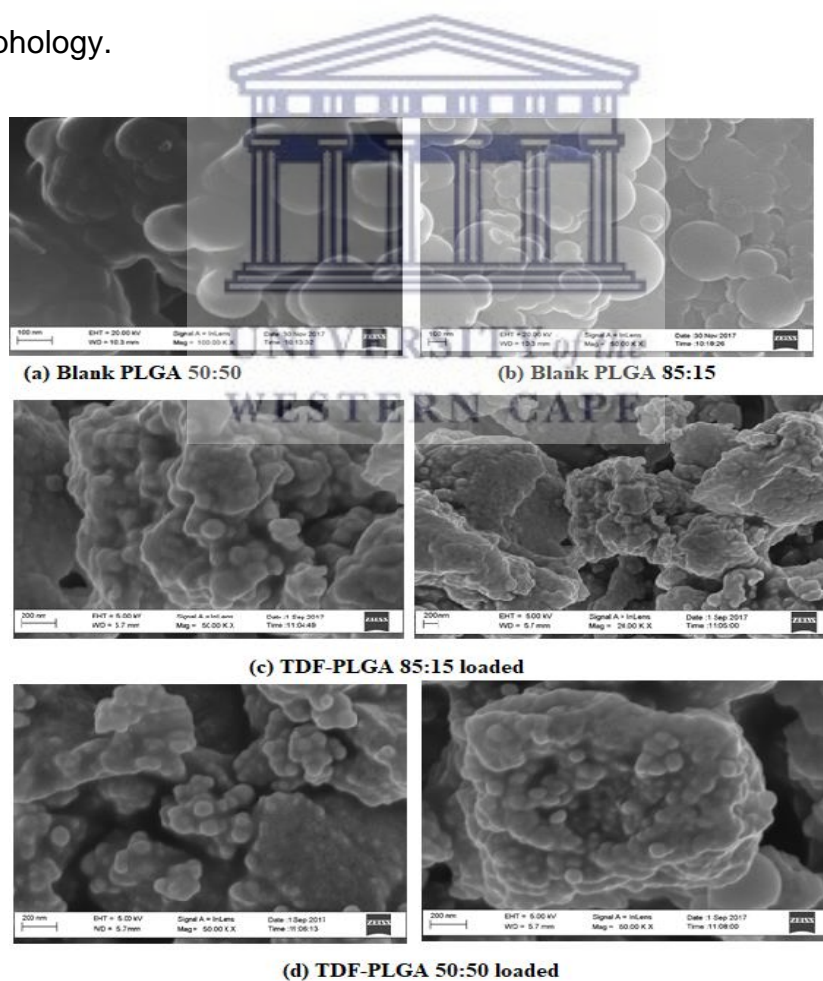
Figure 4.7: *HR-SEM of formulated nanoparticles: (a) Blank PLGA 50:50, (b) Blank PLGA 85:15, (c) TDF-PLGA 85:15 loaded, (d) TDF-PLGA 50:50 loaded*

Figure 4.7d shows images of TDF-PLGA 50:50 taken using the HR-SEM. Similar characteristics to those which were obtained with TDF-PLGA 85:15 were observed (Figure 4.7c); the nanoparticle surface was smooth and spherical, with signs of aggregation and coalescence.

When Figure 4.7a and Figure 4.7b were compared to Figure 4.7c and Figure 4.7d the latter appeared to be less smooth and more coagulated this might be as a result of the presence of TDF in the formulation.

4.3.3 Zeta potential

Following formulation of the TDF-PLGA 50:50 and TDF-PLGA 85:15 loaded nanoparticles, their zeta potentials were determined using the Malvern zeta-sizing system. The mean zeta potential values for TDF-PLGA 50:50 and TDF-PLGA 85:15 were found to be -8.84 ± 0.35 mV and -5.69 ± 0.6 mV, respectively (Table 4.3). These values decreased to -19.1 ± 0.91 mV and -5.72 ± 1 mV, respectively, after washing of the samples. The change in zeta potential for TDF-PLGA 85:15 was not significantly different. The negative charge on the nanoparticles directly affects the cellular uptake of the nanoparticles by inducing a positive charge on the cell membrane, resulting in attraction between the two surfaces. The decrease in the zeta potential values is also an indication of the increased stability of the nanoparticles. A high bioavailability may be obtained due to this increased stability, because the TDF loaded nanoparticles would possibly be able to permeate the cell membrane and be transported to endosomes found within the cell.[9]

Table 4.3: *Zeta potential of TDF-loaded nanoparticles*

Drug Polymer ratio	Zeta potential	
	Before wash	After wash
TDF-PLGA 50: 50	-8.84 ± 0.35 mV	-19.1 ±0.91 mV
TDF-PLGA 85: 15	-5.69 ± 0.6 mV	-5.72 ± 1 mV

4.3.4 Percentage yield

The percentage yield is the total amount of nanoparticles recovered after formulation expressed as a percentage of the total weight of products used for formulation, while drug entrapment efficiency is the ratio of the API amount expected to be loaded *versus* the actual amount of API loaded after formulation and encapsulation efficiency determines the actual amount of drug found in the formulated nanoparticles.

TDF-PLGA 50:50 and TDF-PLGA 85:15 loaded nanoparticles were recovered and weighed after freeze-drying. The values obtained after weighing were 71.2 mg and 61.0 mg, for TDF-PLGA 50:50 and TDF-PLGA 85:15 loaded nanoparticles, respectively (Table 4.4)**.** The percentage yield was calculated as per Equation 3.2

$$Percentage\ yield(\%) = \frac{mass\ of\ nanoparticles\ recovered}{mass\ of\ PLGA, drug\ and\ excipients\ used\ in\ formulation} x100$$

$$Percentage\ yield(\%) = \frac{71.2\ mg}{105\ mg} x100$$

= 67.82% for TDF-PLGA 50:50

$$Percentage\ yield(\%) = \frac{61\ mg}{105\ mg} x100$$

= 58.10% for TDF-PLGA 85:15

The percentage yield was calculated to be 67.82% and 58.10% for TDF-PLGA 50:50 and TDF-PLGA 85:15 loaded nanoparticles, respectively. The loss in mass could be

due to unbound polymer and drug discarded during collection of the formulated

nanoparticles or washing process.

Table 4.4: Mass of TDF-loaded nanoparticles recovered (mg) and percentage yield*.*

Drug polymer combination	Mass of TDF used in formulation(mg)	Mass of polymer used (mg)	Mass of nanoparticle recovered (mg)	Percentage yield (%)
TDF-PLGA 50:50	5	100	71.2	67.82
TDF-PLGA 85:15	5	100	61	58.10

To determine the encapsulation efficiency and entrapment, we first needed to

develop a method (HPLC-DAD and UV-spectrometry method) of which we used to

determine the amount of TDF in the nanoparticles.

4.3.5 Standard calibration plot for determination of TDF (HPLC-DAD and UV-spectrometry method)

To determine linearity of the method, samples were analyzed at an absorbance

frequency of 260 nm, at which TDF is reported to have its maximum absorbance.[10] A

linear regression model was used to study the relationship between absorbance of

TDF and its concentration, and a graph of mean TDF absorbance *versus* TDF

concentration was plotted (Figure 4.8). This model enabled the prediction of TDF

concentration in the prepared nano-formulations by measuring its absorbance in the

sample; data obtained is featured in appendix C (Table C1.1 and Table C1.2).
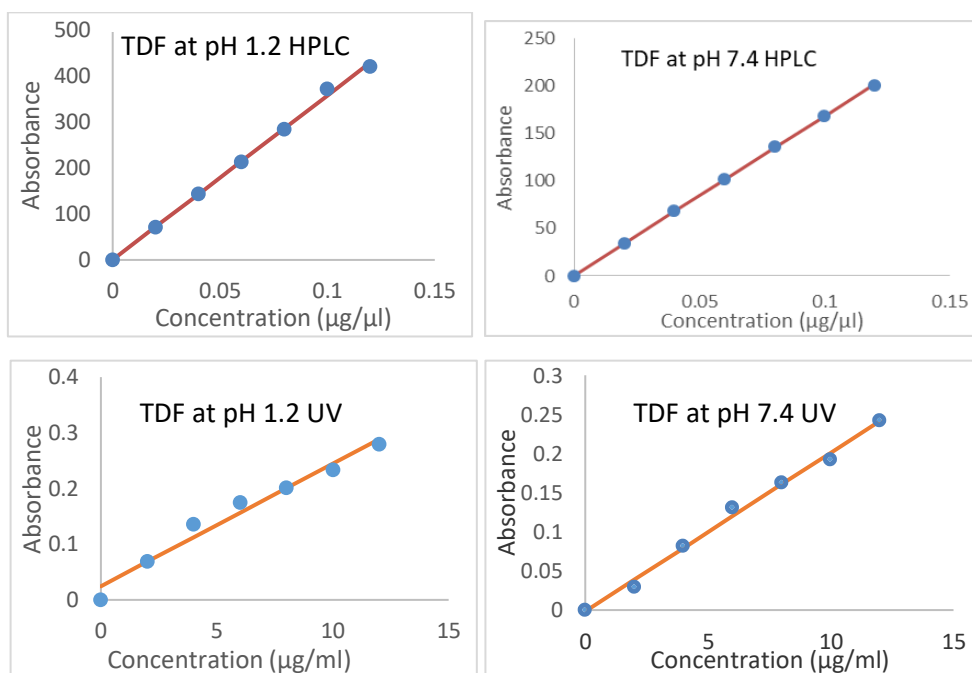
Figure 4.8: Standard calibration graph of Tenofovir disoproxil fumarate (λmax=260nm).

Stock solutions and working standards were prepared in phosphate buffer solution (PBS) at a pH of 1.2 and pH 7.4. Samples were analyzed at 25⁰C. Data values were recorded in triplicate presented as mean ± SD (n=3).

Table 4.5 presents computed data derived from plotting the calibration curves for TDF. The R^2 values at pH 1.2 and pH 7.4 depicted linearity and showed how close the data was to the fitted regression line. The relationship between concentration and absorbance can be expressed by Equation 4.1 with substitutions from Table 4.5. From this, the amount of drug encapsulated within the nanoparticles was determined. Data obtained is featured in appendix C (Table C1.1 and Table C1.2).

$$y = intercept + slope(x)$$

Equation 4.1

where   *y*   =   TDF peak area

             x   =   the standard solution concentration in µg/ml

Table 4.5: Linearity data and quantification limits of Tenofovir disoproxil fumarate at pH 1.2 and 7.4 (*HPLC-DAD and UV-spectrometry methods*).

Validation parameters	HPLC-DAD		UV-spectrometry	
	pH 1.2	pH 7.4	pH 1.2	pH 7.4
R^2	0.9781	0.9999	0.9702	0.9938
Slope ± SD	3578.54±69.44	1677.96±7.86	0.0220±0.002	0.02±0.001
Intercept ± SD	0.32±5.01	0.79±0.567	0.024±0.01	-0.002±0.01
Concentration range (µg/ml)	0.02-0.12	0.02-0.12	200-1200	200-1200
LOD (µg/ml)	0.001	0.01	1.87	0.85
LOQ (µg/ml)	0.003	0.014	5.65	2.5

Analyses with HPLC-DAD presented better linearity values than those with UV-spectrometry, and linearity values obtained at pH 7.4 seemed better than values obtained at pH 1.2 (as shown by the R^2 values); however, it is not clear if these differences in values are statistically significant. The results obtained indicate that the two methods, HPLC-DAD and UV-spectrometry, were sensitive enough to determine the concentration of the API in the standard solutions. However, the concentration ranges, as well as the LOD and LOQ values are lower for the HPLC-DAD method than for the UV-spectrometry method, attesting to the increased sensitivity of the HPLC-DAD compared to the UV-spectrometry method.

The percentage recovery was calculated from the equation of the calibration curve and was found to be between 98% and 102% (Table 4.6). This was acceptable when viewed against the International Conference on Harmonisation (ICH) guidelines for assays using the HPLC-DAD method. The precision (repeatability) of the methods was determined by analyzing replicates of TDF standard solution, at three different concentrations (over the ranges, 0.02-0.12 µg/µl for the HPLC-DAD method and 2-12

µg/µl for the UV-spectrometry method) covering the standard calibration range (Table C1.1 and Table C1.2 in the appendix). The values were expressed as % RSD and found to be less than 2% (Table 4.6); suggesting that the results provided by the methods are reproducible.

Table 4.6: Intra-day and inter-day assay precision and accuracy for Tenofovir disoproxil fumarate at pH 1.2 and 7.4 (HPLC-DAD method).

	pH 1.2			pH 7.4		
TDF(µg/µl)	0.02	0.06	0.12	0.02	0.06	0.12
	Intra-day (n=3)					
	Day 1					
Mean	0.02	0.06	0.12	0.02	0.06	0.12
SD	0.0003	0.0009	0.0006	0.0003	0.0008	0.0007
Precision[1] (%)	1.51	1.51	0.51	2.01	1.32	0.59
Accuracy[2] (%)	99.50	99.30	97.92	99.50	100.80	99.40
	Day 2					
Mean	0.02	0.06	0.12	0.02	0.06	0.12
SD	0.0002	0.0007	0.0012	0.0002	0.0007	0.0005
Precision[1] (%)	1.00	1.17	1.02	1.00	1.13	0.42
Accuracy[2] (%)	100.00	99.83	98.00	99.50	101.80	99.10
	Day 3					
Mean	0.02	0.06	0.12	0.02	0.06	0.12
SD	0.0002	0.0006	0.0009	0.0003	0.0009	0.0009
Precision[1] (%)	1.00	1.00	0.77	1.47	1.50	0.75
Accuracy[2] (%)	100.50	99.50	97.83	99.50	99.50	99.50
	Inter-day (n=9)					
Mean[3]	0.02	0.06	0.12	0.02	0.06	0.12
SD	0.00008	0.0001	0.00008	0.0002	0.0008	0.0002
Precision[1] (%)	0.40	0.12	0.07	1.00	1.32	0.17
Accuracy[2] (%)	100.00	99.50	97.92	100.50	101.00	99.30

The accuracy of the method for assay purposes was determined by measuring the absorbance of TDF at three different concentrations (0.02, 0.06, 0.12 µg/ µl and 2, 6, 12 µg/ µl, for the HPLC-DAD and UV-spectrometry methods, respectively) covering the standard calibration range (Figure 4.8). The accuracy data from the UV-spectrometry method on the other hand provided values within the range, 99-116.7% (Table 4.7). The acceptable recovery range in assays for quality control and drug

registration is between 90 and 110%,[11] and so this method did not meet the requirements for quality control and drug registration. However, since this study is still preliminary and not for quality control or drug registration purposes, the UV spectrometry method was also utilized as a comparison to the HPLC-DAD method for determination of TDF in samples.

Table 4.7: Intra-day and inter-day assay precision and accuracy for Tenofovir disoproxil fumarate at pH 1.2 and 7.4 (UV-spectrometry method).

	pH 1.2			pH 7.4		
TDF(µg/µl)	2	6	12	2	6	12
Intra-day (n=3)						
Day 1						
Mean	2.04	6.90	11.63	1.98	5.95	12.03
SD	0.0006	0.0008	0.0006	0.0002	0.0003	0.0007
Precision[1] (%)	0.03	0.01	0.005	0.08	0.005	0.006
Accuracy[2] (%)	102	115	96.9	99	99.2	100.3
Day 2						
Mean	2.05	6.87	11.52	2.07	6.01	12.19
SD	0.0005	0.0013	0.0020	0.0003	0.0001	0.0002
Precision[1] (%)	0.02	0.02	0.02	0.01	0.002	0.002
Accuracy[2] (%)	102.5	114.5	96.0	103.5	100.1	101.6
Day 3						
Mean	2.04	7.00	11.57	2.09	6.05	12.01
SD	0.0006	0.0006	0.0025	0.0002	0.0001	0.0002
Precision[1] (%)	0.030	0.009	0.020	0.010	0.002	0.002
Accuracy[2] (%)	100.1	116.7	96.4	104.5	100.8	102.0
Inter-day (n=9)						
Mean[3]	2.04	6.92	11.68	2.07	6.00	12.15
SD	0.0002	0.0020	0.0010	0.0005	0.0010	0.0020
Precision[1] (%)	0.01	0.03	0.90	0.02	0.02	0.02
Accuracy[2] (%)	102.00	115.30	97.30	103.50	100.00	101.30

Values obtained in Table 4.6 and Table 4.7 were calculated as follows;

❖ [1]Expressed as % RSD = (SD/mean) × 100.

❖ [2]Calculated as (mean determined concentration/nominal concentration) × 100.

❖ [3]n = 3 days with three replicates per day

4.3.6 Encapsulation efficiency

The encapsulation efficiency was determined using Equation 3.6.

$$Encapsulation\ efficiency(\%)$$

$$= \frac{total\ amount\ of\ drug\ in\ the\ yield}{amount\ of\ drug\ added\ during\ encapsulation}\ x100$$

$$Encapsulation\ efficiency(\%)\ =\ \frac{2.29}{5}x100$$

= 45.8% for TDF-PLGA 50:50

$$Encapsulation\ efficiency(\%)\ =\ \frac{2.49}{5}x100$$

= 49.8 for TDF-PLGA 85:15

The total amount of drug in the yield was determined by dissolving 5 mg of the TDF-loaded nanoparticles in 0.5 ml of ethyl acetate (in a 5 ml Eppendorf tube) with vortexing. The ethyl acetate was evaporated, and 3 ml of phosphate buffer solution (PBS) was added to the Eppendorf tube. The tube was vortexed, and the contents centrifuged at a speed of 10000 rpm for 15 minutes. Thereafter, the supernatant was collected, and the absorbance measured using the UV-spectrometer and HPLC-DAD system. The concentration of the drug in that sample was determined by extrapolating the absorbance value from the calibration plot of TDF in Figure 4.8.

The results obtained from using Equation 3.6 are presented in Table 4.8. The nano-formulations prepared with PLGA 85:15 showed about 4% increase in drug encapsulation when compared to those prepared with PLGA 50:50. The significance of this difference was however not calculated. A possible reason for this could be the high ratio of PLA (hydrophilic nature) in the PLGA 85:15 polymer. The encapsulation efficiency suggests that less than half the initial amount of TDF used during the formulation process was recovered after formulation. The amount of TDF lost might be because of un-encapsulated drug discarded during the washing process.

Table 4.8: *Total amount of drug in recovered TDF-loaded nanoparticles and encapsulation efficiency.*

Drug polymer combination	Amount of drug in nano-formulation (mg)	Encapsulation efficiency (%)
TDF-PLGA 50:50	2.29	45.8
TDF-PLGA 85:15	2.49	49.8

4.3.7 Drug entrapment efficiency

The theoretical drug loading, actual drug loading, and drug entrapment efficiency, were calculated using the following equations

Equation 3.3,

$$Theoretical\ drug\ loading\ (TDL)(\%) = \frac{weight\ of\ drug\ added}{weight\ of\ polymer\ and\ drug\ added}\ x\ 100$$

$$Theoretical\ drug\ loading\ (TDL)(\%) = \frac{5}{105}\ x\ 100$$

$$= 4.76\%\ for\ both\ TDF\text{-}PLGA\ 50:50\ and\ 85:15$$

Equation 3.4,

$$Actual\ drug\ loading\ (\%) = \frac{weight\ of\ drug\ in\ nanoparticles}{weight\ of\ nanoparticles}\ x100$$

$$Actual\ drug\ loading\ (\%) = \frac{2.29}{71.2}\ x100$$

$$= 3.23\%\ for\ TDF\ for\ PLGA\ 50:50$$

$$Actual\ drug\ loading\ (\%) = \frac{2.49}{61}\ x100$$

$$= 4.08\%\ for\ TDF\ for\ PLGA\ 85:15$$

and Equation 3.5;

$$Drug\ Entrapment\ efficiency(\%) = \frac{actual\ drug\ loading}{theoretical\ drug\ loading}\ x100$$

$$Drug\ Entrapment\ efficiency(\%) = \frac{3.23}{4.76}\ x100$$

$$= 67.86\%\ for\ TDF\text{-}PLGA\ 50:50$$

$$Drug\ Entrapment\ efficiency(\%) = \frac{4.08}{4.76}x100$$

= 85.71% for TDF-PLGA 85:15

Table 4.9 presents the results of the calculations. The formulation with PLGA 50:50 had a higher entrapment efficiency of the drug (TDF) than the formulation with PLGA 85:15. The reasons for the difference in entrapment efficiency are yet unknown, our hypothesis is that this might be as a result of differences in the polymer ratios. The significance of this difference was however not calculated.

Table 4.9: Actual and theoretical drug loading values, and drug entrapment efficiency of TDF-PLGA formulations

Drug/polymer combination	Theoretical drug loading (% w/w)	Actual drug loading (% w/w)	Drug entrapment efficiency (% w/w)
TDF-PLGA 50:50	4.76	3.23	67.86
TDF-PLGA 85:15	4.76	4.08	85.71

4.3.8 Fourier Transform Infrared Spectroscopy (FT-IR)

Following drug loading, the nanoparticles were analyzed using FT-IR spectroscopy. Figure 4.9 presents the FT-IR spectra of TDF-PLGA (50:50) and TDF-PLGA (85:15) physical mixtures and loaded nanoparticles. When compared to the FT-IR spectra obtained during analysis of the parent compounds and the physical mixtures, the characteristic intensity bands, that is the peaks obtained with the loaded products mostly corresponded to the polymer (PLGA 50:50 or 85:15) Figure 4.2 a & c. From this, it can be inferred that TDF was encapsulated within the polymer. Comparison of both loaded polymers (loaded formulations of PLGA 50:50 and 85:15) showed the appearance of an extra intensity peak at 2945.29 cm^{-1} (Figure 4.9d) for TDF-PLGA 85:15 loaded nanoparticles, which was not observed with the TDF-PLGA 50:50 loaded nanoparticles (Figure 4.9c) or the physical mixture of TDF-PLGA 85:15. TDF-PLGA

85:15 also presented with the disappearance of a peak at 1674.85 cm^{-1} present in the physical mixture but absent in TDF-PLGA 85:15 loaded nanoparticles, indicating that there is some interaction taking place between the two components . This also further confirmed that TDF was indeed encapsulated within the polymer. Figure 4.10 below shows possible points of interactions between PLGA and TDF.

The differences shown in the FT-IR spectra of both polymers could be due to their ratios, that is, their composition and molecular weight. Comparing TDF-polymer physical mixture to TDF-PLGA loaded nanoparticles, it was noted that the frequency band values for TDF-PLGA loaded nanoparticles had increased; further confirming an interaction (hydrogen bonding) between TDF and PLGA (Table 4.10). This interaction is possibly an encapsulation of TDF within the polymer. It is known that the physicochemical properties of PLGA enable it to entrap drugs for onward delivery to the required site of action[12]. As such, evidence of TDF encapsulation within the polymer may infer a possible improvement in TDF delivery.
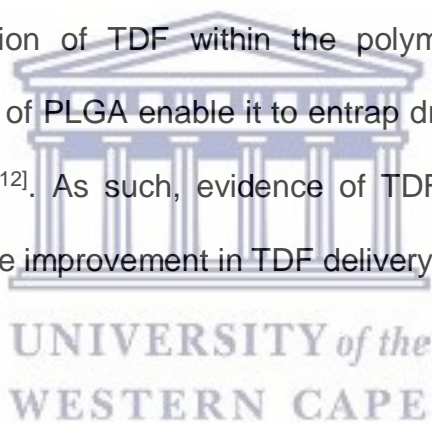
Table 4.10: Selected FTIR data for TDF-PLGA 50:50 and TDF-PLGA 85:15 loaded nanoparticles compared with TDF-PLGA 50:50 physical mixture and TDF-PLGA 85:15 physical mixture.

Analyzed sample	Experimental frequency bands (cm^{-1})	Standard frequency bands (cm-1)	Associated functional groups from IR bands
TDF-PLGA 50:50 loaded	2949.09	3000 - 2500	Chelated O-H stretching bridge
	1748.08	1790 - 1740	Strong C=O stretching of the carbonyl group
TDF-PLGA 85:15 loaded	2995.67	3000 - 2500	Chelated O-H stretching bridge
	2945.29	3000 - 2500	Chelated O-H stretching bridge
	1748.18	1790 - 1740	Strong C=O stretching of the carbonyl group
TDF-PLGA 50:50 physical mixture	2993.81	3000 - 2500	Chelated O-H stretching bridge
	1750.07	1790 - 1740	Strong C=O stretching of the carbonyl group
TDF-PLGA 85:15 physical mixture	2985.88	3000 - 2500	Chelated O-H stretching bridge
	1754.32	1790 - 1740	Strong C=O stretching of the carbonyl group
	1674.85	1685 - 1665	Strong C=0 stretching

Figure 4.9: FT-IR spectra of (a): TDF-PLGA 50:50 physical mixture, (b): TDF-PLGA 85:15 physical mixture(c): TDF-PLGA 50:50 loaded and (d): TDF-PLGA 85:15 loaded nanoparticles.
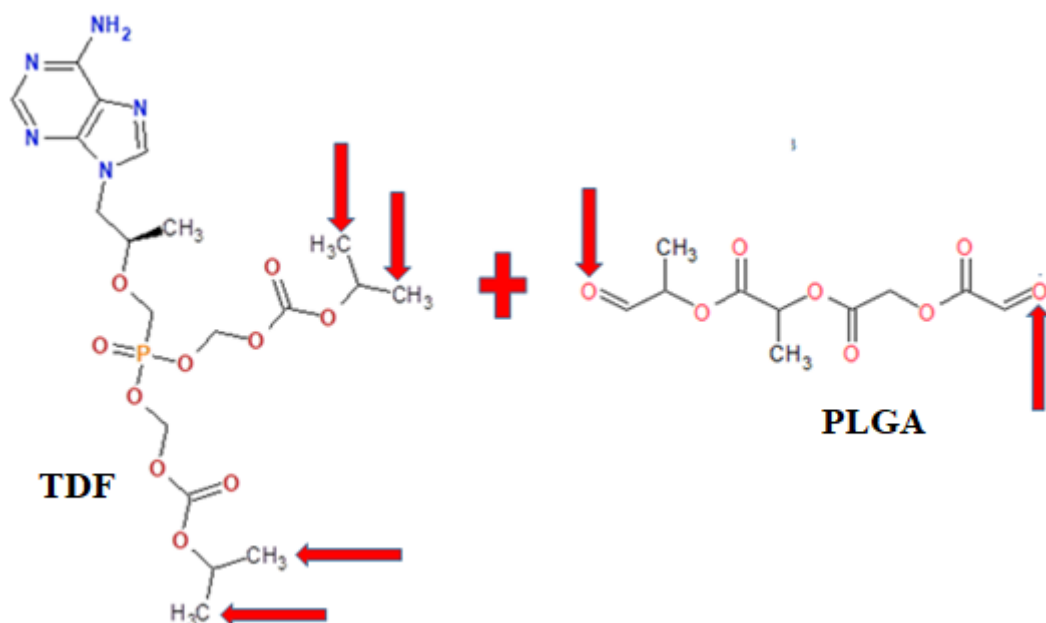
Figure 4.10: Schematic representation of possible functional group interactions between TDF and PLGA.

4.3.9 Hot Stage Microscopy (HSM)

Following collection of the freeze dried TDF-loaded nanoparticles, the samples were analyzed using HSM. Figure 4.11c shows images from the HSM analysis of TDF-PLGA 50:50 loaded nanoparticles.

Changes to the sample because of an increase in temperature were a bit difficult to visualize between 40°C and 60°C; however noticeable changes such as signs of melting were observed at temperatures above 110°C. No appearance of bubbles or visible degradation of the sample was observed. This could be explained by the rationale that the polymer completely encapsulated TDF and therefore protected it from degradation. It may also be because the amount of TDF in the formulation was too small for the degradation process to be visualized.

(a) TDF-PLGA 50:50 mixture   (b) TDF-PLGA 85:15 mixture

(c) TDF-PLGA 50:50 loaded   (d) TDF-PLGA 85:15 loaded
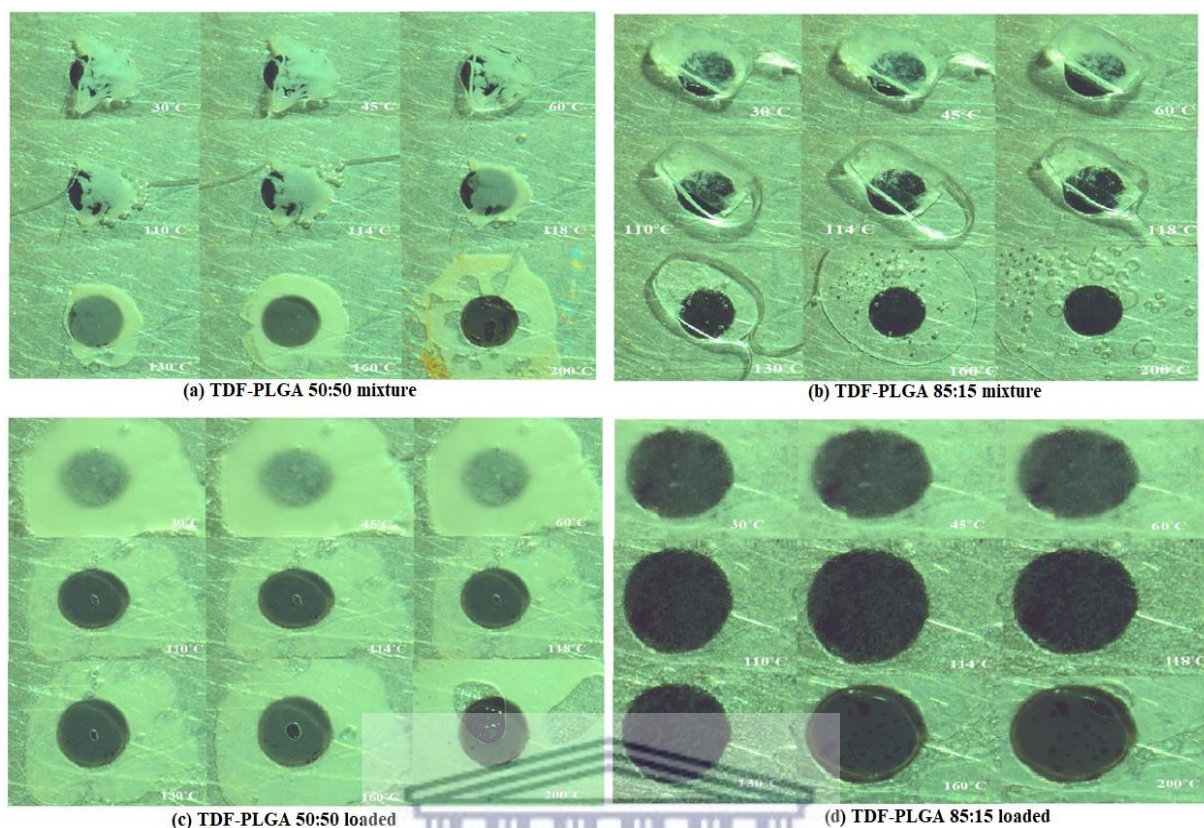
Figure 4.11: *HSM images of TDF-PLGA 50:50 physical mixture, TDF-PLGA 85:15 physical mixture, TDF-PLGA 50:50 loaded, and TDF-PLGA 85:15 loaded nanoparticles.*

Both TDF loaded nanoparticles and physical mixtures showed an increase in thermal stability (Figure 4.11) when compared to the parent compounds. A reference to Figure 4.11c shows that the HSM of TDF-PLGA 50:50 loaded nanoparticles did not show any evidence of being oily or viscous, but rather appeared to dry up at temperatures above 130°C. Figure 4.11d shows images from the HSM of TDF-PLGA 85:15 loaded nanoparticles. Changes to the sample with increase in temperature were a bit difficult to visualize at temperatures between 40°C and 60°C, as was the case with TDF-PLGA 50:50 loaded nanopartilces, with the sample showing signs of melting at temperatures above 110°C. unlike what was observed with Figure 4.11c, the TDF-PLGA 85:15 sample (Figure 4.11d) appeared to be oily and viscous at temperatures above 130°C. This may be because of the difference in polymer ratios used. No appearance of bubbles or visible degradation of the sample was observed on continued heating of

90

TDF-PLGA 85:15. As with TDF-PLGA 50:50, this could be explained by the rationale that the polymer completely encapsulated TDF and therefore protected it from degradation, or that the amount of TDF in the formulation was too small for the degradation process to be visualized. If the former is the case, then the oral delivery of TDF would likely be improved by its encapsulation within the polymer. **(NB melting point of TDF is in the range 114-118 °C).**

4.3.10 Thermogravimetric analysis (TGA)

Thermogravimetric data analysis of TDF-PLGA (50:50 and 85:15) loaded nanoparticles (Figure 4.12) shows the exhibition of two mass loss events. This was different when compared to the single mass loss event exhibited by the TDF-PLGA physical mixtures (Figure 4.4c). The differences in the TGA results between the physical mixture and the nano-formulation could perhaps be a result of change in thermal stability of the nano-formulation.
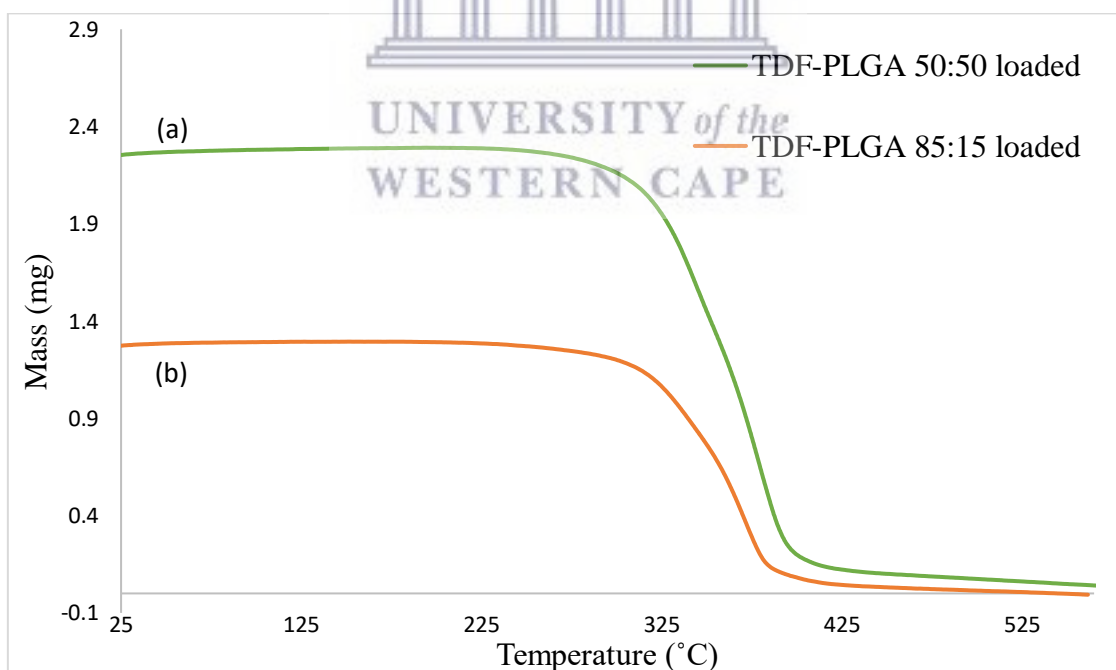
Figure 4.12: *TGA curve of (a) TDF-PLGA 50:50 loaded and (b) TDF-PLGA 85:15 loaded nanoparticles.*

Table C1.5 in the appendix presents data from the thermal analyses of TDF formulated nanoparticles. This shows the temperatures at which sample degradation started, and

when degradation ended. The results indicated that TDF-PLGA 50:50 and TDF-PLGA 85:15 exhibited a total mass loss of about 93 and 91%, with a 7% and 9% inert residue remaining, respectively.

4.3.11 Differential Scanning Calorimetry (DSC)

Figure 4.13 below shows thermograms of TDF-PLGA 50:50 and TDF-PLGA 85:15 loaded nanoparticles. No identifiable peaks of TDF could be found in the thermograms. This could indicate that no crystalline TDF was found in the nanoparticles. It may also indicate that TDF was molecularly dispersed in the polymer matrix, or that the amount of TDF present in the analyzed sample was too small to show any significant peaks. The loaded nanoparticles however showed peaks that agreed with TDF-PLGA physical mixtures (mentioned earlier); that is, it showed melting points of about 56.38°C and 58.88°C for TDF-PLGA 85:15 and TDF-PLGA 50:50. It is however not known if these differences in temperature are significant.
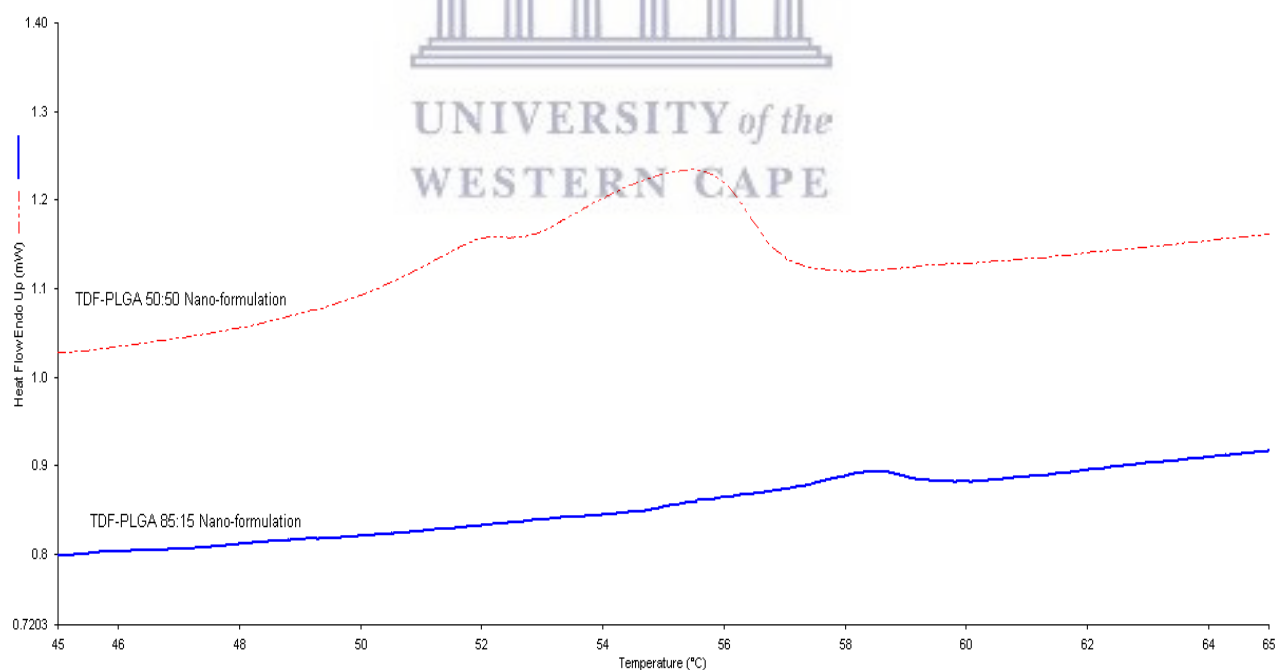
Figure 4.13: DSC thermograms of TDF-PLGA 50:50 and TDF-PLGA 85:15 loaded nanoparticles

4.3.12 Determination of TDF release from TDF-PLGA loaded nanoparticles

Figure 4.14 shows the cumulative percentage of drug released from TDF-loaded nanoparticles at pH 1.2 and pH 7.4 *versus* time. Samples were analyzed using HPLC-DAD and UV-spectrometry. The release profile displayed by both polymers was biphasic; an initial burst of TDF accompanied by a sustained release profile as is commonly seen in core-shell type nanoparticles[13]. This model also confirmed the presence of surface drug on the nanoparticles with the bulk of the TDF encapsulated within the nanoparticles. If this is the case, some level of extended release can be obtained from the nano-formulation without compromise of immediate release. This ensures that the surface drug can be immediately released and delivered to the site of action immediately. This will be followed by gradual release of TDF from the nano-formulation over time, ensuring extending TDF release.
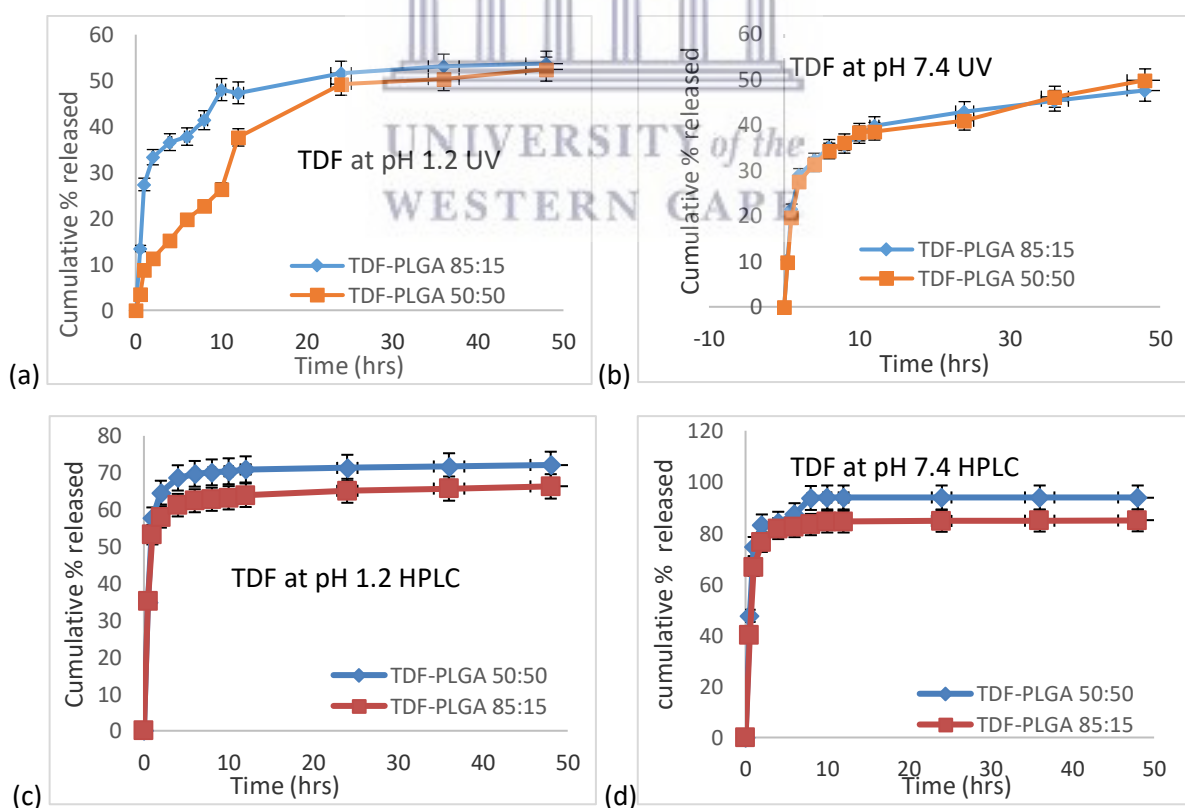
Figure 4.14: In-vitro release of TDF-PLGA 50:50 and TDF-PLGA 85:15 loaded nanoparticles

The release was done at pH 1.2 (Figure 4.14a & c) and pH 7.4 (*Figure* 4.14b & d) at 37˚C over a period of 48h, analyzed using UV-spectrometry (*Figure* 4.14a & b) and HPLC-DAD (*Figure* 4.14c & d). Data was collected in triplicates and is here presented as mean ± SD (n=3).

Table 4.11 shows the total percentage of TDF released in 12 hours from the formulations. The same sample was analyzed using two analytical methods (HPLC-DAD and UV-spectrometry). The results from HPLC-DAD analysis, compared to those from UV spectrometry, showed additional release of TDF from the formulations at both pH values. While human error may be a factor, the low values may very likely be due to the lower sensitivity of the UV-spectrometric method.

Table 4.11: Percentage of TDF released from formulations after 12 hours analysis

Formulation	Percentage of TDF released			
	HPLC-DAD		UV-spectrometry	
	pH 1.2	pH 7.4	pH 1.2	pH 7.4
TDF-PLGA 50:50	63.9%	84.4%	39.82%	47.3%
TDF-PLGA 85:15	70.9%	93.7%	38.62%	37.64%

4.3.13 Mathematical modeling of drug release data

The mechanism of TDF release from TDF-PLGA formulated nanoparticles was evaluated by fitting the release data to four mathematical models namely; Gompertz model, Korsmeyer-Peppas model, Peppas-Sahlin model, and the Weibull model. DDsolver a peer-reviewed modelling program[14] was used for this analysis, the release data was fitted to the four mathematical models (named above) which are commonly used in literature.[15]

94

Best fit model was selected using the adjusted coefficient of determination (R^2 adj) and a model with the highest R^2 adj was deemed to be the best fit model. R^2 adj allows for better comparison of the models when compared to coefficient of determination (R^2).[14] The release data of TDF obtained at both pH 1.2 and 7.4 was fitted to the four models mentioned above. Of these four models, the Weibull model was adjudged the model of best fit according to the R^2 adj value obtained, as illustrated in Table 4.12.

In the Weibull models **α** is a parameter that represents the time scale, **Ti** is the lag time before onset of the dissolution and **β** describes the shape of the curve which can follow either one of the following:

- **β=1** the shape is exponential

- **β>1** the shape is S-shaped (sigmoid) with an upward curvature followed by a turning point.

- **β<1** the shape has a high initial slope followed by a consistent exponential curve.

The Weibull model has four different modifications that generally differ in terms of the absence or presence of the following parameters **F_{max}** and **Ti**. **β** according to literature which can be used as an indicator to describe the mechanism of drug release from a polymer matrix.[16]

Data collected from the different models can be seen in Table 4.12, the Weibull model as earlier mentioned was selected as best fit model for the four samples analyzed. The value of **β** was less than 0.75 for all four formulations thereby conforming that the release was Fickian diffusion which was in line with data from literature.[16]

Release mechanism from polymeric systems using Weibull model can be interpreted as follows:

95

Time exponent	Release mechanism
β≤0.75	Fickian diffusion in fractal or Euclidian spaces
0.75<β<1	Combined release mechanism
β>1	Complex release mechanism

Table 4.12: *Parameter values and R^2 adj values obtained from fitting drug release experimental data to four mathematical models*

pH		**1.2**		**7.4**	
	Parameters	**TDF-PLGA50:50**	**TDF-PLGA85:15**	**TDF-PLGA50:50**	**TDF-PLGA85:15**
Weibull_1	β	0.08	0.01	0.19	0.12
	α	1.01	1.19	0.63	0.75
	Ti	0.5	0.5	0.49	0.5
	R^2adj	0.993	0.998	0.994*	0.991
Gompertz_1	α	0.64	0.71	0.39	0.50
	β	0.56	0.42	1.71	1.01
	R^2adj	0.931	0.951	0.983	0.952
Peppas-Sahlin_1	K1	67.24	63.24	86.5	77.78
	K2	-15.20	-14.94	-19.3	-17.01
	m	0.27	0.24	0.27	0.28
	R^2adj	0.950	0.964	0.965	0.951
Korsmeyer-Peppas with Tlag	n	0.04	0.04	0.04	0.04
	k	63.2	56.8	80.9	74.4
	R^2adj	0.992	0.997	0.989	0.988

4.3.14 Stability of TDF-PLGA loaded nanoparticles

The formulated nanoparticles were stored at temperatures between 2 and 8°C. They were evaluated for stability by measuring parameters such as the zeta potential, particle size and PDI, at the time of preparation and at different time intervals during storage over a period of 90 days.

Particle size

After formulation, the average size of the formulated TDF-PLGA 50:50 nanoparticles was measured to be 117.2 ± 2.33 nm while TDF-PLGA 85:15 was measured to be 111.1 ± 0.02 nm. These values increased to 161.2 ± 4.82 nm and 138.3 ± 0.02 nm after washing, then to 2074 ± 63.3 nm and 1824 ± 70.02 nm after freeze drying for TDF-PLGA 50:50 and TDF-PLGA 85:15 respectively, with no significant difference between the means (p<0.0001). Subsequently, the size increased steadily to about 4520 ± 93.1 nm and 5598 ± 82.7 nm after 90 days (Figure 4.15).
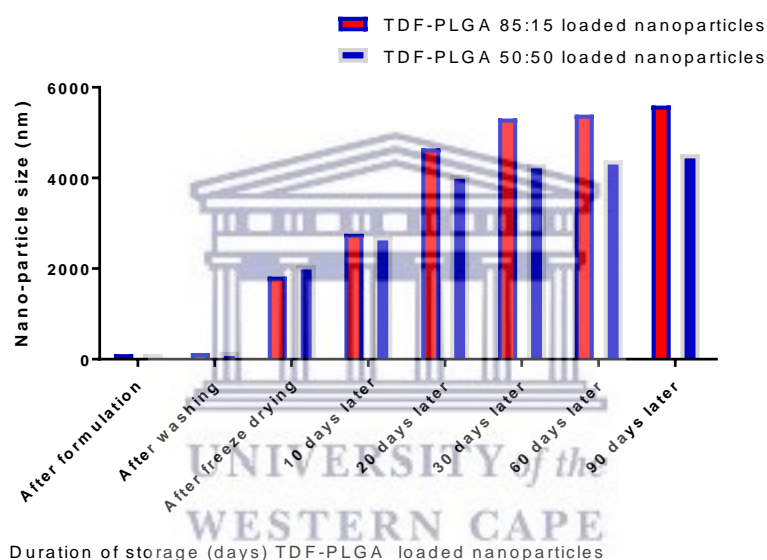
Figure 4.15: Changes in nanoparticle size of TDF-PLGA 50:50 and 85:15 freeze dried loaded nanoparticles

Comparing both formulations, the particles sizes of TDF-PLGA 50:50 formulations were less than those of TDF-PLGA 85:15, at every measurement. The two formulations showed the same trend, an increase in particle size that was proportional (perhaps not necessarily directly) to the duration of storage.

The postulated mechanisms to show how particles pass through the gastrointestinal and physiological barriers highlights endocytosis as one of the mechanisms, for particles < 500 nm. It can therefore be seen that the nanoparticle sizes immediately

after formulation and after washing favors uptake *via* endocytosis. Following the freeze-drying and 90-days storage processes however, the increase in particle size as mentioned above was such that endocytosis may not be favorable as an uptake mechanism. There may however be some success with uptake *via* lymphatic passage, with absorption by cells in Peyer's patches, especially for particles less than 5 µm. It can be seen that the nanoparticle size increased after the washing process, possibly due to agglomeration of these particles. We propose that more assessments can be carried out to assess ways to limit such agglomeration in the washing process, perhaps by the use of suitable surface-active agents. Such an intervention may slow / prevent agglomeration, ensuring that particle sizes remain close to the values obtained immediately after formulation. This will enhance penetration through physiological barriers and hence improve bioavailability.

Zeta potential

The average zeta potential of the formulated nanoparticles was also assessed and found to be -6.74 ± 0.02 mV and -5.32 ±4.1 mV for TDF-PLGA 50:50 and TDF-PLGA 85:15 respectively (Figure 4.16), the zeta potential values further decreased after washing and freeze drying, indicating an increase in stability. On assessing the samples after 10 days of storage, the zeta potential had increased, indicating a decrease in stability of the nano-formulation with increase in time. However, on day 30, the samples showed some discrepancy indicating an increase in stability. The zeta potential further increased from day 60 through 90 Figure 4.16, indicating a decrease in stability.
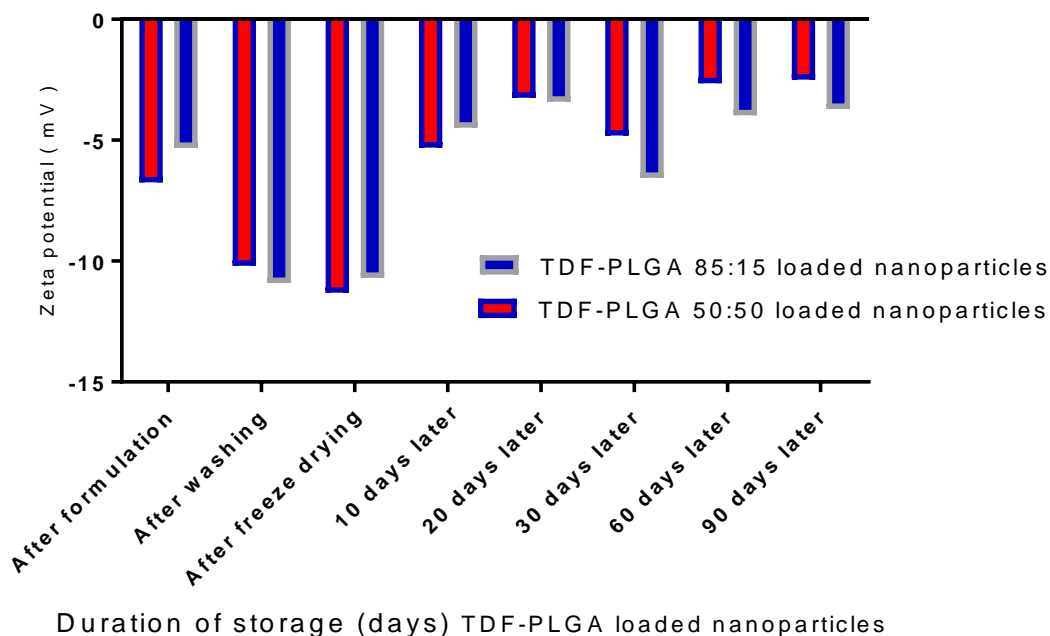
Figure 4.16: Changes in zeta potential of TDF-PLGA 50:50 and 85:15 freeze dried loaded nanoparticles

Comparing the stability of both formulations, the data indicated that TDF-PLGA 50:50 seemed more stable than TDF-PLGA 85:15, until day 20 when TDF-PLGA 85:15 seemed to be more stable than TDF-PLGA 50:50 until day 90. It may not be easy to tell at this point, without further studies, if these seeming differences in stability are significant – statistically, pharmaceutically, physiologically or therapeutically.

Polydispersity index

The PDI of the formulated nanoparticles were also assessed immediately and the values were 0.149 ± 1.3 and 0.191 ± 3.1 for TDF-PLGA 50:50 and TDF-PLGA 85:15 respectively. The PDI value further increased which indicated coalescence of the nanoparticles after washing and freeze drying (Figure 4.17). The PDI value after day 10 of storage showed signs of increased coalescence of the nanoparticles. A steady increase in the PDI values was expected; however, on day 10, 20 and 30, and 90 for both formulations, a decrease in the PDI values was noticed, indicating less coalescence, and an increase was noticed in these values from day 60 to 90 (Figure

99

4.17). These changes could be due to more samples aggregating during this period of storage.
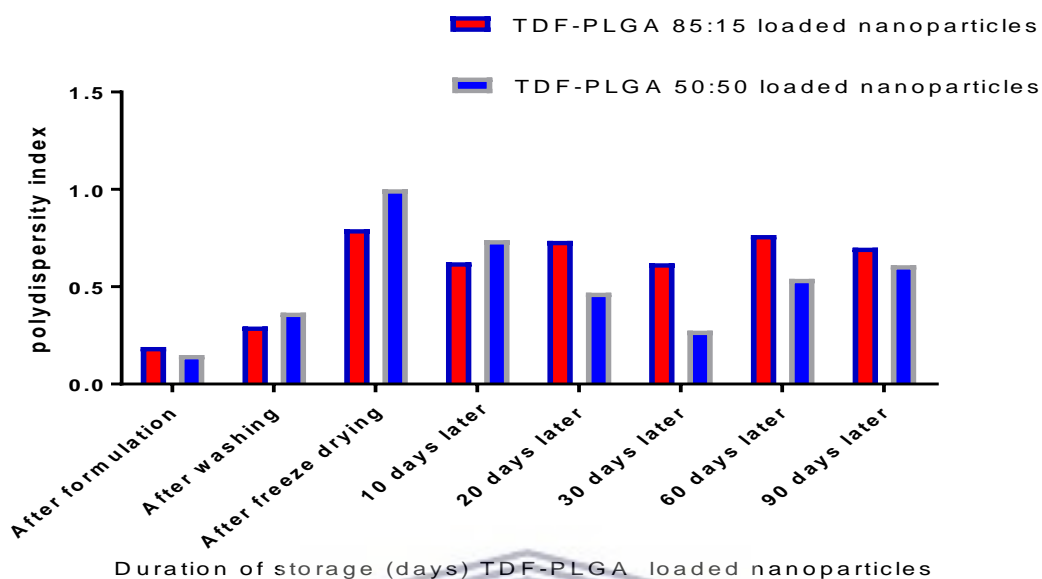
Figure 4.17: Changes in PDI of TDF-PLGA 50:50 and 85:15 freeze dried loaded nanoparticles

Comparing both formulations from the data presented, it could be inferred that TDF-PLGA 50:50 was more monodispersed than TDF-PLGA 85:15 after formulation until day 10 when TDF-PLGA 85:15 became more monodispersed. It is our hypothesis that the molecular weight and copolymer ratios may be a factor for these differences.

The overall changes in the nanoparticle size, zeta potential and PDI over the duration of storage were indicative of a decrease in stability of the formulated nanoparticles over time.

Comparing the results obtained from characterizing TDF-loaded nanoparticles with other studies we observed that the encapsulation efficiency was less than that obtained by Shailender *et al.,* 2017 and Destache *et al.,* 2016 64% and 52.9%, respectively. However, the particle size range obtained for this study was less than that obtained by the aforementioned studies, with zeta potential higher than that

reported by Shailender *et al.,* 2017 (-4.8 mv) but less than what Destache *et al.*, 2016 (-26.7 mv) reported. Shailender *et al.,* 2017 reported a biphasic release profile which was similar to what we obtained with this study. Shailender *et al.,* 2017 also reported that the nanoparticles were stable after 3 months of storage between 2 and 8°C, which was the opposite of what we obtained.

Chapter 5 will follow with the results obtained during formulation and characterization of nanoparticles formulated with AZT, PLGA 50:50 and PLGA 85:15.

UNIVERSITY *of the*
WESTERN CAPE

Bibliography

1. Wilkie, C. A., and Morgan, A. B., (2009). 'Thermal and fire performance of polymer nano composites and mechanisms. *In Fire retardancy of polymeric materials*', (2nd ed., pp. 279-285).

2. Gomes, E., Ercole de Carvalho, I., Fialho, S., Barbosa, J., Yoshida, M. and da Silva Cunha Júnior, A., (2017) 'Mixing method influence on compatibility and polymorphism studies by DSC and statistical analysis', *Journal of Thermal Analysis and Calorimetry*, 131(3), pp.2123-2128.

3. Lee, E., Smith, D., Fanwick, P., and Byrn, S., (2010) 'Characterization and Anisotropic Lattice Expansion/Contraction of Polymorphs of Tenofovir Disoproxil Fumarate', Crystal Growth & Design, 10(5), pp.2314-2322.

4. Gomes, E., Mussel, W., Resende, J., Fialho, S., Barbosa, J., Carignani, E., Geppi, M., and Yoshida, M., (2015) 'Characterization of Tenofovir Disoproxil Fumarate and Its Behavior under Heating', Crystal Growth & Design, 15(4), pp.1915-1922.

5. Jani, P.U., Halbert, G.W., Langridge, J., Florence, A.T., (1990) 'Nanoparticle uptake by the rat gastrointestinal mucosa: Quantitation and particle size dependency', *J. Pharm. Pharmacol*, 42(N/A), pp. 821–826.

6. Gref, R., Minamitake, Y., Peracchia, M.T., Trubetskoy, V., Torchilin, V., Langer, R., (1994) 'Biodegradable long-circulating polymeric nanospheres', *Science*, 263 (5153), pp.1600–1603.

7. Bhattacharjee, S., (2016) 'DLS and zeta potential – What they are and what they are not?', Journal of Controlled Release, 235, pp.337-351.

8. Fonte, P., Andrade, F., Azevedo, C., Pinto, J., Seabra, V., Van de Weert, M., Sarmento, B., (2016). 'Effect of the freezing step in the stability and bioactivity of protein-loaded PLGA nanoparticles upon lyophilization', *Pharmaceutical research*, *33*(11), pp. 2777-2793.

9. Cui, L., Liu, Z., Yu, D., Zhang, S., Bligh, S. and Zhao, N. (2014). Electrosprayed core-shell nanoparticles of PVP and shellac for furnishing biphasic controlled release of ferulic acid. *Colloid and Polymer Science*, 292(9), pp.2089-2096.

10. Abdelhay, M., Gazy, A., Shaalan, R., and Ashour, H., (2015). 'Selective RP-HPLC DAD method for determination of tenofovir fumarate and emtricitabine in bulk powder and in tablets', *Acta Chromatographica*, 27(1), pp.41-54.

11. Shabir G. A., (2005). 'Step-by-step analytical methods validation and protocol in the quality system compliance industry', *JVT* 10(N/A), pp. 314-325.

12. Makadia, H. K., and Siegel, S. J., (2011). 'Poly Lactic-co-Glycolic acid (PLGA) as biodegradable controlled drug delivery carrier', *Polymers*, 3(4), pp. 1377–1397.

13. Panyam, J., Labhasetwar, V., (2003). 'Biodegradable nanoparticles for drug and gene delivery to cells and tissue', *Adv Drug Deliv Rev*, 55(N/A), pp.329-347.

14. Zhang, Y., Huo, M., Zhou, J., Zou, A., Li, W., Yao, C. and Xie, S., (2010). 'DDSolver: An Add-In Program for Modeling and Comparison of Drug Dissolution Profiles', *The AAPS Journal*, 12(3), pp.263-271.

15. Maryam, J., Babak, K., 'Mathematical Kinetic Modeling on Isoniazid Release from Dex-HEMA-PNIPAAm Nanogels', *Nanomed research journal,* 1(2), pp.90-96.

16. Papadopoulou, V., Kosmidis, K., Vlachou, M. and Macheras, P., (2006). 'On the use of the Weibull function for the discernment of drug release mechanisms', *International Journal of Pharmaceutics*, 309(1-2), pp.44-50.

17. Pirooznia, N., Hasannia, S., Lotfi, A. and Ghanei, M., (2012). 'Encapsulation of Alpha-1 antitrypsin in PLGA nanoparticles: In Vitro characterization as an effective aerosol formulation in pulmonary diseases', *Journal of Nanobiotechnology*, 10(1), p.20.

18. Shailender, J., Ravi, P., Saha, P., Dalvi, A., and Myneni, S., (2017). 'Tenofovir disoproxil fumarate loaded PLGA nanoparticles for enhanced oral absorption: Effect of experimental variables and in vitro, ex vivo and in vivo evaluation', *Colloids and Surfaces B: Biointerfaces*, 158, pp.610-619.

19. Destache, C., Mandal, S., Yuan, Z., Kang, G., Date, A., Lu, W., Shibata, A., Pham, R., Bruck, P., Rezich, M., Zhou, Y., Vivekanandan, R., Fletcher, C. and Li, Q. (2016). 'Topical Tenofovir Disoproxil Fumarate Nanoparticles Prevent HIV-1 Vaginal Transmission in a Humanized Mouse Model', *Antimicrobial Agents and Chemotherapy*, 60(6), pp.3633-3639.

CHAPTER 5: RESULTS AND DISCUSSION FOR ZIDOVUDINE LOADED

NANOPARTICLES

This chapter presents the results obtained and discussion following when Zidovudine (AZT) was analyzed. Emphasis is placed on the different ratios of poly-lactic-co-glycolic acid (PLGA 50:50 and 85:15) used in this study.

5.1 Introduction

The objectives of this study were twofold of which the formulation of AZT as a nanoparticle presented the following specific sub-objectives:

- ❖ to characterize AZT and PLGA

- ❖ to formulate non-covalent complexes of AZT with PLGA of different ratios (50:50 and 85:15);

- ❖ to characterize and compare physicochemical properties of the formulated complexes using various analytical techniques;

- ❖ to compare the pharmaceutical properties (i.e. particle size, stability and *in-vitro* release) of both formulations (AZT-PLGA 50:50 and AZT-PLGA 85:15) as a means of addressing some of the limitations associated with optimal delivery of AZT (e.g., short plasma half-life and extensive first pass metabolism).

5.2 Characterization of AZT and PLGA (50:50 and 85:15)

Prior to formulation of the nanoparticle proper, AZT and two PLGA ratios (PLGA 50:50 and PLGA 85:15) were characterized individually, and in combination as a physical mixture (AZT-PLGA 50:50 and AZT-PLGA 85:15). The results of the characterization assessments were as follows;

5.2.1 Fourier-transform infra-red (FT-IR) spectroscopy

Figure 5.1 below shows the structure of AZT and PLGA while Figure 5.2 shows the FT-IR spectra of AZT, PLGA (50:50, and 85:15), and AZT-PLGA (50:50 and 85:15)

physical mixtures. The physical mixtures were prepared in a similar manner as discussed in chapter 4 section 4.2.1. The FTIR spectra of these physical mixtures were compared to those of the single component compounds (AZT, PLGA 50:50 and PLGA 85:15) to identify characteristic functional groups as a physical mixture, as well as the appearance of or disappearance of such functional groups in the combination (Figure 5.2 and Table 5.1).

Table 5.1: Selected FTIR data for AZT, PLGA (50:50 and 85:15), AZT-PLGA 50:50 physical mixture, and AZT-PLGA 85:15 physical mixture

Analyzed sample	Experimental frequency bands (cm^{-1})	Standard frequency bands (cm-1)	Associated functional groups from IR bands
AZT	3458.92	3500 - 3300	Medium N-H stretching bands
	2974.83	3200 - 2500	O-H stretching
	2813.97		
	2081.50	2160-2120	Strong N=N=N stretching
	1669.58	1685-1666	Strong C=O stretching
PLGA 50:50	2950.52	2960 - 2850	Chelated O-H stretching bridge
	1750.32	1800 – 1750	C=O stretching of the carbonyl group
PLGA 85:15	2996.25	3000 - 2500	Chelated O-H stretching bridge
	1746.64	1790 - 1740	Strong C=O stretching of the carbonyl group
AZT-PLGA 50:50 physical mixture	3461.12	3500 - 3300	Medium N-H stretching bands
	3023.15	3000 - 2500	Chelated O-H stretching bridge
	2814.57	3200 - 2500	O-H stretching
	2082.39	2160-2120	Strong N=N=N stretching
	1751.54	1770 - 1710	Strong C=O stretching
	1679.98	1685-1666	Strong C=O stretching
AZT-PLGA 85:15 physical mixture	3460.60	3500 - 3300	Medium N-H stretching bands
	3023.04	3000 - 2500	Chelated O-H stretching bridge
	2082.15	2160-2120	Strong N=N=N stretching
	1750.91	1770 - 1710	Strong C=O stretching
	1677.09	1685-1666	Strong C=O stretching

FT-IR spectra of pure PLGA 50:50 and PLGA 85:15 was the same as discussed in chapter 4 Figure 4.2 b & c. AZT on the other hand shared characteristic peaks similar to TDF (Figure 4.2a). Similarities such as N-H, and O-H groups at 3458.92 cm^{-1} and

2974.83 cm^{-1} stretching vibrations respectively, however AZT also presented with differences such as lack of the C=C (1752.31 cm^{-1}) found in TDF and the presence of N$_3$ group present at 2081.50 cm^{-1} in AZT but absent in TDF. These unique stretching areas were expected given the respective structures below.
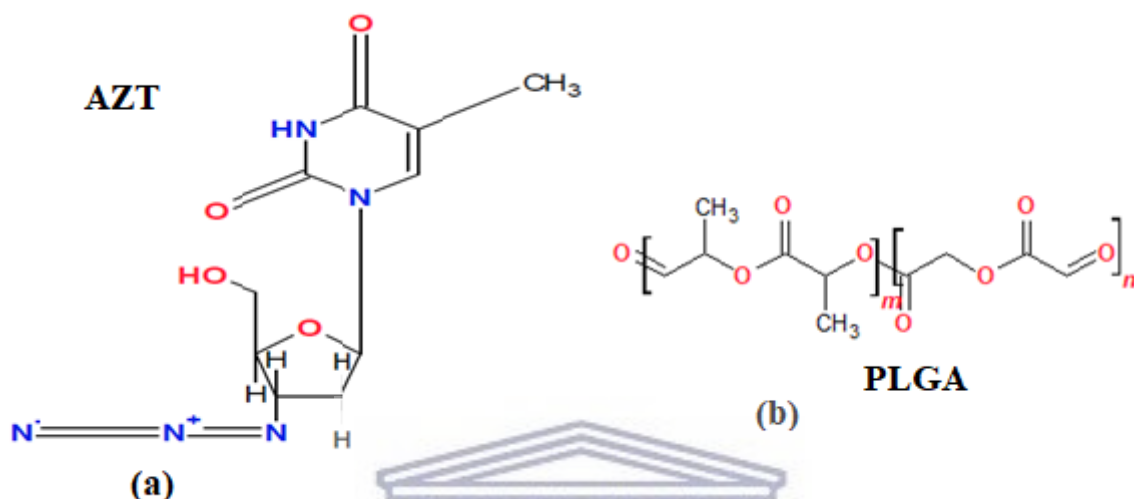
*Figure 5.1: Structure of (a) AZT and (b) PLGA (**n** represents the number of lactic acid units while **m** represents the number of glycolic acid units)*
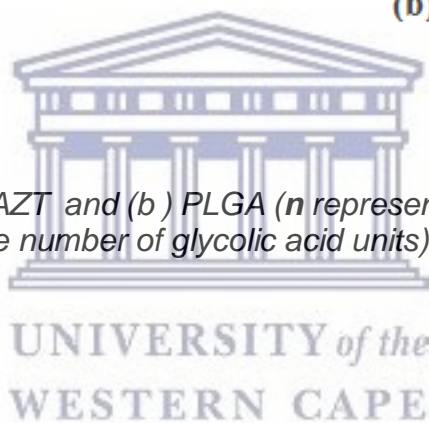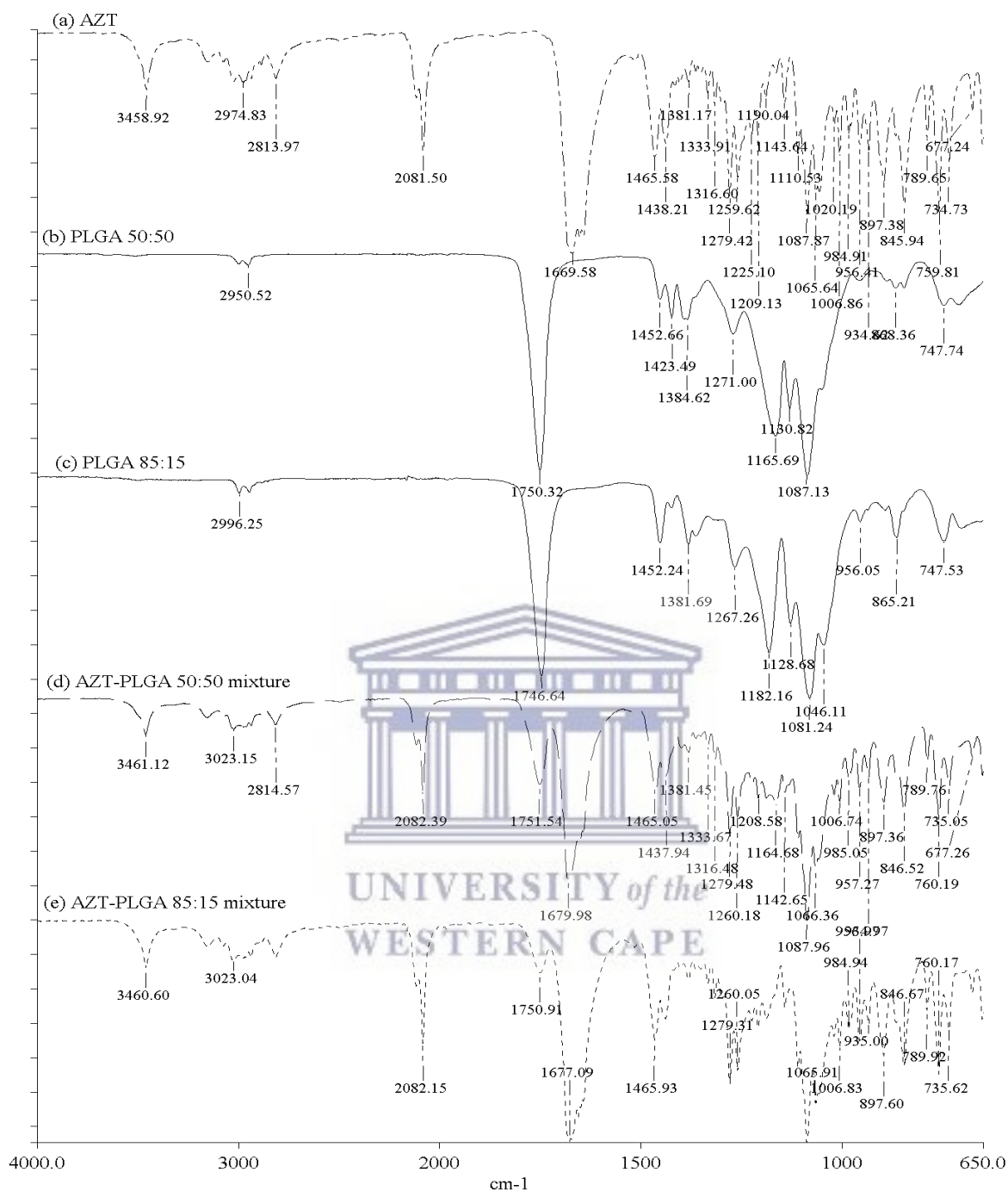
Figure 5.2: FT-IR spectra of (a) AZT, (b) PLGA 50:50, (c) PLGA 85:15, (d) AZT-PLGA 50:50 physical mixture, (e) AZT-PLGA 85:15 physical mixture

When compared to the FT-IR spectrum of either AZT or the polymer alone, the physical mixture of AZT-PLGA 50:50 and AZT-PLGA 85:15 (Figure 5.2(d) and (e), respectively) showed slight shifts in the bands of the resulting physical mixture as well as indicated some physiochemical interaction in the spectrum. AZT-PLGA 50:50

108

showed bands at 3461.12 cm^{-1}, attributed to OH stretching; at 3023.15 cm^{-1} which were attributed to C-H stretching vibration; at 2814.57 cm^{-1} which was attributed to strong CH$_3$ stretching vibration; at 2082.39 cm^{-1}, attributed to N$_3$ asymmetric stretching vibration; as well as at 1751.54 cm^{-1} and 1679.98 cm^{-1} which were attributed to C=O stretching vibrations. In Figure 5.2(e), AZT-PLGA 85:15 showed bands at 3460.60 cm^{-1} attributed to OH stretching; at 3023.04 cm^{-1} attributed to C-H stretching vibration; at 2082.15 cm^{-1} attributed to N$_3$ asymmetric stretching vibration; and at 1750.91 cm^{-1} and 1677.09 cm^{-1} attributed to C=O stretching vibrations. AZT-PLGA 85:15 also presented with the disappearance of the O-H stretching vibration (2813.97 cm^{-1}) which is present in the AZT-PLGA 50:50 physical mixture these may be because of the differences in PLGA ratios. No new peaks were observed, but the intensity of certain characteristic peaks such as 2950.52 cm^{-1} and 2996.25 cm^{-1} increased while those at 1750.32 cm^{-1} and 1746.64 cm^{-1} decreased in the physical mixture for PLGA 50:50 and PLGA 85:15 respectively when compared to the parent compound further confirming an interaction taking place.

Overall, both physical mixtures showed slight shifts and disappearance of characteristic peaks when compared to the parent compounds, thus indicating an interaction between AZT and PLGA.

5.2.2 Hot stage microscopy

The results presented below were obtained during sample analysis using hot stage microscopy (HSM). The compounds were analyzed individually as AZT, PLGA 50:50, PLGA 85:15, and in combination that is as a physical mixture of the polymer with AZT (mixed by grinding). The samples were heated up to a maximum temperature of 200°C at a temperature increase rate of 10°C per min.
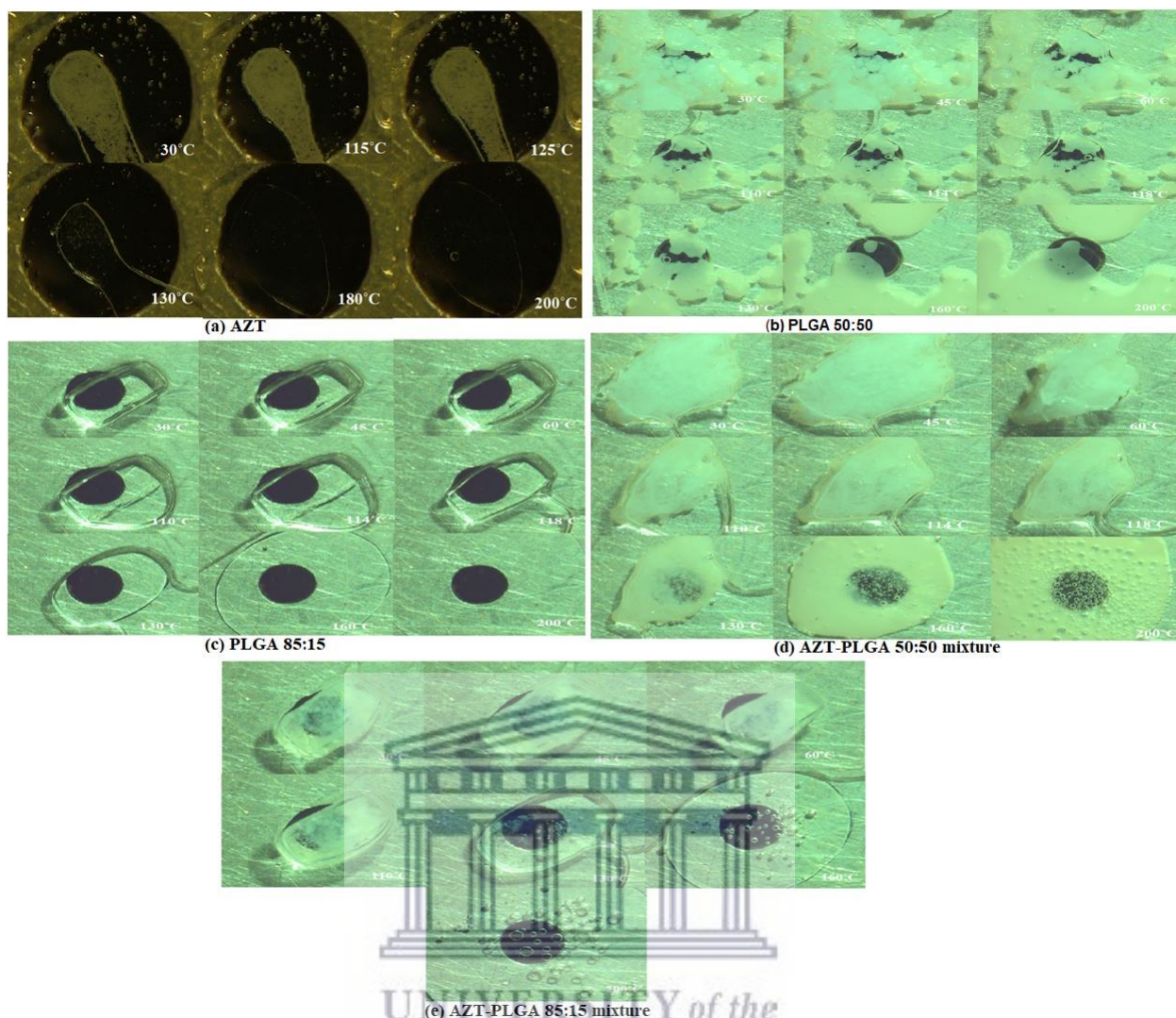
Figure 5.3: *HSM of (a)AZT, (b)PLGA 50:50, (c)PLGA 85:15, (d)AZT-PLGA 50:50 physical mixture, (e)AZT-PLGA 85:15 physical mixture*

Figure 5.3(a) shows images taken during HSM analysis of AZT. The melting of AZT commenced at 120°C and continued up till 125°C. No bubbles were observed during this process, indicating that no moisture was contained in the sample. At 130°C, the sample had completely melted. The degradation of AZT, observed by discoloration of the sample, started at about 180°C. The results obtained from this analysis were in line with the certificate of analysis which indicated that the melting point of AZT is between 120°C and 127°C. Figure 5.3b & c are HSM images of PLGA 50:50 and PLGA 85:15, which have been discussed in chapter 4, section 4.2.2.

110

Figure 5.3d shows HSM images of the copolymer and AZT physical mixture (AZT-PLGA 50:50). Melting commenced at about 30°C, with the appearance of bubbles observed at about 110°C. The appearance of bubbles was an indication of moisture being trapped under the slide covering the sample. Unlike the case with TDF-PLGA 50:50 physical mixture (Figure 4.3 d), the bubbles did not disappear, however; as noticed with TDF-PLGA 50:50 physical mixture, sign of degradation such as browning of the sample was noticed at a temperature of about 160°C.

Figure 5.3e shows images from HSM analysis of AZT and the polymer (AZT-PLGA 85:15 physical mixture). As with AZT-PLGA 50:50 physical mixture, melting commenced at about 30°C, with the appearance of bubbles, noticed at about 120°C. This temperature is around the melting point of AZT, thus confirming the presence of AZT in the physical mixture. The appearance of the bubble was an indication of moisture being trapped under the slide covering the sample. The bubbles did not disappear on continued heating but rather increased in size. Degradation, such as browning of the sample appeared at about 160°C. Since the initial polymer did not show any sign of degradation under HSM analysis (Figure 5.3c) whereas AZT degraded (Figure 5.3a), such degradation in AZT-PLGA 85:15 physical mixture could further infer the presence of AZT in the sample.

5.2.3 Thermogravimetric analysis (TGA)

Changes in thermal stability, organic solvent evolution and the degradation form of AZT, PLGA 50:50, PLGA 85:15, and a combination of both polymers with AZT (mixed by grinding) was evaluated using TGA. Figure 5.4 shows the curves obtained when the samples were analyzed. There was release of volatile species, and weight loss due to moisture was observed.
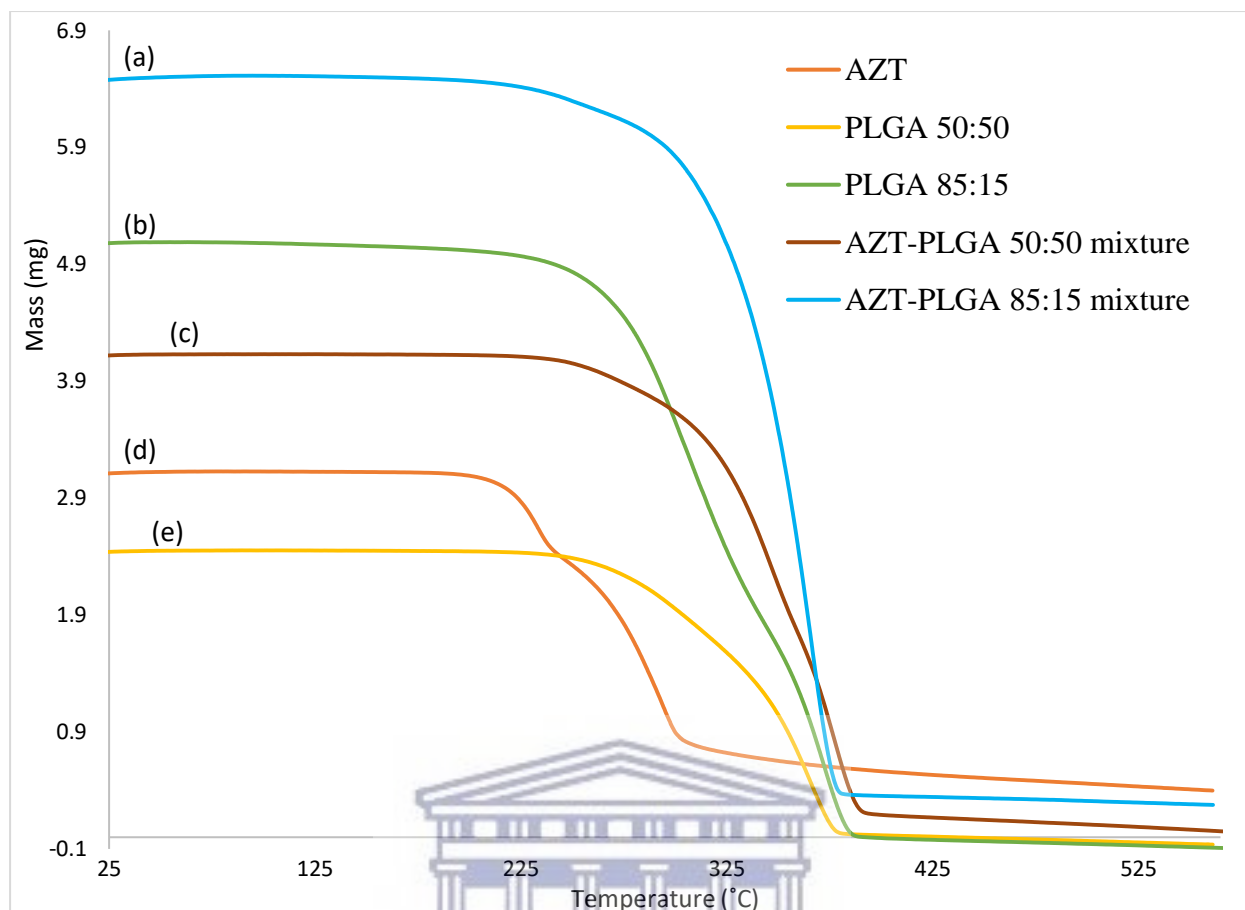
Figure 5.4*: TGA curves of (a) AZT-PLGA 85:15 physical mixture, (b) PLGA 85:15, (c) AZT-PLGA 50:50 physical mixture, (d) AZT, (e) PLGA 50:50*

Both polymers (PLGA 50:50 and PLGA 85:15) showed two mass loss events associated with the degradation process [Figure 5.4 (b) and (e)]. The first mass losses for PLGA 50:50 and PLGA 85:15 were about 30% and 65%, respectively. The second mass loss peak showed values of about 68% and 35% for PLGA 50:50 and PLGA 85:15, respectively. Unlike PLGA 85:15, PLGA 50:50 did not exhibit a 100% mass loss event; it had about 2% inert residue.

The drug-polymer physical mixtures (AZT-PLGA 50:50 and AZT-PLGA 85:15) were also analyzed via TGA [Figure 5.4 (a) and (c)]. The physical mixture with PLGA 50:50 showed two mass loss events while the physical mixture with PLGA 85:15 which showed a single mass loss event. The individual components (polymer and AZT)

showed two mass loss events. These differences in the TGA results between the individual components and the resulting physical mixture could be a result of differences in the polymer ratios and molecular weights (Appendix C, Table C1.8). The percentage weight loss for AZT-PLGA 50:50 and AZT-PLGA 85:15 were about 94% and 97%, respectively. The T_{onset} values however were at a lower temperature when compared to that of either polymer or AZT alone.

5.2.4 Differential Scanning Calorimetry (DSC)

Figure 5.5a presents the thermogram of AZT; the peak indicated that the melting point of AZT was about 124.80°C which was in accordance with the melting point of AZT in literature.[1] The thermograms for PLGA 50:50 and 85:15 Figure 4.5a are discussed in chapter 4 section 4.2.4.

(a)

(b)
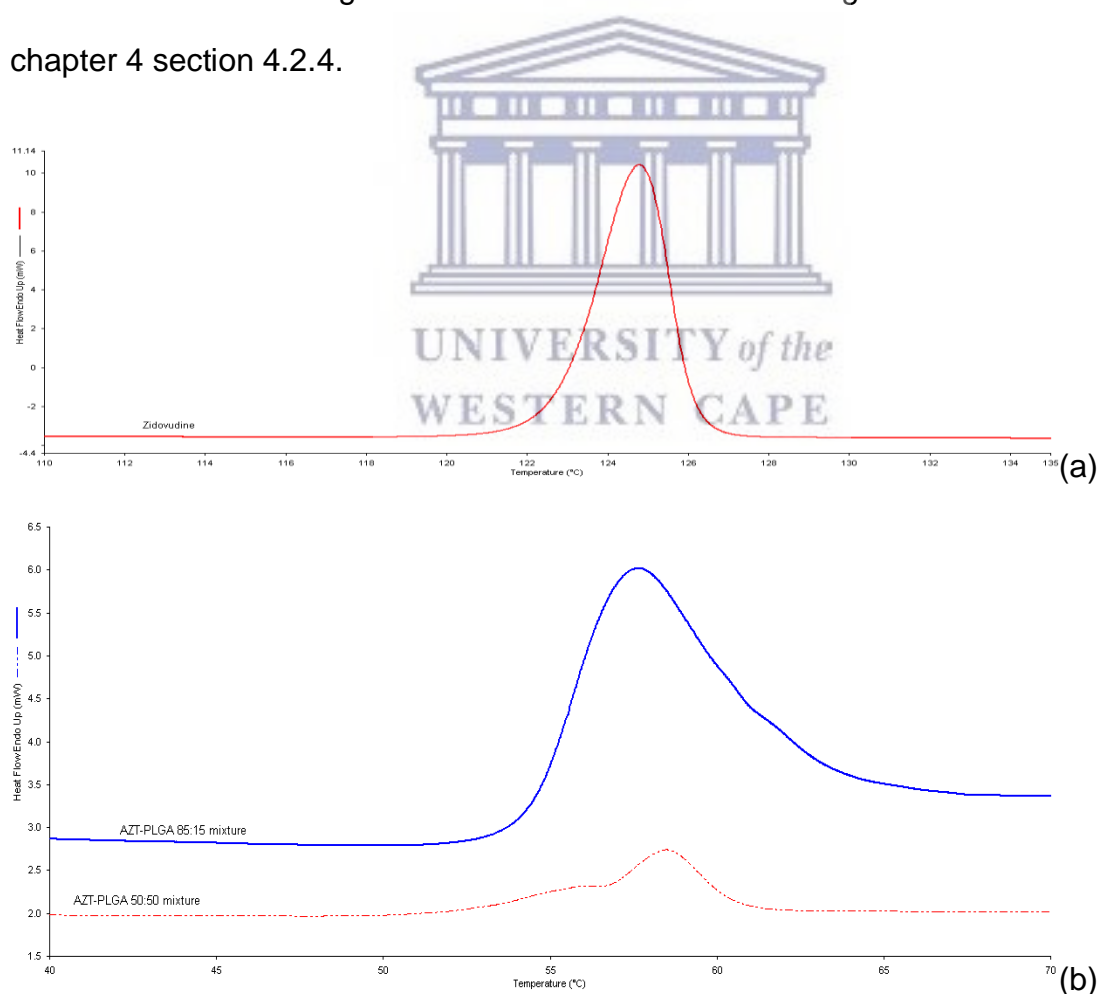
Figure 5.5: DSC Thermograms of Zidovudine, AZT-PLGA 50:50 and AZT-PLGA 85:15 physical mixtures

113

Figure 5.5b above presents thermograms of AZT when it was mixed and ground separately with PLGA 50:50 and PLGA 85:15. The thermograms indicated both physical mixtures had single peaks which indicated the melting point started from 57.48°C to 58.51°C for physical mixtures of AZT-PLGA 50:50 and AZT-PLGA 85:15 respectively. Comparing the physical mixture to PLGA alone (Figure 4.5), the plot indicated that the presence of AZT increased the stability of PLGA; however, a peak indicating the presence of AZT could not be seen. The lack of an AZT peak may perhaps be because too little of the AZT was used.

5.3   Formulation and characterization of AZT loaded nanoparticles

Figure 5.6 below shows diagrammatically each step in the formulation of AZT-loaded nanoparticles, formulation was done using the water-in-oil-in-water double emulsion solvent evaporation and diffusion method by Liu *et al.*, 2010 with modifications to decrease nanoparticle size and increase encapsulation efficiency.
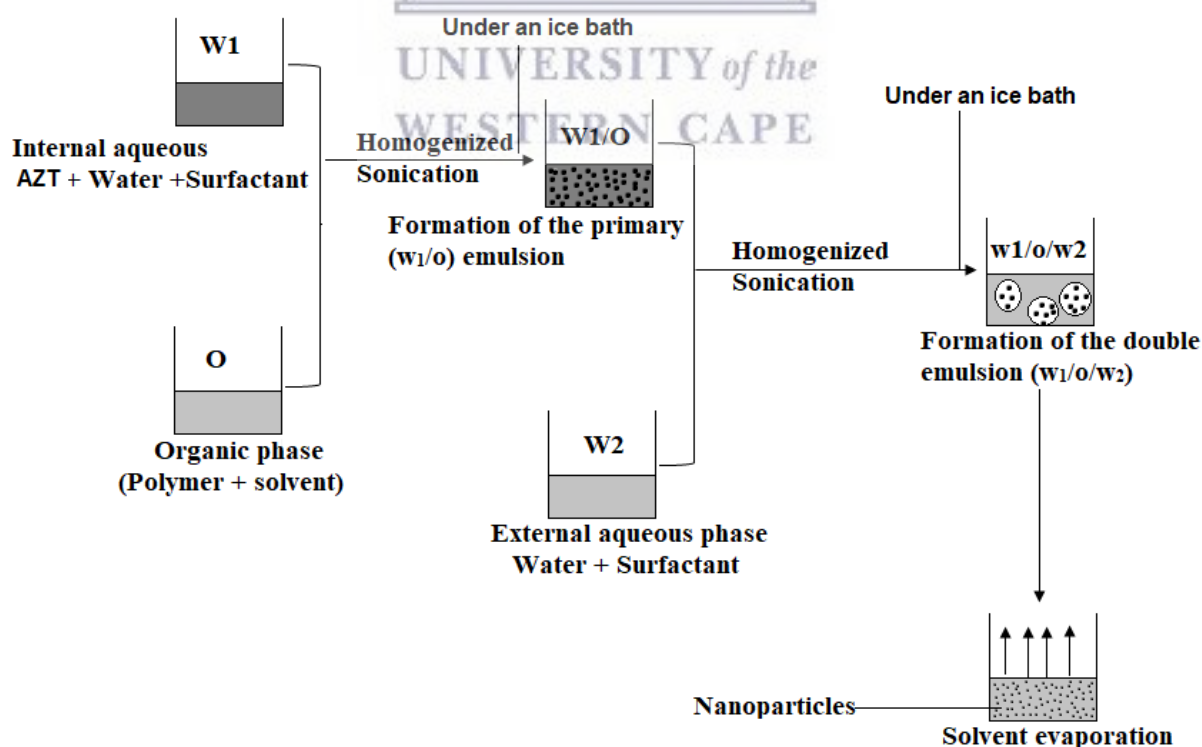
Figure 5.6: Schematic presentation of AZT-loaded nanoparticle formulation process

5.3.1 Particle size and distribution (polydispersity index, PDI)

The particle sizes of AZT-PLGA (50:50 and 85:15) loaded nanoparticles were measured, immediately after formulation and evaporation of the organic solvents from the sample, using dynamic light scattering (Malvern system). The mean particle sizes for AZT-PLGA 50:50 and AZT-PLGA 85:15 were found to be 110.6 ± 0.42 nm and 112.0 ± 2.43 nm, respectively (Table 5.2).

Table 5.2: *Particle size of AZT-loaded nanoparticles.*

Formulated nanoparticles	Particle size (nm)	
	Before wash	**After wash**
AZT-PLGA 50:50	110.6 ± 0.42	154.3 ± 3.1
AZT-PLGA 85:15	112.0 ± 2.43	160.4 ± 1.7

The postulated mechanisms to show how particles pass through the gastrointestinal and physiological barriers highlights endocytosis as one of the mechanisms, for particles < 500 nm. The particle sizes of the nanoparticles increased after they were washed three times with distilled water. The average size for AZT-PLGA 50:50 and AZT-PLGA 85:15 nanoparticles after washing was found to be 154.3 ± 3.1 nm and 160.4 ± 1.7 nm respectively (Table 5.2). The increase in particle size could be a result of the particle aggregation after surfactants and emulsifiers had been removed by the washing process. Particles size of formulated nanoparticles plays an important role in drug pharmacokinetics. The smaller the particle sizes of the drug / formulation, the higher the rate of particle absorption from the intestine into the blood stream.[1,2] A high uptake of particles can be expected because of the relatively small sizes of the nanoparticles formulated.

The polydispersity index (PDI) values for AZT-PLGA 50:50 and AZT-PLGA 85:15 after formulation were found to be an average of 0.165 ± 0.004 and 0.152 ± 0.015,

respectively. These values increased to 0.418 ± 0.004 and 0.376 ±0.17 for AZT-PLGA

50:50 and AZT-PLGA 85:15, respectively, after the washing process (Table 5.3).

Table 5.3: Polydispersity index of AZT-loaded nanoparticles.

Formulated nanoparticles	Polydispersity index	
	Before wash	After wash
AZT-PLGA 50:50	0.165 ± 0.004	0.418 ± 0.004
AZT-PLGA 85:15	0.152 ± 0.015	0.376 ± 0.17

The PDI values are indicative of a largely homogenous distribution of the

nanoparticles.[3] Values of PDI closer to one (1) indicate a heterogeneous distribution

of nanoparticles while values closer to zero (0) indicate a homogenous distribution of

nanoparticles[4] The increase in PDI value could be as a result of formulated pellets

fusing together after removal (washing off) of the surfactants and emulsifiers, hence

making the distribution more heterogeneous when compared to the characteristic prior

to the washing process.

5.3.2 Evaluation of surface morphology of the nanoparticle

The morphology (shape and properties) of the nanoparticles was determined using a

high-resolution scanning electron microscopy (HR-SEM). Figure 5.7 shows images of

blank nanoparticles of PLGA 50:50 and PLGA 85:15, AZT-PLGA 85:15 and AZT-

PLGA 50:50 loaded nanoparticles. [Figure 5.7 (a) and (b)] are blank HR-SEM images

of blank nanoparticles of PLGA 50:50 and PLGA 85:15, respectively; the images

showed the particles were spherical in shape with smooth surfaces.

Figure 5.7(c) shows HR-SEM images of AZT-PLGA 85:15 loaded nanoparticles. From

the image, it was observed that the particles were spherical in shape with smooth

surfaces, with an average particle size above 200 nm (which was greater than the

maximum size observed with the zeta sizer (160 nm). The increase in size might be a

result of aggregation and coalescence of the small nanoparticles. Such aggregating

116

and coalescing behavior may be a consequence of the freeze-drying process, which may cause the nanoparticles to irreversibly fuse, hence increasing the particle size. Freezing of the samples can also cause mechanical stress on the nanoparticles leading to a change in particle morphology. As earlier mentioned, (Section 4.3.2), aggregation of formulated nanoparticles may be minimized (Pirooznia *et al.*, 2012).
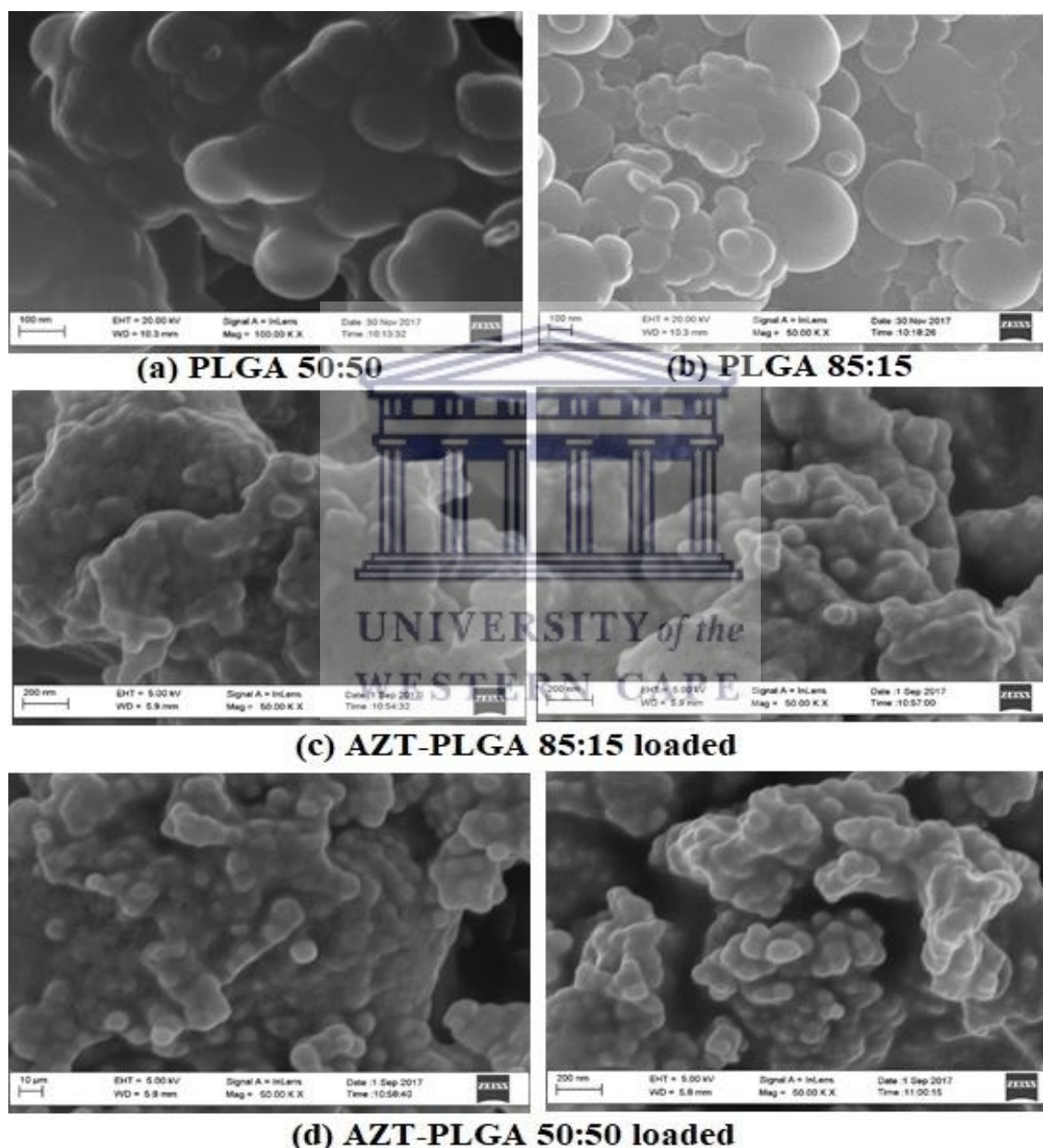
Figure 5.7: *HR-SEM of formulated nanoparticles (a) Blank PLGA 50:50, (b) Blank PLGA 85:15, (c) AZT-PLGA 85:15 loaded, and (d) AZT-PLGA loaded nanoparticles*

117

Figure 5.7d shows images of AZT-PLGA 50:50 loaded nanoparticles taken with HR-SEM. Similar characteristics to those of AZT-PLGA 85:15 (Figure 5.7c) were observed; the nanoparticle surface was smooth and spherical, with signs of aggregation and coalescence.

When Figure 5.7 (a) and (b) were compared to Figure *5.7*c and Figure 5.7d, the latter appeared to be less smooth and more coagulated; this might be as a result of the presence of AZT in the formulation.

5.3.3 Zeta potential

The zeta potential after formulation of the AZT-PLGA 50:50 and AZT-PLGA 85:15 loaded nanoparticles (Table 5.4) was determined using the Malvern system. The mean zeta potential for AZT-PLGA 50:50 and AZT-PLGA 85:15 were found to be -4.82 ± 0.62 mV and -5.41 ± 0.02 mV, respectively. These values had decreased to -15.3 ± 0.5 mV and -12.2 ± 0.6 mV, respectively, after washing of the samples, an indication that the stability of the nanoparticles had increased. The negative charge on the nanoparticles directly affects the cellular uptake of the nanoparticles by inducing a positive charge on the cell membrane, resulting in attraction between the two surfaces. This may result in higher bioavailability of AZT, as the drug-loaded nanoparticles may be better able to permeate the cell membrane and be transported to endosomes found within the cell.[6]

Table 5.4: *Zeta potential of AZT-loaded nanoparticles.*

Drug Polymer ratio	Zeta potential	
	Before wash	**After wash**
AZT-PLGA 50: 50	-4.82 ± 0.62 mV	-15.3 ± 0.5 mV
AZT-PLGA 85: 15	-5.41 ± 0.02 mV	-12.2 ± 0.6 mV

5.3.4 Percentage yield

After freeze drying, the AZT-PLGA 50:50 and AZT-PLGA 85:15 loaded nanoparticles were recovered and weighed. The values obtained after weighing were 83.1 mg and 67.02 mg, respectively (Table 5.5). The percentage yield, calculated as detailed in Equation 3.2,

$$Percentage\ yield(\%) = \frac{mass\ of\ nanoparticles\ recovered}{mass\ of\ PLGA, drug\ and\ excipients\ used\ in\ formulation} x100$$

$$Percentage\ yield(\%) = \frac{83.1}{105\ mg} x100$$

$$= 79.14\%\ for\ AZT\text{-}PLGA\ 50{:}50$$

$$Percentage\ yield(\%) = \frac{67.02}{105\ mg} x100$$

$$= 63.83\%\ for\ AZT\text{-}PLGA\ 85{:}15$$

The percentage yield was calculated to be 79.14% and 63.83%, respectively. The unbound polymer and drug could have been washed out and discarded during the washing process, resulting in the observed mass loss.

Table 5.5: *Mass of AZT-loaded nanoparticles recovered (mg) and percentage yield.*

Drug polymer combination	Mass of AZT used in formulation (mg)	Mass of polymer used (mg)	Mass of nanoparticle recovered (mg)	Percentage yield (%)
AZT-PLGA 50:50	5	100	83.1	79.14
AZT-PLGA 85:15	5	100	67.02	63.83

5.3.5 Standard calibration plot for determination of AZT (HPLC-DAD and UV-spectrometry method)

The linearity of the methods was determined by analyzing the samples at an absorbance frequency of 266 nm, at which AZT had been proven to have its maximum absorbance.[7] A linear regression model was used to study the relationship between

absorbance of AZT and its concentration, and a graph of mean AZT absorbance *versus* AZT concentration was plotted (Figure 5.8). This model enabled the prediction of AZT concentration in the prepared nano-formulations by measuring its absorbance in the sample; data obtained is featured in appendix C (Table C1.6 and Table C1.7)
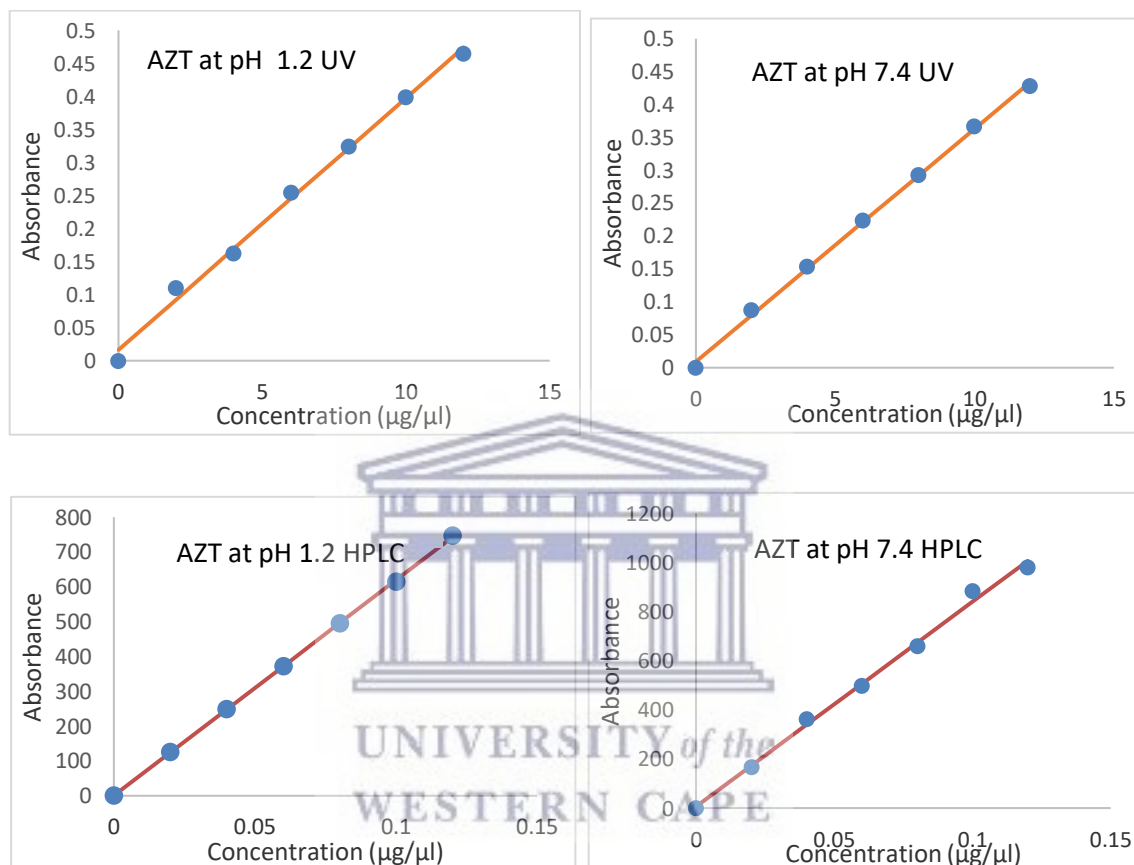
Figure 5.8: Standard calibration graph of Zidovudine ($λ_{max}$=266nm).
Stock solutions and working standards were prepared in PBS at a pH of 1.2 and pH 7.4. Samples were analyzed at 25⁰C. Data values were recorded in triplicate and are presented as mean ± SD (n=3)*.*

Table 5.6 presents computed data derived from plotting the calibration curves for AZT. The R^2 values at pH 1.2 and pH 7.4 depicted linearity and showed how close the data was to the fitted regression line. The relationship between concentration and absorbance can be expressed using Equation 5.1 with substitutions from Table 5.6

120

the amount of drug encapsulated within the nanoparticles was determined. Data obtained is featured in appendix C (Table C1.6 and Table C1.7).

$$y = intercept + slope(x)$$

Equation 5.1

Where y = AZT peak area

x = the standard solution concentration in µg/ml

Table 5.6: Linearity data and quantification limits of AZT at pH 7.4 and 1.2 (HPLC-DAD and UV-spectrometry methods).

Validation parameters	HPLC-DAD		UV-spectrometry	
	pH 1.2	pH 7.4	pH 1.2	pH 7.4
R^2	0.9999	0.9979	0.9951	0.9986
Slope ± SD	6181.304±27.59	8334.304±241.78	0.0381±0.0012	0.0654±0.00058
Intercept ± SD	0.8246±1.99	6.1803±17.44	0.0164±0.0086	0.00921±0.0042
Concentration range (µg/ml)	0.02-0.12	0.02-0.12	200-1200	200-1200
LOD (µg/ml)	0.001	0.007	0.75	0.40
LOQ (µg/ml)	0.001	0.021	2.26	1.19

Unlike what was obtained with the calibration plot for TDF, HPLC-DAD did not necessarily present better linearity values than analyses done with UV-spectrometry. The values obtained at pH 7.4 were also not necessarily better than those obtained at pH 1.2. It seems the HPLC-DAD method was more precise than the UV-spectrometry method at pH 1.2, while the UV-spectrometry method was more precise than the HPLC-DAD method at pH 7.4. However, the concentration ranges, as well as the LOD and LOQ values are lower for the HPLC-DAD method than for the UV-spectrometry

method (as was obtained with TDF analyses), attesting to the increased sensitivity of the HPLC-DAD compared to the UV-spectrometry method.

Repeatability, precision and accuracy of the methods (HPLC-DAD and UV-spectrometry methods) were assessed by analyzing replicates of AZT standard solution over a period of three days. Three different concentrations (0.02,0.06, 0.12 and 2, 6 and 12 μg/ μl) covering the standard calibration range of AZT were selected and analyzed to determine the inter-day and intra-day variability as shown in Table 5.7 and Table 5.8. The intermediate precision and precision of the method at both pH 1.2 and 7.4 were expressed as % RSD and found to be less than 2% for both HPLC-DAD and UV-spectrometry which suggested that the above methods were reproducible.

Table 5.7: Intra-day and inter-day assay precision and accuracy for Zidovudine at pH 1.2 and 7.4 (HPLC-DAD method)

	pH 1.2			pH 7.4		
AZT (µg/ µl)	0.02	0.06	0.12	0.02	0.06	0.12
Intra-day (n=3)						
Day 1						
Mean	0.0203	0.0599	0.1207	0.0192	0.0591	0.1167
SD	0.0002	0.0010	0.0012	0.0001	0.0008	0.0020
Precision[1] (%)	0.99	1.67	0.99	0.52	1.40	1.70
Accuracy[2] (%)	101.5	99.8	100.58	96	98.5	97.25
Day 2						
Mean	0.0204	0.0600	0.1205	0.0193	0.0591	0.1167
SD	0.0004	0.0010	0.0020	0.00012	0.0008	0.0005
Precision[1] (%)	1.96	1.67	1.66	0.62	1.35	0.43
Accuracy[2] (%)	102.00	100.00	100.4	96.5	98.5	97.3
Day 3						
Mean	0.0201	0.0597	0.1207	0.0190	0.0588	0.1166
SD	0.0001	0.0009	0.0018	0.0002	0.0003	0.0007
Precision[1] (%)	0.50	1.51	1.49	1.05	0.50	0.60
Accuracy[2] (%)	100.5	99.5	100.6	95	98	97.2
Inter-day (n=9)						
Mean[3]	0.0203	0.0599	0.1206	0.0192	0.059	0.1167
SD	0.00012	0.00012	0.000094	0.00012	0.00014	0.000047
Precision[1] (%)	0.59	0.20	0.08	0.63	0.24	0.04
Accuracy[2] (%)	101.5	99.83	100.5	96	98.33	97.25

The results for accuracy (expressed as percentage of the mean determined concentration / nominal concentration) fell within the range, 95-102%. The acceptable mean recovery range in assays for quality control and drug registration is between 90

and 110%.[7] Thus, the accuracy and validity of the HPLC-DAD and UV-spectrometry method for AZT analyses was proven.

Table 5.8: Intra-day and inter-day assay precision and accuracy for Zidovudine at pH 1.2 and 7.4 (UV-spectrometry method).

	pH 1.2			pH 7.4		
AZT (µg/ µl)	2	6	12	2	6	12
Intra-day (n=3)						
Day 1						
Mean	0.0920	0.2547	0.4644	0.0820	0.2303	0.4630
SD	0.0007	0.0001	0.0007	0.0001	0.0001	0.0002
Precision[1] (%)	0.76	0.04	0.15	0.14	0.04	0.05
Accuracy[2] (%)	99.12	104.1	97.9	102.8	104.1	106.8
Day 2						
Mean	0.0923	0.2546	0.4656	0.0779	0.2185	0.44697
SD	0.0018	0.0002	0.0002	0.0002	0.0002	0.0003
Precision[1] (%)	1.95	0.08	0.04	0.26	0.10	0.07
Accuracy[2] (%)	99.52	104.1	98.16	97.0	98.5	103.1
Day 3						
Mean	0.0924	0.2543	0.4637	0.0804	0.2193	0.4391
SD	0.0015	0.0003	0.0029	0.000006	0.0001	0.00064
Precision[1] (%)	1.62	0.12	0.63	0.07	0.05	0.15
Accuracy[2] (%)	99.65	104.0	97.75	100.6	99.0	103.1
Inter-day (n=9)						
Mean[3]	0.0922	0.2545	0.4646	0.080121	0.22271	0.449701
SD	0.0002	0.0002	0.0010	0.002083	0.006584	0.012198
Precision[1] (%)	0.22	0.08	0.22	2.60	2.96	2.71
Accuracy[2] (%)	99.39	104.06	97.94	100.2	100.5	103.7

The values in Table 5.7 and Table 5.8 was calculated as follows;

❖ [1]Expressed as % RSD = (SD/mean) × 100.

❖ [2]Calculated as (mean determined concentration/nominal concentration) × 100.

❖ [3]n = 3 days with three replicates per day

5.3.6 Encapsulation efficiency

The encapsulation efficiency was determined using Equation 3.6,

$$Encapsulation\ efficiency(\%)$$

$$= \frac{total\ amount\ of\ drug\ in\ the\ yield}{amount\ of\ drug\ added\ during\ encapsulation}\ x100$$

$$Encapsulation\ efficiency(\%)\ =\ \frac{3.69}{5}\ x100$$

= 73.82% for AZT-PLGA 50:50

$$Encapsulation\ efficiency(\%)\ =\ \frac{2.38}{5}\ x100$$

= 47.6% for AZT-PLGA 85:15

Table 5.9 below presents the encapsulation efficiency and the total amount of drug in the yield. This was determined by dissolving 5 mg of the AZT-loaded nanoparticles in 0.5 ml of ethyl acetate (in a 5 ml Eppendorf tube) with vortexing. The ethyl acetate was evaporated, and 3 ml of phosphate buffer solution (PBS) was added to the Eppendorf tube. The tube was vortexed, and the contents centrifuged at a speed of 10000 rpm for 15 minutes. Thereafter, the supernatant was collected, and the absorbance measured using the UV-spectrometer and HPLC-DAD system. The concentration of the drug in that sample was determined by extrapolating the absorbance value from the calibration plot of AZT in Figure 5.8.

Table 5.9: *Total amount of AZT in recovered nanoparticles and encapsulation efficiency*

Drug polymer combination	Amount of drug in nano-formulation (mg)	Encapsulation efficiency (%)
AZT-PLGA 50:50	3.69	73.82
AZT-PLGA 85:15	2.38	47.6

125

the above results indicated that formulation with PLGA 50:50 showed about 26.22% increase in encapsulation efficiency of AZT when compared to formulation with PLGA 85:15. Possible reasons for this could be the differences in the molecular weights and polymer ratios of PLGA 50:50 and PLGA 85:15. The encapsulation efficiency of AZT-PLGA 85:15 suggested that less than half the initial amount of AZT used during the formulation process was recovered after formulation. The amount of AZT lost might be because of un-encapsulated drug discarded during the washing process.

5.3.7 Drug entrapment efficiency

The theoretical, actual loading and drug entrapment efficiency were calculated using the following equations;

Equation 3.3,

$$Theoretical\ drug\ loading\ (TDL)(\%) = \frac{weight\ of\ drug\ added}{weight\ of\ polymer\ and\ drug\ added}\ x\ 100$$

$$Theoretical\ drug\ loading\ (TDL)(\%) = \frac{5}{105}\ x\ 100$$

$$= 4.76\%\ for\ both\ AZT\text{-}PLGA\ 50{:}50\ and\ 85{:}15$$

Equation 3.4

$$Actual\ drug\ loading\ (\%) = \frac{weight\ of\ drug\ in\ nanoparticles}{weight\ of\ nanoparticles}\ x100$$

$$Actual\ drug\ loading\ (\%) = \frac{3.69}{83.1}\ x100$$

$$= 4.44\%\ for\ AZT\ for\ PLGA\ 50{:}50$$

$$Actual\ drug\ loading\ (\%) = \frac{weight\ of\ drug\ in\ nanoparticles}{weight\ of\ nanoparticles}\ x100$$

$$Actual\ drug\ loading\ (\%) = \frac{2.38}{67.02}\ x100$$

$$= 3.57\%\ for\ AZT\text{-}PLGA\ 85{:}15$$

and Equation 3.5,

$$Drug\ Entrapment\ efficiency(\%) = \frac{actual\ drug\ loading}{theoretical\ drug\ loading} x100$$

$$Drug\ Entrapment\ efficiency(\%) = \frac{4.44}{4.76} x100$$

$$= 93.23\%\ for\ AZT\text{-}PLGA\ 50\text{:}50$$

$$Drug\ Entrapment\ efficiency(\%) = \frac{3.57}{4.76} x100$$

$$= 75\%\ for\ AZT\text{-}PLGA\ 85\text{:}15$$

Table 5.10 below presents data derived from the above calculations. The formulation with PLGA 50:50 showed higher encapsulation of the drug compared to the formulation with PLGA 85:15. The reasons for the difference in entrapment efficiency are yet unknown, our hypothesis (similar to that with the TDF formulations) is that this might be as a result of differences in the polymer ratios. The significance of this difference was however not calculated.

Table 5.10: *Actual and theoretical drug loading values, and drug entrapment efficiency of TDF-PLGA formulations.*

Drug polymer combination	Theoretical drug loading (% w/w)	Actual drug loading (% w/w)	Drug entrapment efficiency (% w/w)
AZT-PLGA 50:50	4.76	4.44	93.23
AZT-PLGA 85:15	4.76	3.57	75

5.3.8 Fourier Transform Infrared Spectroscopy (FT-IR)

Figure 5.9 (c) and (d) present data from the FT-IR analysis of AZT-PLGA 50:50 and AZT-PLGA 85:15 loaded nanoparticles, respectively. The different intensity peaks showed that AZT was encapsulated within the polymer because, when compared to the FT-IR data obtained prior to formulation (Figure 5.9a and b), the characteristic intensity bands mostly corresponded to the polymer. The loaded AZT-PLGA 50:50 and AZT-PLGA 85:15 nanoparticles (Figure 5.9c & d) produced significantly less pronounced spectra. In the FT-IR spectra of the nano-formulation several peaks once

again shifted (compared to the parent compound), disappeared and even new peaks appeared (comparatively to the physical mixtures). What this suggests is a clear indication of a more pronounced interaction between AZT and the polymers as well as that the polymer is indeed loaded with AZT.

Figure 5.9d showed the appearance of an extra intensity peak at 2995.93 cm^{-1}. This peak was not present in Figure 5.9c and may be because of differences in the polymers used. The loaded nanoparticles also indicated the disappearance of certain peaks such as at 3461.12 cm^{-1} and 3460.60 cm^{-1} (N-H stretching vibration), 2814.57 cm^{-1} (O-H stretching) as well as 1751.54 cm^{-1} and 1750.91 cm^{-1} (C=O stretching) for AZT-PLGA 50:50 and AZT-PLGA 85:15 respectively. Figure 5.10 indicates the possible functional groups that may interact between AZT and PLGA based on the FTIR analysis obtained below.
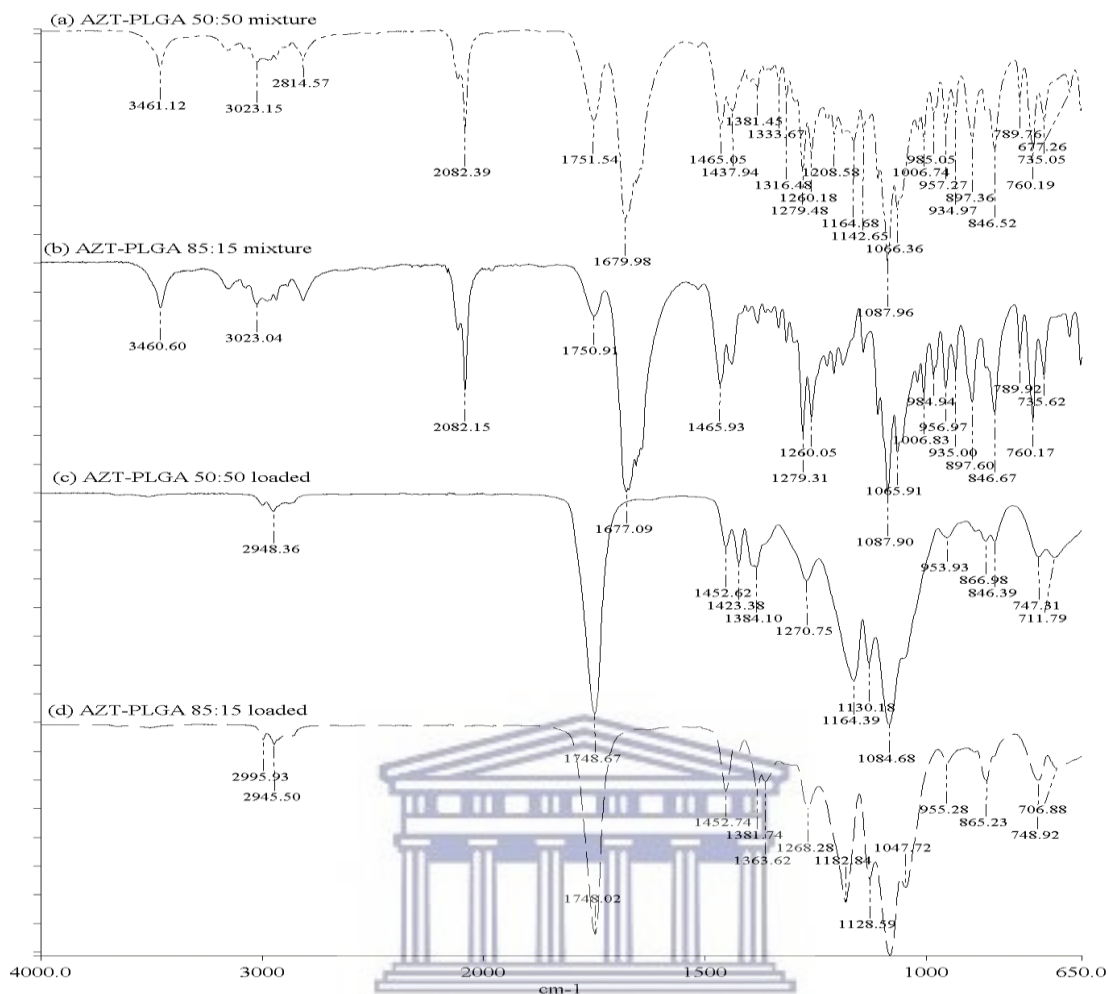
Figure 5.9**:** *FT-IR spectra of (a) AZT-PLGA 50:50 physical mixture, (b) AZT-PLGA 85:15 physical mixture, (c) AZT-PLGA 50:50 loaded, and (d) AZT-PLGA 85:15 loaded nanoparticles*
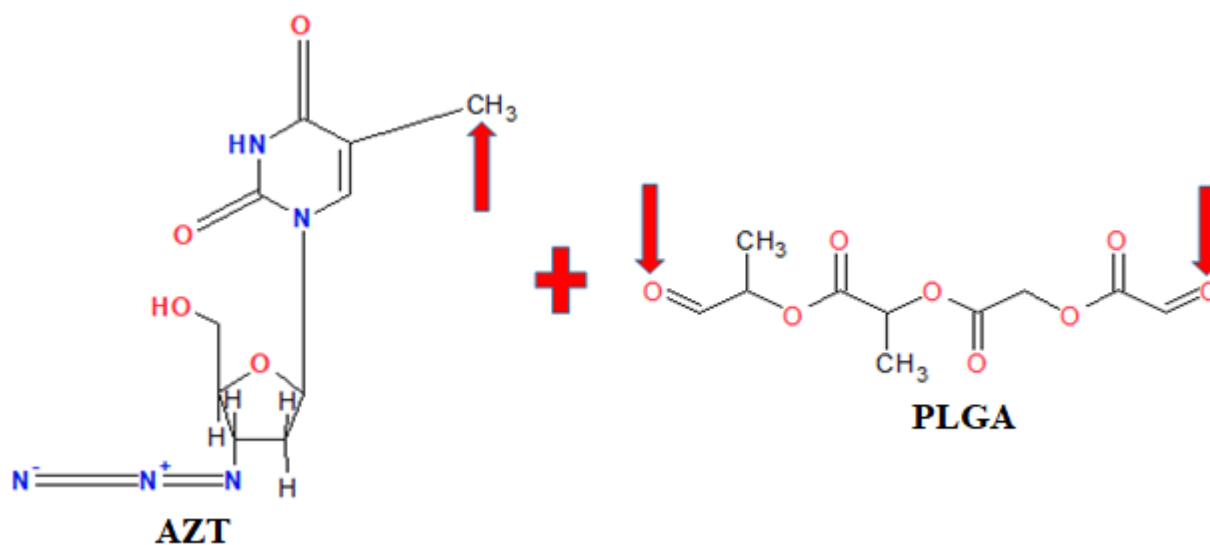
Figure 5.10: *Schematic representation of possible functional group interactions between AZT and PLGA*

129

5.3.9 Hot stage microscopy

Following collection of the freeze-dried AZT-loaded nanoparticles, the samples were analyzed using HSM. Figure 5.11a & b (AZT-PLGA 50:50 and AZT-PLGA 85:15 physical mixtures) are as discussed in section 5.2.2 (Figure 5.3 d and e), respectively. Figure 5.11c shows images from the HSM analysis of AZT-PLGA 50:50 loaded nanoparticles. Melting of the sample with increase in temperature was noticeable around 45°C; however, sample melting was challenging to visualize. At 110°C, clear change such as melting of the sample was observed. There was no appearance of bubbles or visible degradation of the sample; this may be explained by the inference that the polymer completely encapsulated AZT and therefore protected it from degradation. It could also be because the amount of AZT in the formulation was too small for the degradation process to be visualized. At temperatures above 130°C, the sample appeared oily and viscous with no further changes observed with increase in temperature.
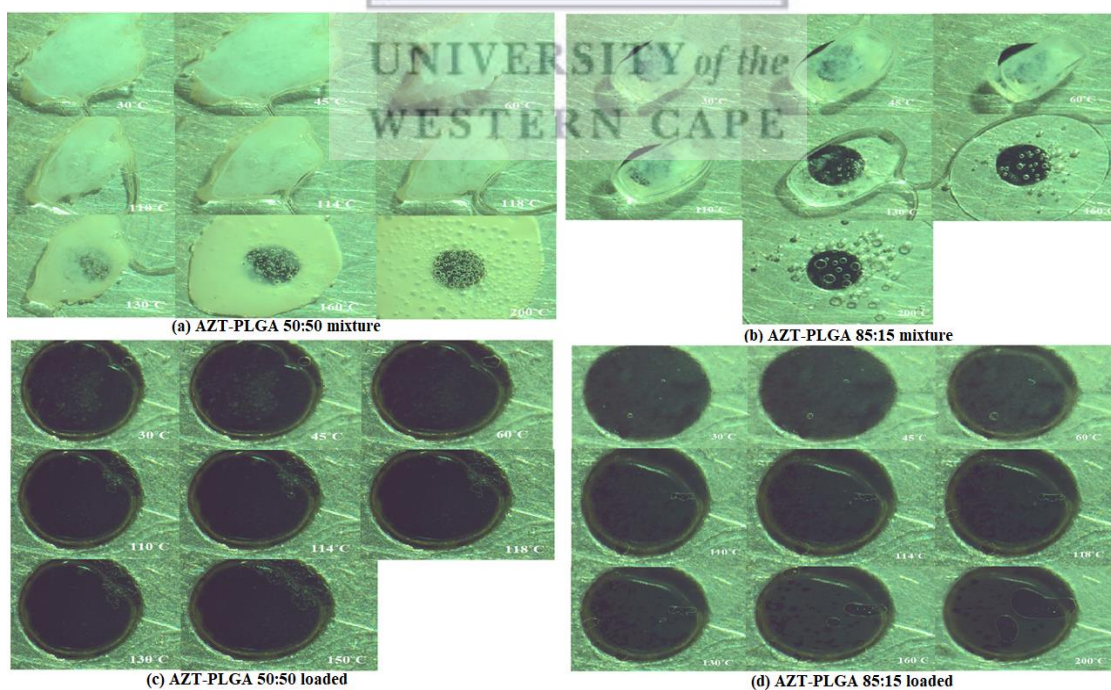
Figure 5.11: HSM images of (a) AZT-PLGA 50:50 physical mixture, (b) AZT-PLGA 85:15 physical mixture, (c) AZT-PLGA 50:50 loaded and (d) AZT-PLGA 85:15 loaded

Figure 5.11d above presents images from the HSM analysis of AZT-PLGA 85:15 loaded nanoparticles. Melting of the sample with increase in temperature was a bit difficult to visualize at temperature changes between 30°C and 60°C; however, noticeable change such as melting of the sample was observed at temperatures above 110°C. There was no appearance of bubbles, and no visible degradation of the sample was observed. This could possibly be explained by the fact that the polymer completely encapsulated AZT and therefore protected it from degradation. It may also be that the amount of AZT in the formulation was too small for the degradation process to be visualized. Unlike the case with AZT-PLGA 50:50 nano-formulation, the sample appeared to dry up when the temperature increased above 130°C.

5.3.10 Thermogravimetric analysis (TGA)

In Figure 5.12, data from the TGA of AZT-PLGA 50:50 and AZT-PLGA 85:15 loaded nanoparticles are presented. The AZT-PLGA 50:50 loaded nanoparticles exhibited a single mass loss event unlike AZT-PLGA 85:15 loaded nanoparticles which exhibited two mass loss events. This can be attributed to differences in polymer ratios and their molecular weights. During pre-formulation analysis however, the reverse was the case; the physical mixture of AZT-PLGA 50:50 exhibited two mass loss events while AZT-PLGA 85:15 exhibited a single mass loss event.
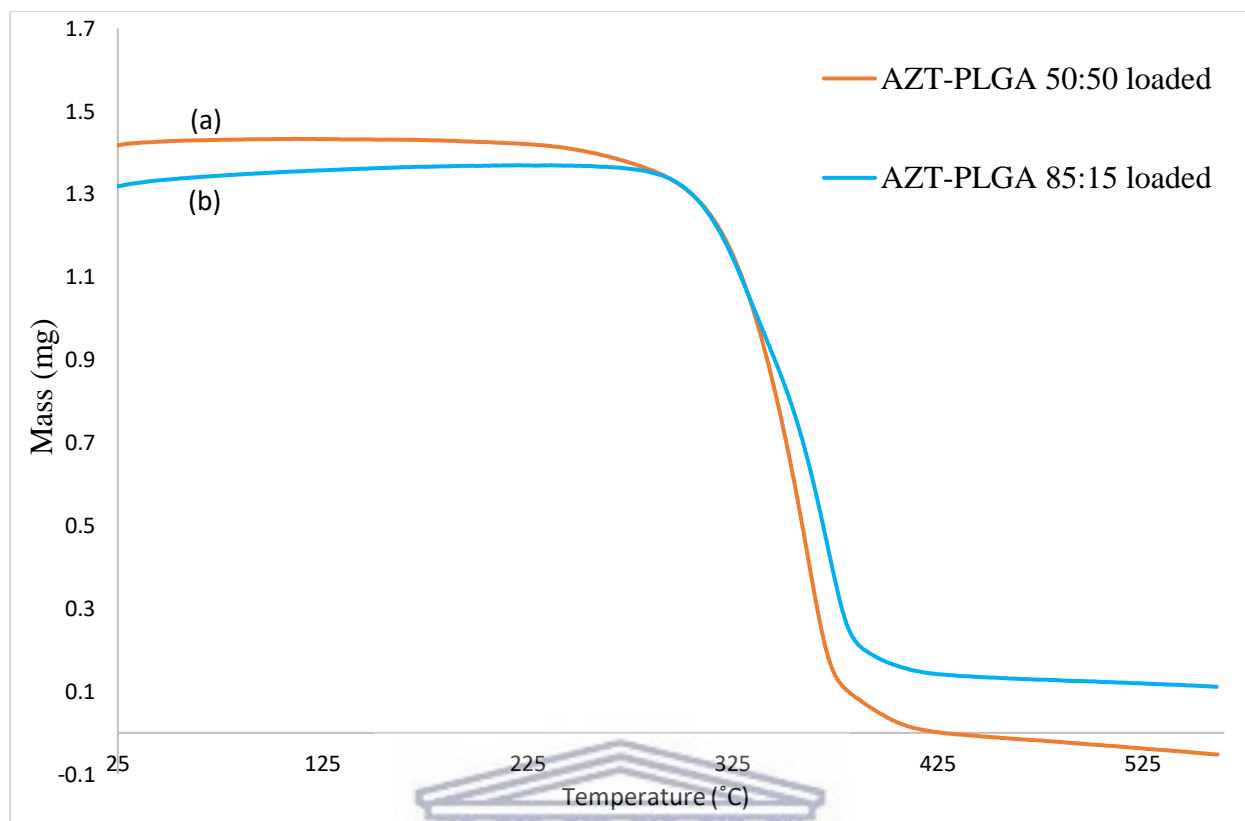
Figure 5.12: TGA curve of (a) AZT-PLGA 50:50 loaded and (b) AZT-PLGA 85:15 loaded nanoparticles.

These differences could perhaps be a result of insufficient trituration of the physical mixture and its components. It may also be due to a change in thermal stability of the products. These are only hypothetical currently; hence, may require further investigation.

Table C1.10 appendix C presents data from the thermal analyses of AZT formulated nanoparticles.

5.3.11 Differential Scanning Calorimetry (DSC)

Figure 5.13 shows thermograms of AZT-PLGA 50:50 and AZT-PLGA 85:15 loaded nanoparticles. As was the case with TDF, no identifiable peaks of AZT could be seen in the thermograms. The reason for this could be that no crystalline AZT was found in the nanoparticles. It may also indicate that the amount of AZT present in the sample was too small to show any peaks, or that AZT is molecularly dispersed in the polymer

matrix. The loaded nanoparticles showed peaks that were present when AZT physical mixtures were analyzed (Figure 5.5b), with melting points of 55.25°C and 56.09°C for AZT-PLGA 85:15 and AZT-PLGA 50:50 respectively. It is however not known if these differences in temperature are significant.
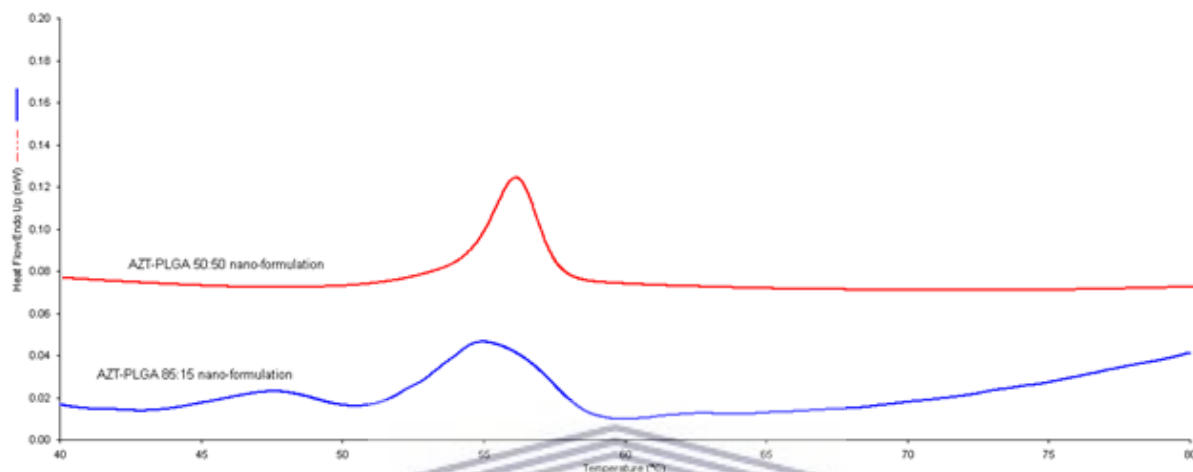
Figure 5.13: DSC thermograms of AZT-PLGA 50:50 and AZT-PLGA 85:15 loaded nanoparticles

5.3.12 Determination of AZT release from AZT-PLGA loaded nanoparticles

Figure 5.14 shows the cumulative percentage of AZT released from AZT-PLGA loaded nanoparticles at a pH 1.2 and pH 7.4 *versus* time. Samples were analyzed using two analytical methods, HPLC-DAD and UV-spectrometry. The release profiles from both analytical methods showed a biphasic release model with an initial burst of AZT followed by sustained release. This is typical of core-shell type nanoparticles.[8] The release profile also confirmed the presence of surface drug present on the nanoparticles, with the bulk of the AZT encapsulated within the nanoparticles. With such release kinetics, some level of extended release may possibly be obtained from the AZT-PLGA formulations. If this is the case, there may be no need for twice daily

dosing of AZT, thus making a formulation with once daily dosing, which can improve

patient compliance and adherence to therapy.

(a)

(b)

(c)

(d)
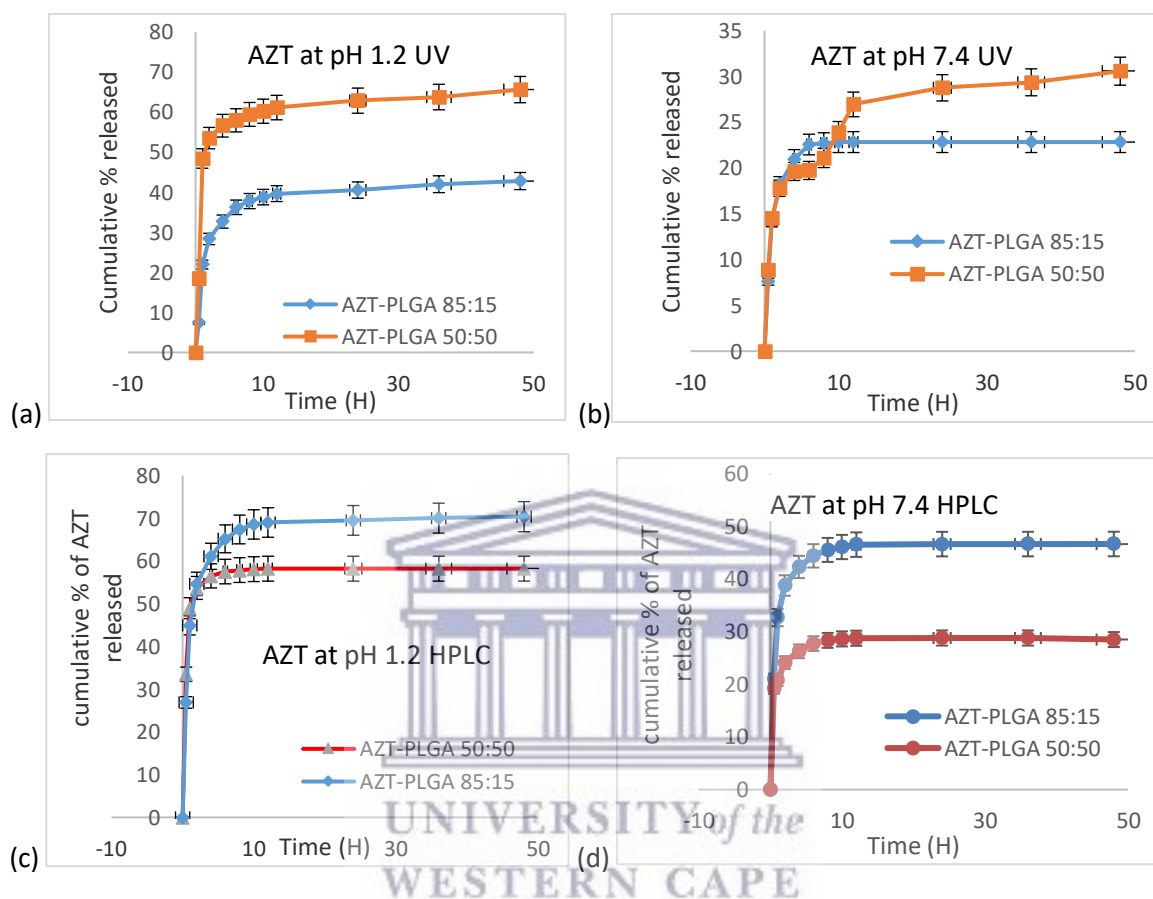
Figure 5.14: In-vitro release of AZT-PLGA 50:50 and AZT-PLGA 85:15 loaded nanoparticles

The release studies were done at pH 1.2 (Figure 5.14 a & c) and pH 7.4 (Figure 5.14

b & d) at 37˚C over a period of 48h, using the UV-spectrometry (Figure 5.14 a & b)

and HPLC-DAD (Figure 5.14 c & d) analytical methods. Data was collected in

triplicates and presented as mean ± SD (n=3).

Table 5.11 indicates an approximation of the total percentage of AZT released within

12 hours. Drug release from the same sample was quantified using two analytical

equipment's. Some differences were observed when the release curves from one

method were compared to the other method. Could this be a result of human error, or some other reason not yet fully understood?

Table 5.11: Percentage of AZT released (12 hours analysis)

AZT	HPLC-DAD		UV-spectrometry	
	pH 7.4	pH 1.2	pH 7.4	pH 1.2
PLGA 50:50	28.7 %	58%	27%	61%
PLGA 85:15	46.1%	68%	23%	39%

After the initial burst, more of AZT was released from the nano-formulations over a period of time before a constant release was attained. The release profiles of both formulations indicated that more of AZT was released from the AZT-PLGA 85:15 formulation when compared to the AZT-PLGA 50:50 formulation at pH 1.2 and pH 7.4 when analyzed using the HPLC-DAD method; however, the reverse was the case when the sample was analyzed using UV-spectrometry. This difference may be due to differences in the different polymers with respect to molecular weight, ratio and composition.
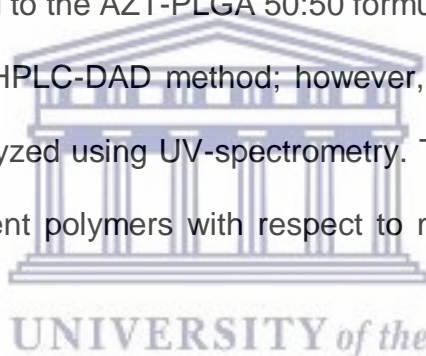
5.3.13 Mathematical modeling of drug release data

The release mechanism of AZT from AZT-PLGA formulated nanoparticles was evaluated by fitting the release data to four mathematical models, namely; Gompertz model, Korsmeyer-Peppas model, Peppas-Sahlin model, and Weibull model. DDsolver, a peer-reviewed modelling program [9], was used for this analysis. The release data was fitted to each of the four mathematical models listed above; these models are the ones commonly used in literature.[10]

The best fit model was selected by using the adjusted coefficient of determination (R^2 adj) and a model with the highest R^2 adj was deemed to be the best fitting model. R^2 adj allows for better comparison of the models when compared to the coefficient of

determination (R^2).[11] The release data of AZT obtained at both pH 1.2 and 7.4 was fitted to the four models mentioned above and it was determined that a majority of the formulations (3 out of 4) were best fit by the Weibull model. The exception was AZT-PLGA 50:50 at pH 7.4 whose best fit model (according to the R^2 adj value) was the Peppas-Sahlin model (Table 5.12).

Table 5.12 below presents parameter values and R^2adj values obtained from fitting drug release experimental data to the four mathematical models. The asterisked values correspond to the highest value of R^2adj obtained when the four models were compared, for each sample.

Parameters explaining the Weibull model are as discussed in chapter 4 section 4.3.13, The following samples were best fitted by Weibull model AZT-PLGA 85:15 at pH 7.4, AZT-PLGA 50:50 and AZT-PLGA 85:15 at pH 1.2, All three sample models displayed a **β** value less than 0.75, which implied that the release mechanism was by Fickian diffusion.

Parameters in Peppas-Sahlin can be described as follows **K1** is the constant that is related to Fickian kinetics (Fickian diffusion), **K2** is the constant that is related to case-II relaxation kinetics (matrix relaxation/erosion) and **m** is the diffusional exponent (ranges between 0 and 1).

As mentioned earlier, AZT-PLGA 50:50 at pH 7.4 did not fit with the other release data for Weibull model; its model of best fit was the Peppas-Sahlin model (Table 5.12). The release parameters for AZT-PLGA 50:50 under the Peppas-Sahlin model showed that the **k2** values were all negative. This indicates that **k1** was the only mechanism of release, which inferred that AZT release from the formulation was by Fickian diffusion.

Table 5.12: Parameter values and R^2adj values obtained from fitting drug release experimental data to four mathematical models

pH		1.2		7.4	
	Parameters	**AZT-PLGA50:50**	**AZT-PLGA85:15**	**AZT-PLGA50:50**	**AZT-PLGA85:15**
Weibull_1	B	0.15	0.05	0.07	0.07
	A	1.32	1.22	3.67	3.67
	Ti	0.49	0.5	0.47	0.47
	R^2adj	0.982*	0.993*	0.977	0.981*
Gompertz_1	A	0.84	0.77	1.50	1.13
	B	0.70	0.30	0.14	0.32
	R^2adj	0.957	0.937	0.969	0.930
Peppas-Sahlin_1	K1	51.42	59.9	28.19	38.33
	K2	-9.03	-14.88	-6.75	-7.54
	M	0.33	0.24	0.24	0.30
	R^2adj	0.971	0.968	0.998*	0.978
Korsmeyer-Peppas with Tlag	N	0.08	0.03	0.06	0.07
	K	53.9	53.0	23.9	38.0
	R^2adj	0.976	0.992	0.976	0.980

5.3.14 Stability of AZT-PLGA loaded nanoparticles

The formulated nanoparticles were stored at temperatures between 2 and 8°C. They were subsequently evaluated for stability by measuring parameters such as the particle size, zeta potential and PDI at the time of preparation and at different time intervals over a duration of 90 days.

Particle size

The average nanoparticle size after formulation was determined to be 122.4 ±1.48 nm and 110.4 ± 0.02 which increased to 155.3 ± 0.8 nm and 182.7 ± 3.7 nm after washing. These values further increased to 1941.3 ±32.21 nm and 1600 ± 74.8 nm after freeze

drying of the nanoparticles for AZT-PLGA 50:50 AZT-PLGA 85:15, respectively. During storage, the nanoparticles showed a steady pattern of increasing nanoparticle size with time (Figure 5.15). This was indicative of an increase in coalescence of the nanoparticles, and as such a decrease in stability with time.
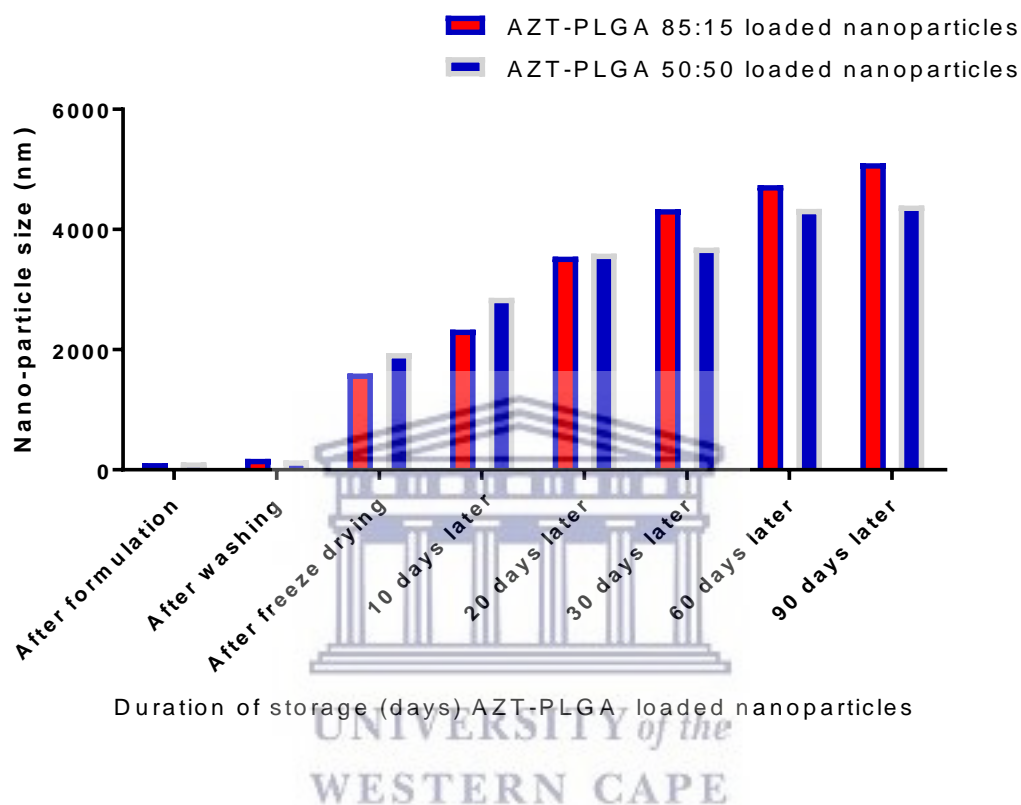
Figure 5.15: Changes in nanoparticle size of TDF-PLGA 50:50 and 85:15 freeze dried loaded nanoparticles

Upon comparison of the particle sizes, AZT-PLGA 85:15 showed a steady increase in particle over time, This was similar to the observation made with TDF-PLGA 85:15 (Figure 4.15) As noted with TDF-PLGA 50:50, the particle sizes of AZT-PLGA 50:50 also increased with time, albeit at a seemingly slower rate than was observed with AZT-PLGA 85:15. These differences in the rate of particle size increase may be due to differences in the copolymer ratios and their molecular weights.

The postulated mechanisms to show how particles pass through the gastrointestinal and physiological barriers highlights endocytosis as one of the mechanisms, for

138

particles < 500 nm. It can therefore be seen that the nanoparticle sizes immediately after formulation and after washing favors uptake *via* endocytosis. Following the freeze-drying and 90-days storage processes however, the increase in particle size as mentioned above was such that endocytosis may not be favorable as an uptake mechanism. There may however be some success with uptake *via* lymphatic passage, with absorption by cells in Peyer's patches, especially for particles less than 5 µm. It can be seen that the nanoparticle size increased after the washing process, possibly due to agglomeration of these particles. As with the TDF formulations a proposal may be made for more assessments of to limit such agglomeration after the washing process, perhaps by making use of suitable surface-active agents. Such an intervention may slow / prevent agglomeration, ensuring that particle sizes remain close to the values obtained immediately after formulation. This will enhance penetration through physiological barriers and hence improve bioavailability.

Zeta potential

The average zeta potential after formulation was determined to be -9.94 ± 0.02 mV and -5.11 ± 2.1 mV for AZT-PLGA 50:50 and AZT-PLGA 85:15, respectively. These values further decreased after washing, indicating an increase in stability. During storage, the zeta potential showed a steady increase in value, which is an indication of a decrease in stability of the nano-formulation with increase in time; however, on day 30, the sample showed some discrepancy indicating an increase in stability. The zeta potential further decreased from day 60 through day 90 (Figure 5.16).

The same trend was also noticed with the TDF formulations (section 4.3.14 and Figure 4.16). Was there perhaps some condition that improved stability on day 30, only to compromise such stability afterwards? This may be the subject of further studies.
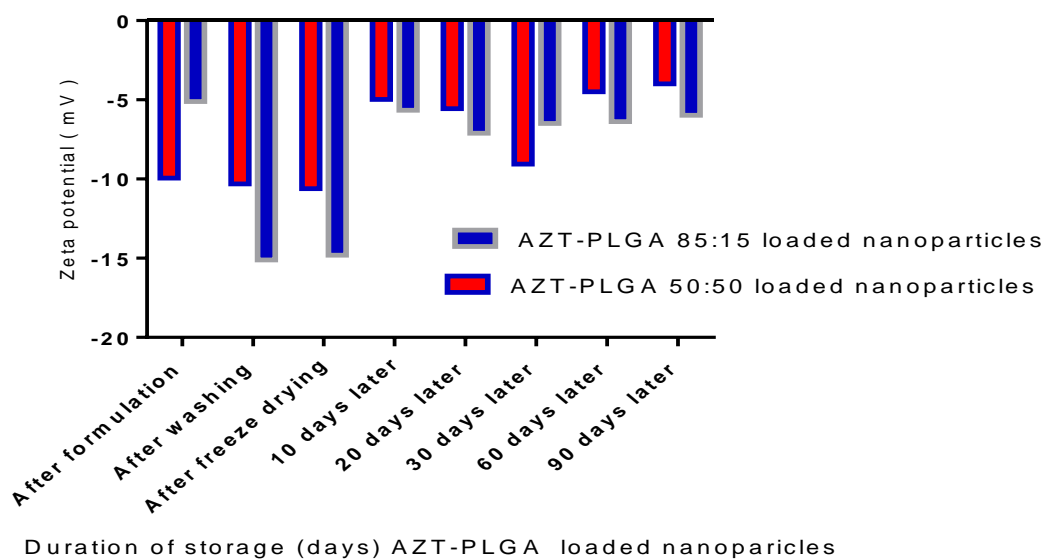
Figure 5.16: *Changes in zeta potential of AZT-PLGA 50:50 and AZT-PLGA 85:15 freeze dried loaded nanoparticles.*

Polydispersity index

The PDI values of the formulated nanoparticles were also assessed immediately after formulation. The values were 0.193 ±1.2 and 0.159 ± 0.02 for AZT-PLGA 50:50 and AZT-PLGA 85:15 respectively. The PDI values after day 10 of storage showed signs of increased coalescence of the nanoparticles. A steady increase in the PDI values was expected over time, however, on days 20, 30, 60 and 90, a drop was noticed in the PDI values, indicating less coalescence. It is our hypothesis that the molecular weight and copolymer ratios may be a factor responsible for these differences. (Figure 5.17).
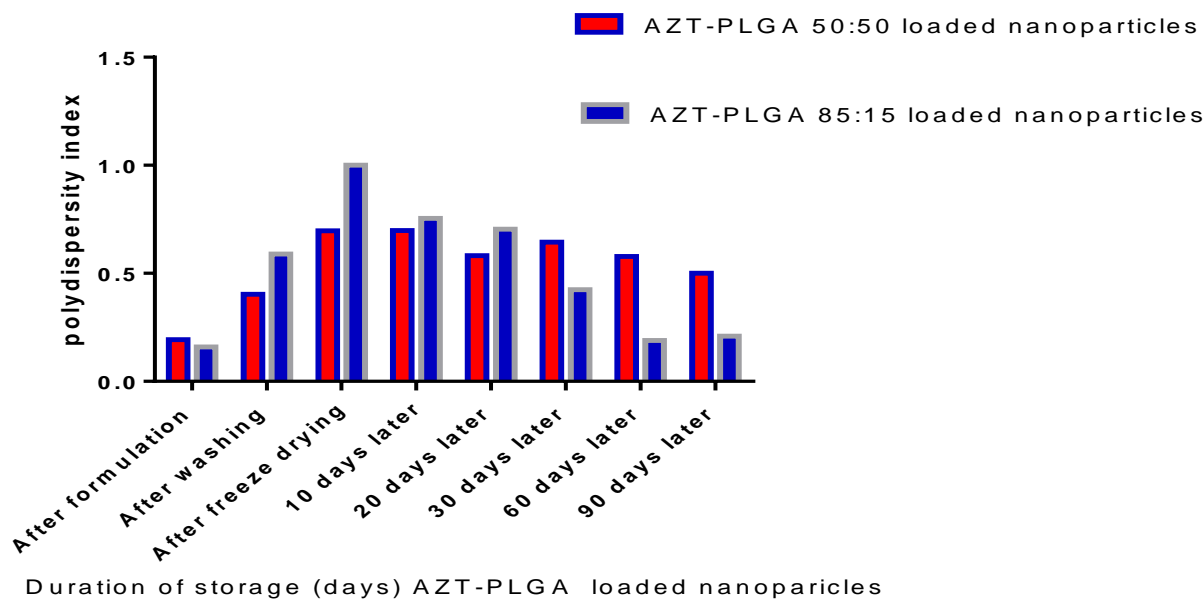
Figure 5.17*: Changes in PDI of AZT-PLGA 85:15 and AZT-PLGA 50:50 freeze dried loaded.*

The overall changes in the nanoparticle size, zeta potential and PDI over the duration of storage were indicative of a decrease in stability of the formulated nanoparticles over time.

Comparing the results obtained from characterizing AZT-loaded nanoparticles with the work done by Peter Christoper *et al.,* 2014 it could be determined that the author formulated nanoparticles which were less than 100 nm in size as opposed to the values obtained in the preset study (particle sizes greater than 100 nm). The present formulation with AZT-PLGA 50:50 yielded a higher encapsulation efficiency (73.8%) when compared to the value (59.50%) obtained by Peter Christoper *et al.,* 2014. Peter Christoper *et al.,* 2014 also modeled the drug release profile and found it to fit the Higuchi model while for this study, the release profile fit best to the Weibull and Peppas-Sahlin models.

Chapter 6 will follow with an overall conclusion of the study.

141

Bibliography

1. Peter, C. G., Vijaya R. C., Siddharth, K., Siva S. K. M., and Hari, P. R., (2014). 'Formulation and optimization of coated PLGA – Zidovudine nanoparticles using factorial design and in vitro in vivo evaluations to determine brain targeting efficiency', *Saudi Pharmaceutical Journal*, *22*(2), pp 133-140.

2. Jani, P.U., Halbert, G.W., Langridge, J., Florence, A.T., (1990) 'Nanoparticle uptake by the rat gastrointestinal mucosa: Quantitation and particle size dependency', *J. Pharm. Pharmacol*, 42(N/A), pp. 821–826.

3. Gref, R., Minamitake, Y., Peracchia, M.T., Trubetskoy, V., Torchilin, V., Langer, R., (1994) 'Biodegradable long-circulating polymeric nanospheres', *Science*, 263 (5153), pp.1600–1603.

4. Bhattacharjee, S., (2016) 'DLS and zeta potential – What they are and what they are not?', *Journal of Controlled Release*, 235, pp.337-351.

5. Masarudin, M. J., Cutts, S. M., Evison, B. J., Phillips, D. R., Pigram, P. J., (2015). 'Factors determining the stability, size distribution, and cellular accumulation of small, monodisperse chitosan nanoparticles as candidate vectors for anticancer drug delivery: application to the passive encapsulation of [14C]-doxorubicin', *Nanotechnology, Science and Applications*, 8(N/A), pp. 67-80

6. Panyam, J., Labhasetwar, V., (2003). 'Biodegradable nanoparticles for drug and gene delivery to cells and tissue', *Adv Drug Deliv Rev*, 55(N/A), pp.329-347.

7. Shabir G. A., (2005). 'Step-by-step analytical methods validation and protocol in the quality system compliance industry', *JVT* 10(N/A), pp. 314-325.

8. Cui, L., Liu, Z., Yu, D., Zhang, S., Bligh, S. and Zhao, N. (2014). Electrosprayed core-shell nanoparticles of PVP and shellac for furnishing biphasic controlled release of ferulic acid. *Colloid and Polymer Science*, 292(9), pp.2089-2096.

9. Zhang, Y., Huo, M., Zhou, J., Zou, A., Li, W., Yao, C. and Xie, S., (2010). 'DDSolver: An Add-In Program for Modeling and Comparison of Drug Dissolution Profiles', *The AAPS Journal*, 12(3), pp.263-271.

10. Maryam, J., Babak, K., 'Mathematical Kinetic Modeling on Isoniazid Release from Dex-HEMA-PNIPAAm Nanogels', *Nanomed research journal,* 1(2), pp.90-96.

11. Papadopoulou, V., Kosmidis, K., Vlachou, M. and Macheras, P. (2006). 'On the use of the Weibull function for the discernment of drug release mechanisms', *International Journal of Pharmaceutics*, 309(1-2), pp.44-50.

12. Pirooznia, N., Hasannia, S., Lotfi, A. and Ghanei, M., (2012). 'Encapsulation of Alpha-1 antitrypsin in PLGA nanoparticles: In Vitro characterization as an effective aerosol formulation in pulmonary diseases', *Journal of Nanobiotechnology*, 10(1), p.20.

CHAPTER 6: CONCLUSION AND RECOMMENDATIONS

Co-formulation of TDF and AZT with PLGA to produce TDF-PLGA and AZT-PLGA nanoparticles, respectively, was the overall aim of this study. Producing these nanoparticles would in turn improve absorption and reduce the dose of drug required to attain therapeutic concentrations, thereby improving bioavailability and reducing the adverse effects associated with the use of these APIs when administered orally.

The overall objectives of the study were:

❖ to characterize AZT, TDF and PLGA

❖ to formulate non-covalent complexes of TDF and AZT with PLGA of different ratios (50:50 and 85:15);

❖ to characterize and compare physicochemical properties of the formulated complexes using various analytical techniques;

❖ to compare the pharmaceutical properties (i.e. particle size, stability and *in-vitro* re*lease st*udies) of the formulated complexes as a means of addressing some of the limitations associated with the optimal delivery of TDF and AZT (e.g. low permeability, low bioavailability).

The above objectives were achieved by formulating nanoparticles using a modified water in oil in water (w/o/w) double emulsion solvent evaporation and diffusion method which had been proven to be efficient in encapsulating hydrophilic drugs.[1] Part of the hypothesis was successfully achieved when AZT and TDF were successfully co-formulated to produce AZT-loaded and TDF-loaded nanoparticles.

Nanoparticles of relatively small sizes in the range of 103 to 160 nm were successfully formulated, with PDI and zeta potential values indicating good homogeneity (PDI of less than 0.4) and good stability of the formulated nanoparticles (zeta potential of up to -19 mV). These smaller particle sizes play an important role as they are likely to be absorbed from the small intestine in greater proportions than the larger nanoparticles.

144

Analysis on FTIR provided spectra which were indicative of TDF and AZT encapsulation within the formulated nanoparticles. This was characterized by shifts, disappearance, appearance, increase or decrease in the intensity of the characteristic peaks when both formulations where compared to the parent compounds and physical mixtures of TDF and AZT with the polymers.

A significant visual difference was noticed when the nanoparticles where analyzed using SEM; the blank nanoparticles showed surfaces that were smother than the loaded nanoparticles. This difference was explained by the APIs presence in the nanoparticles. This study recommends both TEM and SEM analysis be performed on the APIs and physical mixtures with PLGA based on the absence of such data in previous studies and comparative analysis with loaded samples.

TEM on the loaded nanoparticles based on magnification of microscopic image may provide physical image of the loaded PLGA with the API visible in the micelle. Further structural elucidation could be determined using X-ray diffraction.

Both formulated nanoparticles of TDF and AZT showed high percentage yields greater than 50%, with high entrapment values (67-85% for TDF and 75-93% for AZT) and low encapsulation efficiency of less than 50%. An exception was the AZT-PLGA 50:50 formulation which presented with an encapsulation efficiency as high as 73.82%, a value which is 24.02% more than the second highest encapsulation efficiency obtained from the four formulations (TDF-PLGA 85:15). It is uncertain at this stage if this difference is significant. The limitations to this value are highlighted in chapters 4 and 5.

The developed method of formulation was sound and the API to polymer ratio should be reviewed for a possible increase in concentration of API to be included in subsequent studies.

The *in vitro* release profile of both formulations (TDF and AZT) suggested that the release profile was biphasic; firstly, there was an initial burst of the API which confirmed the presence of surface API in the formulated nanoparticles, followed by a sustained release. Overall, the release profile revealed that more of the API was released at pH 1.2 when compared to the release profile of the same formulation at pH 7.4 (Table 4.11 and Table 5.11). This was confirmed by both HPLC-DAD and UV-spectrometry analyses and it agreed with studies by Pamula and Menaszek *et la*, 2007 who stipulated that the surrounding medium influences the degradation process.

The total percentage of API released proposed that not all of the encapsulated drug was released within the 48-hour period. Hence, 48 hours is not sufficient time to achieve complete polymer swelling and degradation to facilitate drug diffusion from the nanoparticles.

Chapters 4 and 5 release data fit well to four Mathematical models, i.e. with the Peppas-Sahlin (only for AZT-PLGA 50:50 at pH 7.4) and the Weibull models (for all other formulations) as the best fit models. This also confirmed that the main mechanism of drug release from the formulated nanoparticles was by Fickian diffusion of the drug molecule from the nanoparticle core. Dissolution is a kinetic process and is quantified by the drug's rate of solubility in solution. Solubility quantifies the dynamic equilibrium state achieved when the rate of dissolution equals the rate of precipitation. Since release studies were not performed for the free drugs, the nanoparticle release profile was compared to the free drug release profile performed by Shailender *et al.*, 2017 and Uronnachi *et al.*, 2014 for TDF and AZT, respectively and to the calibration curve used to analyse the HPLC data. Shailender *et al.*, 2017 and Uronnachi *et al.*, 2014 established that the free drugs were completely released in less than four hours of testing. This confirmed that sustained release was achieved which can led to an

improvement in bioavailability and reduction of adverse effects associated with the use of these APIs thereby proving the hypothesis. *In-vivo* studies are however recommended to further test this hypothesis.

All drug formulations have to be tested for stability. The shelf-life of the product is dependent on such studies. Gradual changes in the stability of the nanoparticles was noticed after just 10 days of storage (2°C to 8°C). The sample showed a decrease in stability; however, these changes were not drastic, therefore the samples were not stable for a duration of 90 days at temperatures between 2°C to 8°C. It is our recommendation that the stability of samples be evaluated at room temperature at well.

According to literature, there are several factors and different mechanisms of polymer degradation to release encapsulated drugs.[2] (mentioned in chapter 2). Firstly, PLGA containing both *D-* and *L-* forms of PLA was purchased, a combination of both forms prevents concerns of prolong or fast degradation. In 1999 Tracy *et la*, stated that PLGA with acid terminated ends showed a 2-3-fold increase in degradation rate when compared to ester terminated PLGA. Thus, this influenced the purchase of ester terminated PLGA for this study which has been proven to degrade slower.[3] .

Finally, the results obtained showed that non-covalent nanoparticles were successfully formulated. Evaluation of the formulated nanoparticles revealed that future studies are needed to improve encapsulation efficiency, i.e., further work is needed to minimized wastage to improve the overall yield and stability, which can translate to a high percentage yield. Further work on *in vivo* analysis could also be performed to assess the ability of the nano-formulations to attenuate the limitations of the APIs.

Bibliography

1. Liu, J., Qiu, Z., Wang, S., Zhou, L., and Zhang, S., (2010). 'A modified double-emulsion method for the preparation of daunorubicin-loaded polymeric nanoparticle with enhancedin vitroanti-tumor activity', *Biomedical Materials*, 5(6), pp. 065002.

2. Lanao, R. P. F., Jonker, A. M., Wolke, J. G. C., Jansen, J. A., van Hest, J. C. M., and Leeuwenburgh, S. C. G., (2013). 'Physicochemical properties and applications of Poly(lactic-co-glycolic acid) for use in bone regeneration', *Tissue Engineering Part B: Reviews*, 19(4), pp. 380–390.

3. Tracy, M., (1999). Factors affecting the degradation rate of poly(lactide-co-glycolide) microspheres in vivo and in vitro. *Biomaterials*, 20(11), pp.1057-1062.

4. Shailender, J., Ravi, P., Saha, P., Dalvi, A., and Myneni, S., (2017). 'Tenofovir disoproxil fumarate loaded PLGA nanoparticles for enhanced oral absorption: Effect of experimental variables and in vitro, ex vivo and in vivo evaluation', *Colloids and Surfaces B: Biointerfaces*, 158, pp.610-619.

5. Uronnachi, E., Ogbonna, J., Kenechukwu, F., Chime, S., Attama, A., and Okore, V., (2014). 'Formulation and Release Characteristics of Zidovudine-Loaded Solidified Lipid Microparticles', *Tropical Journal of Pharmaceutical Research*, 13(2), p.199.

Appendices

Appendix A: Method development for formulation of TDF and AZT loaded nanoparticles

Appendix A presents the different methods assessed to achieve the desired method for formulation of TDF and AZT loaded nanoparticles utilized in this study. The following general method was applied to prepare the nanoparticles, NP (methods A-F).

The general method

1. 100 mg of polymer was weighed and dissolved in 10 ml of ethyl acetate: acetone (4:1 ratio) containing 5% v/v tween 80 in a beaker.
2. 5 mg of API was dissolved in 1 ml of distilled water in a separate beaker.
3. (2) was **sonicated** in (1) at a speed of 5000 rpm for 30 seconds, in an ice bath. The mixture was then **homogenized** at 87 kHz for 2 minutes in the ice bath to form the primary emulsion (w/o).
4. (3) was added dropwise into 40 ml of water and **sonicated** at a speed of 12000 rpm for a further 2 minutes to form the secondary emulsion (w/o/w). Thereafter, the mixture was **homogenized** at 87 kHz for 3 minutes.
5. The w/o/w double emulsion was then poured gradually into a beaker containing 0.05% w/v gelatin dissolved in water while stirring with a magnetic stirrer at 400 rpm.
6. The solution (5) was then continuously stirred at 400 rpm at a temperature of 30 degrees centigrade for 6 hrs. This served to evaporate the organic solvents i.e. ethyl acetate and acetone completely, leaving a white cloudy emulsion (the formed nanoparticles).

7. The nanoparticles where spun in a centrifuge at a speed of 16000 rpm for 30 min to collect the pellets (loaded nanoparticles).

8. The pellets where washed three times with distilled water.

ORGANIC SOLVENT

The first organic solvents (dichloromethane and acetone) used were selected because of its ready availability in the laboratory. However, neither of the two solvents could dissolve the polymer, and when used in combination, the polymer precipitated after homogenization (Appendix, Figure A1.1). The goal at this stage was to select an organic solvent that could solubilize the polymer to continue the study.

A. Organic solvent: Dichloromethane / Acetone

Dichloromethane and acetone were used alone and in combination (ratio 4:1), (Figure A1.1a). The organic solvents (was able to dissolve the polymer completely; however, the polymer precipitated upon addition of the aqueous phase during homogenization/ sonication (Figure A1.1 b). Thus, the sample and the method with selected solvent mixture used was rejected.

(a)   (b)
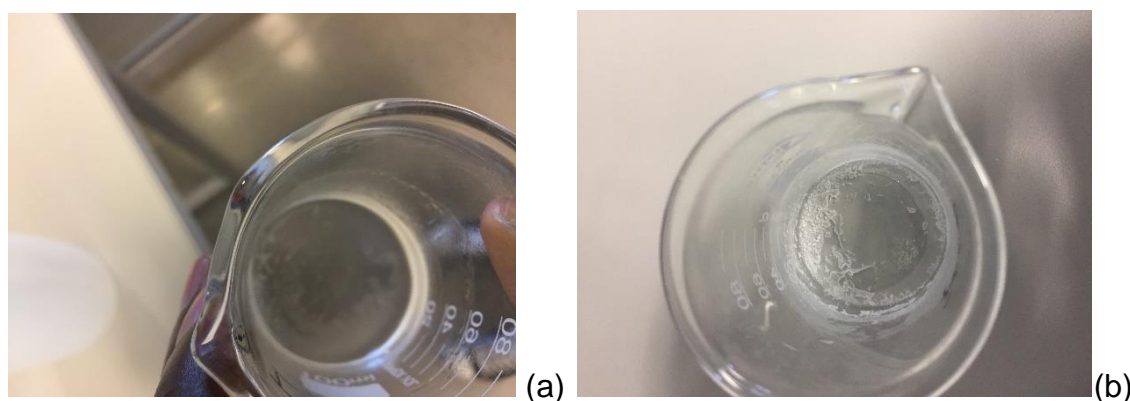
Figure A1.1: *Result of polymer dissolution in the organic solvents (dichloromethane and acetone)*

B. Organic solvent: chloroform

Chloroform was used alone as the organic solvent at this stage of experimentation, because the goal was to select a suitable organic solvent with a low boiling point thus capable of evaporating quickly. NPs were successfully produced but were not subjected to washing because the particle sizes obtained were larger than the expected value of less than 150 nm (Table A1.1). Chloroform had proven to solve the issue (precipitation of the polymer after homogenization) encountered with dichloromethane and acetone; however, it still presented its own shortcomings as particle size obtained was larger than required.

Table A1.1: Particle size, polydispersity index and zeta potential of formulated AZT or TDF nanoparticle obtained with chloroform as the organic solvent.

Solvent	Particle size (nm)		Polydispersity index		Zeta potential	
	Before wash	After wash	Before wash	After wash	Before wash	After wash
Chloroform	354.1	-	0.198	-	-0.361	-

151

C. Organic solvent: Ethyl acetate

Ethyl acetate was also tested as an organic solvent. The results are presented in Table

A1. 2.

Table A1. 2: *Particle size, polydispersity index and zeta potential of formulated nanoparticles obtained with ethyl acetate and changes in gelatin concentration.*

Solvent Ethyl acetate	Gelatin (%) w/v	Particle size (nm)		Polydispersity index		Zeta potential	
		Before wash	After wash	Before wash	After wash	Before wash	After wash
Sample 1 (TDF)	0.5	1859	-	1	-	-	-
Sample 2 (TDF)	0.5 sonicated	185	-	1	-	4	
Sample 3 (TDF)	0.2	392.4	-	0.371	-	3.01	-
Sample 4 (TDF)	0.1	1603	-	0.274	-	-	-
Sample 5 (TDF)	0.05	312	-	1	-	2.91	
Sample 6 (TDF)	0.05 sonicated	237.1	-	1	-	3.94	-
Sample 7 (AZT)	0.05	400	-	1	-	-2	
Sample 8 (AZT)	0.05 sonicated	93	-	0.98	-	6	
Sample 9 (AZT)	0.1	839	-	1	-	-3.5	
Sample 10 (AZT)	0.2	501.2	-	0.917	-	-2.91	-
Sample 11 (AZT)	0.5 sonicated	117.1	-	0.528	-	5.61	-
Sample 12 (AZT)	0.5	1890	-	1	-	-8	

Ethyl acetate was preferred over chloroform because it is less toxic than the latter.

Further experimentation was carried out with ethyl acetate as the organic solvent.

Changes were made to the concentration of gelatin in this exercise. Some gelatin

samples were sonicated to aid with solubility before use because it was apparent that

the size of the formulated NPs were affected by concentration and effects of sonication

as seen in Table A1.3. When gelatin was sonicated before use, the nanoparticle sizes

were of a lower value compared to the same concentration when gelatin was not

sonicated. The concentration of gelatin was also varied and its effect on particle size

investigated.

D. Organic solvent: ethyl acetate/acetone ratio 4:1

Samples in this category were homogenized before sonication, unlike the samples previously prepared which were homogenized after sonication, to determine which sequence will yield the smallest particles sizes. The concentration of gelatin was kept constant at 0.05% w/v and the gelatin stock solution was sonicated before use. An exception was sample 3 which was not sonicated, this was to determine if there would be any difference in particle size, PDI and zeta potential when there is sonication and when there is no sonication (Table A1.3).

Table A1.3: *Particle size, polydispersity index and zeta potential of formulated nanoparticles obtained when samples were homogenized before sonication.*

Solvent Ethyl acetate / Acetone (4:1)	Particle size (nm)		Polydispersity index		Zeta potential	
	Before wash	After wash	Before wash	After wash	Before wash	After wash
Sample 1	99.66	360	0.412	3.12	3.12	-8.63
Sample 2	126.9	278	0.385	0.365	2.85	-9.05
Sample 3*	1895	1688	1	1	-	-

*samples not sonicated

E. Reduction of sample size

Organic solvent: ethyl acetate/acetone ratio 4:1

The sample was prepared using the general method earlier reported with the exception that the w/o/w double emulsion prepared was not poured into 200 ml of water containing 0.05% gelatin but instead was directly transferred to the rotavapor for solvent evaporation at 400 rpm for 4 hrs. This step did not yield much difference in the particle size because the NPs were still not within the desired particle size range of 100-200 nm (Table A1.4).

153

Table A1.4: *Particle size, polydispersity index and zeta potential of formulated nanoparticles obtained when sample size was reduced.*

Solvent	Particle size (nm)		Polydispersity index		Zeta potential	
	Before wash	After wash	Before wash	After wash	Before wash	After wash
Ethyl acetate / Acetone (4:1)	1237	-	1	-	-	-

F. Organic solvent less than 10ml i.e. ethyl acetate and acetone (4:1)

The emulsion was prepared with the general method reported above, with slight modification in the total volume of organic solvent (ethyl acetate and acetone) used. Instead of using a total volume of 10 ml, we tested 5 ml and 6 ml of the organic solvent in the same combination and ratio as above. The organic solvents were used individually as well to dissolve the polymer. A portion of the polymer precipitated during the process (Figure A1.2); and the sample was therefore discarded.
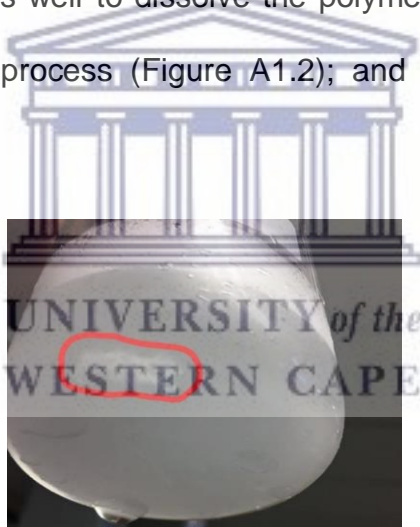
Figure A1.2: *Precipitation of sample (AZT and TDF) when less than 10ml of the organic solvent (ethyl acetate and acetone) was used.*

Appendix B

Reduction of total sample size from 251 ml to 91 ml using d-*α*-tocopheryl polyethylene glycol 1000 succinate (TPGS) and tween 80.

The general method previously described (appendix A) produced a total sample volume of 251 ml and this was very cumbersome and time consuming to centrifuge. In addition, some of the sample was lost during this process. There was thus a need to reduce the total sample size. The gelatin which was used as a surfactant affected the particle sizes of the NPs hence the change to TPGS. The general method below was used to accommodate these changes.

Method

1) 100 mg of polymer was weighed and dissolved in 10 ml of a mixture of 4:1 ethyl acetate/acetone and vortexed to ensure that it was completely dissolved.

2) 5 mg of the API was dissolved in (1) ml of water containing 0.2% w/v tween 80.

3) (2) was homogenized in 1 at a speed of 5000 rpm for 2 min and sonicated at 87 kHz for 30 seconds under an ice bath to produce the primary emulsion.

4) (3) was added dropwise into 40 ml of external water containing 0.12% TPGS and homogenized for 3 min at a speed of 12000 rpm. The mixture was then sonicated at 87 kHz for 2 min.

5) The w/o/w double emulsion was poured gradually into a beaker containing 40 ml of 0.2% tween 80 while stirring with a magnetic stirrer at 800 rpm.

6) The solution was evaporated using the rotavapor at a speed of 400 rpm and temperature between 30-35 degrees for 6 hrs to completely evaporate the organic solvents.

7) The nanoparticles where spun at a speed of 16500 rpm for 60 min to collect the pellets which settled at the bottom.

8) The pellets where washed three times with distilled water.

G. Sample preparation without TPGS

The sample was prepared using the method described above, however only with tween 80 (and no TPGS) as follows: The TPGS in step 4 was replaced with tween 80 thus in the final stage no surfactant was used. However, following centrifugation at a temperature of 4°C and speed of 16500 rpm for 30 mins, the nanoparticles could not be collected. A possible reason for this might have been that the particle sizes were too small, and a higher centrifugation speed was needed for the nanoparticles formed to settle and be collected from the sample. This sample was rejected (Table B1.1).

Table B1.1: *Particle size, polydispersity index and zeta potential of formulated nanoparticles obtained when sample size was reduced and preparation was without TPGS.*

Solvent	Particle size (nm)		Polydispersity index		Zeta potential	
	Before wash	After wash	Before wash	After wash	Before wash	After wash
Ethyl acetate / Acetone (4:1)	89.92	-	0.232	-	-4.94	-

H. Sample preparation with TPGS

The sample was prepared as described previously by the general method in appendix B. Formulation data from this activity are presented in Table B1.2. Following preparation, the samples were spun at a speed of 26000 rpm for 30 mins. In the process, the Eppendorf tubes containing the samples were broken, leading to loss of samples. A possible reason proffered for this was the centrifuge speed, which may have been too high for the tubes used.

Table B1.2: *Particle size, polydispersity index and zeta potential of formulated nanoparticles obtained when sample size was reduced and preparation was with TPGS.*

Solvent	Particle size (nm)		Polydispersity index		Zeta potential	
	Before wash	After wash	Before wash	After wash	Before wash	After wash
Ethyl acetate / Acetone (4:1)	107.7	-	0.161	-	-5.71	-

I. Sample prepared with TPGS

The samples prepared in section H above confirmed the method to be used. The prepared sample was collected by centrifuging at a lower speed of 16500 rpm for one hour. The collected pellets were washed and freeze-dried. Data obtained from this activity is presented in Table B1.3.

Table B1.3: *Particle size, polydispersity index and zeta potential of formulated nanoparticles obtained when sample size was reduced, reduced collection speed (16500) and preparation was with TPGS.*

Solvent Ethyl acetate / Acetone (4:1)	Particle size (nm)		Polydispersity index		Zeta potential	
	Before wash	After wash	Before wash	After wash	Before wash	After wash
Sample 1	111.5	156.9	0.128	0.317	-10.9	-16.6
Sample 2	117.3	153.2	0.160	0.303	-8.84	-19.1

Appendix C : Validation of UV-VIS assay method for tenofovir disoproxil fumarate and zidovudine in PBS at pH 1.2 and pH 7.4.

The tables presented by appendix C are computational data used for a standard callibration curve for both AZT and TDF. It also provides data used to prove the accuracy and precission of the of HPLC-DAD and UV-spectrometry method used for the prediction of TDF and AZT.

Table C1.1: Calibration plot of TDF at pH 7.4 and pH 1.2 (HPLC-DAD analyses).

Concentration (µg/ml)	Mean Absorbance		%RSD	
	pH 7.4	pH 1.2	pH 7.4	pH 1.2
0.02	34.15	71.40	0.42	1.2
0.04	68.27	143.55	2.06	2.0
0.06	102.31	213.44	0.28	3.0
0.08	135.92	284.22	0.86	1.7
0.10	168.55	371.71	0.39	3.0
0.12	201.07	420.0	0.96	0.5

Table C1.2: Calibration plot of TDF at pH 7.4 and pH 1.2 (UV-spectrometry analyses)

Concentration (µg/ml)	Mean Absorbance		%RSD	
	pH 7.4	pH 1.2	pH 7.4	pH 1.2
2	0.0295	0.0696	0.71	4.9
4	0.0817	0.1358	1.22	0.13
6	0.1306	0.1745	0.27	0.10
8	0.1630	0.2018	0.18	0.05
10	0.1927	0.2337	0.05	0.04
12	0.2424	0.2794	0.04	0.14

Table C1.3: Selected FTIR data for TDF, PLGA 50:50, PLGA 85:15, TDF-PLGA 50:50 physical mixture, and TDF-PLGA 85:15 physical mixture

Analyzed sample	Experimental frequency bands (cm^{-1})	Standard frequency bands (cm-1)	Associated functional groups from IR bands
TDF	3459.12	3400-3500	Medium N-H stretching
	2981.38	2300-3300	Strong broad O-H stretching
	2814.22	2850 - 2810	Medium $-OCH_3$ stretching
	2018.44	2140 - 1990	Strong and broad $-N=C=S$ stretching
	1752.31	1800 - 1750	Strong C=0 stretching
	1671.87	1685 - 1665	
PLGA 50:50	2950.52	2960 - 2850	Chelated O-H stretching bridge
	1750.32	1800 – 1750	C=O stretching of the carbonyl group
PLGA 85:15	2996.25	3000 - 2500	Chelated O-H stretching bridge
	1745.64	1790 - 1740	Strong C=O stretching of the carbonyl group
TDF-PLGA 50:50 physical mixture	2993.81	3000 - 2500	Chelated O-H stretching bridge
	1750.07	1790 - 1740	Strong C=O stretching of the carbonyl group
TDF-PLGA 85:15 physical mixture	2985.88	3000 - 2500	Chelated O-H stretching bridge
	1754.32	1790 - 1740	Strong C=O stretching of the carbonyl group
	1674.85	1685 - 1665	Strong C=0 stretching

Table C1.4: Thermogravimetric analysis of data for TDF, polymers and TDF-polymer physical mixture

Sample	Mass loss events	$T_{onset} \pm 1$ (°C)	$T_{deg.max.} \pm 1$ (°C)	$T_{endset} \pm 1$ (°C)	Total mass loss (%)
PLGA 50:50	1st	236	322	324	98
	2nd	335	376	378	
PLGA 85:15	1st	221	311	313	100
	2nd	318	389	390	
TDF-PLGA 50:50		215	399	400	93
TDF-PLGA 85:15		217	396	397	98
TDF	1st	135	199	201	87
	2nd	203	275	276	

Table C1.5: Thermal properties of TDF-PLGA loaded nanoparticles

Drug polymer combination	Mass loss events	T_{onset} (°C)	$T_{deg.max.}$ (°C)	T_{endset} (°C)	Total mass loss (%)
TDF-PLGA 50:50 loaded	1st	206	355	356	93
	2nd	356	424	425	
TDF-PLGA 85:15 loaded	1st	234	340	341	91
	2nd	343	396	397	

Table C1.6: Calibration plot of AZT at pH 7.4 and pH 1.2, (HPLC-DAD analyses)

Concentration (µg/ml)	Mean Absorbance		%RSD	
	pH 7.4	pH 1.2	pH 7.4	pH 1.2
0.02	165.83	124.97	0.72	0.85
0.04	330.59	249.14	0.17	0.99
0.06	495.44	391.12	0.28	0.19
0.08	656.09	494.27	0.02	0.4
0.10	824.70	614.31	0.13	0.32
0.12	976.90	745.93	0.2	0.2

Table C1.7: Calibration plot of AZT at pH 7.4 and pH 1.2 (UV-spectrometry analyses)

Concentration (µg/ml)	Mean Absorbance		%RSD	
	pH 7.4	pH 1.2	pH 7.4	pH 1.2
2	0.0869	0.1100	0.24	0.18
4	0.1539	0.1625	0.10	0.06
6	0.2231	0.2539	0.09	0.37
8	0.2927	0.3248	0.07	0.06
10	0.3666	0.3993	0.27	0.09
12	0.428	0.4649	0.19	0.08

Table C1.8: Thermal properties of AZT, polymers and AZT-polymer physical mixture

Sample	Mass loss events	T_{onset} (°C)	$T_{deg.max.}$ (°C)	T_{endset} (°C)	Total mass loss (%)
AZT-PLGA 50:50	1st	218	353	355	94
	2nd	357	398	399	
AZT-PLGA 85:15		220	386	387	97
AZT	1st	172	247	257	76
	2nd	249	317	318	

Table C1.9: Selected FTIR data for AZT-PLGA 50:50 loaded nanoparticles, AZT-PLGA 85:15 loaded nanoparticles, AZT-PLGA 50:50 physical mixture, and AZT-PLGA 85:15 physical mixture

Compound	Experimental frequency bands (cm^{-1})	Standard frequency bands (cm-1)	Associated functional groups from IR bands
AZT-PLGA 50:50 loaded	2948.36	3000 - 2500	Chelated O-H stretching bridge
	1748.67	1770 - 1710	Strong C=O stretching
AZT-PLGA 85:15 loaded	2995.93	2960 - 2850	Strong C-H bending
	2945.50	3000 - 2500	Chelated O-H stretching bridge
	1748.02	1770 - 1710	Strong C=O stretching
AZT-PLGA 50:50 physical mixture	3461.12	3500 - 3300	Medium N-H stretching bands
	3023.15	3000 - 2500	Chelated O-H stretching bridge
	2814.57	3200 - 2500	O-H stretching
	2082.39	2160-2120	Strong N=N=N stretching
	1751.54	1770 - 1710	Strong C=O stretching
	1679.98	1685-1666	Strong C=O stretching
AZT-PLGA 85:15 physical mixture	3460.60	3500 - 3300	Medium N-H stretching bands
	3023.04	3000 - 2500	Chelated O-H stretching bridge
	2082.15	2160-2120	Strong N=N=N stretching
	1750.91	1770 - 1710	Strong C=O stretching
	1677.09	1685-1666	Strong C=O stretching

Table C1.10: Thermal properties of AZT-PLGA loaded nanoparticles

Drug polymer combination	Mass loss events	T_{onset} (°C)	$T_{deg.max.}$ (°C)	T_{endset} (°C)	Total mass loss (%)
AZT-PLGA 50:50 loaded	1st	225	414	415	100
AZT-PLGA 85:15 loaded	1st	234	334	335	93
	2nd	335	402	403	